

EXPERIMENTAL INVESTIGATION OF  
BENDABLE HEAT PIPES

Dhananjay Dilip Odhekar

A Thesis

Submitted to

the Graduate Faculty of

Auburn University

in Partial Fulfillment of the

Requirements for the

Degree of

Master of Science

Auburn, Alabama  
August 8, 2005

EXPERIMENTAL INVESTIGATION OF  
BENDABLE HEAT PIPES

Except where reference is made to the work of others, the work described in this thesis is my own or was done in collaboration of my advisory committee.  
This thesis does not include proprietary or classified information.

---

Dhananjay Dilip Odhekar

Certificate of Approval:

---

Daniel W. Mackowski  
Associate Professor  
Mechanical Engineering

---

Daniel K. Harris, Chair  
Associate Professor  
Mechanical Engineering

---

Jay Khodadadi  
Professor  
Mechanical Engineering

---

Stephen L. McFarland  
Acting Dean  
Graduate School

EXPERIMENTAL INVESTIGATION OF  
BENDABLE HEAT PIPES

Dhananjay Dilip Odhekar

Permission is granted to Auburn University to make copies of this thesis at its discretion,  
upon request of individuals or institutions and at their expense.  
The author reserves all publication rights.

---

Signature of Author

---

Date

Copy sent to:

Name

Date

## VITA

Dhananjay Dilip Odhekar, son of Dilip K. Odhekar and Suniti D. Odhekar, was born on November 9, 1977 in Dhule, Maharashtra, India. In August 1995, he entered the K. K. Wagh College of Engineering at University of Pune, Maharashtra, India and earned the degree of Bachelor of Mechanical Engineering in June 1999 with first class. He worked for Mahindra Tractors Limited, India as Trainee Engineer in manufacturing for a period of one year. Dhananjay worked for Syndicate Services, Nasik, India as an Assistant Engineer in 2001. He then entered the Graduate School at Auburn University in August 2002.

THESIS ABSTRACT

EXPERIMENTAL INVESTIGATION OF

BENDABLE HEAT PIPES

Dhananjay Dilip Odhekar

Master of Science, August 8, 2005  
(B.E. Mech, K.K.W.C.O.E., University of Pune, 1999)

126 Typed Pages

Directed by Dr. Daniel K. Harris

Heat pipes are highly conductive heat transfer devices. They use the latent heat of the working fluid for efficient heat transfer over a very small temperature drop. They have been a subject of numerous studies since the early 1950s and are commercially available in a variety of forms. This thesis is an investigation of the effect bending has on the performance of heat pipes. Flexible and pre-bent heat pipes have been studied and successfully demonstrated in the past. Bendable heat pipes, which can be bended after fabrication as needed are a novel device developed during this study. The effect of bending on temperature drop, performance and performance limits was investigated. The heat pipes used for testing were made using oxygen free copper for the container and water as the working fluid. The wick was made from sintered copper felt and provided the post fabrication bendability feature of these heat pipes. The concept of copper equivalence to compare disparate data is also developed and explained. It is used to benchmark the test data against copper conductivity.

## ACKNOWLEDGEMENTS

I would like to acknowledge the Dana Corporation contract at Auburn University through Auburn Thermal Management Laboratory for providing the funding.

I would like to thank my advisor, Dr. Daniel K. Harris for his guidance and suggestions throughout this research. I would also like to thank Bhavin Vadgama for his assistance in designing and fabricating heat pipes.

Most importantly, I am sincerely grateful to my parents. The unselfish support they provided so that I could go back to school will always encourage me to walk in their footsteps.

Style manual or journal used:

IEEE

Computer software used:

Microsoft Office System 2003

## TABLE OF CONTENTS

LIST OF FIGURES .....	xi
LIST OF TABLES.....	xiv
1 HEAT PIPES .....	1
1.1 Introduction.....	1
1.2 Heat Pipe.....	2
1.3 Construction.....	2
1.4 Operation .....	3
1.5 Operating Limits.....	7
1.5.1 Capillary Limit.....	7
1.5.2 Sonic Limit.....	8
1.5.3 Boiling Limit.....	9
1.5.4 Entrainment Limit.....	9
1.5.5 Viscous Limit.....	9
1.5.6 Condenser Limit.....	10
2 BACKGROUND .....	12
2.1 Scope of Bendable Heat Pipe .....	12
2.2 Review .....	13
3 FACTORS AFFECTING DESIGN AND PERFORMANCE.....	32
3.1 Introduction.....	32
3.2 Working Fluid.....	32
3.2.1 Compatibility with Wick and Container.....	34
3.2.2 Thermal Stability .....	34
3.2.3 Wetting of Wick and Container .....	34
3.2.4 High Latent Heat and Thermal Conductivity.....	35
3.3 Container.....	35



3.4	Capillary Structure.....	36
3.4.1	Homogeneous Wicks .....	36
3.4.2	Composite Wicks.....	37
4	TESTING AND PERFORMANCE EVALUATION.....	39
4.1	Performance Evaluation.....	39
4.1.1	Testing Procedure .....	40
4.1.2	Conductance.....	42
4.2	Copper Equivalence.....	42
4.2.1	Measurement Errors and Losses .....	44
4.2.2	Parasitic Losses.....	45
4.2.3	Benchmarks.....	46
4.2.4	Concept of Copper Equivalence .....	48
4.2.5	Why Copper Equivalence Works?.....	49
4.2.6	Application.....	50
5	BENDABLE HEAT PIPES .....	53
5.1	Introduction.....	53
5.2	Bendable Wicks.....	53
5.3	Performance Limit.....	57
5.3.1	Vapor Pressure Drop.....	57
5.3.2	Other Pressure Drops .....	62
5.3.3	Capillary Limit.....	63
5.3.4	Other Limits .....	66
5.3.5	Bend Loss.....	66
5.3.5.1	Bend Loss Coefficient for Vapor Flow .....	68
5.3.6	Capillary Limit for Bended Heat Pipe .....	69
5.4	Testing and Evaluation .....	71
5.4.1	Specifications of HP01 .....	73

5.4.2	HP01 Bending Test Results .....	73
5.4.3	Capillary Limits for HP01 .....	79
5.4.4	Specifications of HP02 .....	84
5.4.5	HP02 Bending Test Results .....	84
5.4.6	Capillary Limits for HP02 .....	94
5.5	Results.....	103
5.5.1	Possible Capillary Limit .....	104
5.5.2	Boiling Limit Encountered .....	104
5.5.3	Condenser Limit.....	105
5.5.4	Bending Issues .....	105
6	DISCUSSION.....	106
6.1	Conclusion.....	106
6.2	Future Work.....	107
	BIBLIOGRAPHY.....	109

## LIST OF FIGURES

Figure 1.1: Schematic of construction and operation of a typical heat pipe.....	5
Figure 1.2: Pressure variation along a heat pipe.....	6
Figure 1.3: Operating limits for a heat pipe.....	11
Figure 2.1: Flexible cryogenic heat pipe [10].....	16
Figure 2.2: Heat pipe bends [16].....	20
Figure 2.3: $\Delta T$ between evaporator exit and end of condenser versus bend angle of heat pipe [26] .....	23
Figure 3.1: Homogeneous wicks.....	38
Figure 3.2: Composite wicks .....	38
Figure 4.1: Heat pipe test setup for conductance measurement.....	41
Figure 4.2: Steady state temperature curves during testing .....	43
Figure 4.3: Heat pipe conductance against input power applied .....	43
Figure 4.4: Estimation of parasitic losses .....	47
Figure 4.5: Conductance corrected to account for parasitic losses.....	47
Figure 4.6: Schematic of heater blocks used .....	51
Figure 4.7: Comparison of copper rod data on heater blocks.....	52
Figure 5.1: Wick separation near heat pipe wall due to bending.....	55
Figure 5.2: Bending effects on heat pipe wall and wick.....	56
Figure 5.3: Heat Pipe Nomenclature.....	60
Figure 5.4: The correction function $a(z)$ [38] .....	61
Figure 5.5: Hydrostatic pressure drops in a bended heat pipe .....	65
Figure 5.6: Resistance to flow with Dean number.....	70
Figure 5.7: Schematic of bending configurations for HP01 .....	72
Figure 5.8: Test results for HP01 in straight horizontal position.....	75
Figure 5.9: Test results for HP01 in straight vertical gravity assist position.....	75
Figure 5.10: Test results for HP01 in 15° bended vertical gravity assist position.....	76

Figure 5.11: HP01 Test results for HP01 in 30° bended vertical gravity assist position.....	76
Figure 5.12: Test results for HP01 in 45° bended vertical gravity assist position.....	77
Figure 5.13: Test results for HP01 in 60° bended vertical gravity assist position.....	77
Figure 5.14: Test results for HP01 in 90° bended vertical gravity assist position.....	78
Figure 5.15: $\Delta T$ across HP01 for various bend angles .....	78
Figure 5.16: Capillary limit for HP01 in straight horizontal orientation .....	80
Figure 5.17: Capillary limit for HP01 in straight vertical orientation .....	80
Figure 5.18: Capillary limit for HP01 in 15° bended vertical orientation .....	81
Figure 5.19: Capillary limit for HP01 in 30° bended vertical orientation .....	81
Figure 5.20: Capillary limit for HP01 in 45° bended vertical orientation .....	82
Figure 5.21: Capillary limit for HP01 in 60° bended vertical orientation .....	82
Figure 5.22: Capillary limit for HP01 in 90° bended vertical orientation .....	83
Figure 5.23: Effect of bending angle on capillary limit for HP01 .....	83
Figure 5.24: Test results for HP02 in straight horizontal orientation .....	86
Figure 5.25: Test results for HP02 in straight vertical orientation .....	86
Figure 5.26: Test results for HP02 in 15° bended horizontal orientation .....	87
Figure 5.27: Test results for HP02 in 15° bended vertical orientation .....	87
Figure 5.28: Test results for HP02 in 30° bended horizontal orientation .....	88
Figure 5.29: Test results for HP02 in 30° bended vertical orientation .....	88
Figure 5.30: Test results for HP02 in 45° bended horizontal orientation .....	89
Figure 5.31: Test results for HP02 in 45° bended vertical orientation .....	89
Figure 5.32: Test results for HP02 in 60° bended horizontal orientation .....	90
Figure 5.33: Test results for HP02 in 60° bended vertical orientation .....	90
Figure 5.34: Test results for HP02 in 90° bended horizontal orientation .....	91
Figure 5.35: Test results for HP02 in 90° bended vertical orientation .....	91
Figure 5.36: $\Delta T$ across HP02 for various bend angles in horizontal orientation.....	92
Figure 5.37: $\Delta T$ across HP02 for various bend angles in vertical orientation.....	92

Figure 5.38: Evaporator of HP02 could not attain steady state at 40W power input in 90° bended vertical orientation .....	93
Figure 5.39: Heater of HP02 could not attain steady state at 40W power input in 90° bended vertical orientation.....	93
Figure 5.40: Capillary limit for HP02 in straight horizontal orientation .....	95
Figure 5.41: Capillary limit for HP02 in straight vertical orientation .....	95
Figure 5.42: Capillary limit for HP02 in 15° bended horizontal orientation .....	96
Figure 5.43: Capillary limit for HP02 in 15° bended vertical orientation .....	96
Figure 5.44: Capillary limit for HP02 in 30° bended horizontal orientation .....	97
Figure 5.45: Capillary limit for HP02 in 30° bended vertical orientation .....	97
Figure 5.46: Capillary limit for HP02 in 45° bended horizontal orientation .....	98
Figure 5.47: Capillary limit for HP02 in 45° bended vertical orientation .....	98
Figure 5.48: Capillary limit for HP02 in 60° bended horizontal orientation .....	99
Figure 5.49: Capillary limit for HP02 in 60° bended vertical orientation .....	99
Figure 5.50: Capillary limit for HP02 in 90° bended horizontal orientation .....	100
Figure 5.51: Capillary limit for HP02 in 90° bended vertical orientation .....	100
Figure 5.52: Effect of bending angle on capillary limit for HP02 in vertical orientation .....	101

## LIST OF TABLES

Table 2.1: Summary of published work on flexible heat pipes .....	30
Table 2.2: Summary of published work on flexible heat pipes .....	31
Table 3.1: Thermo physical properties of working fluids used at AuTherMML [3].....	33
Table 4.1: Conductance values of copper 101 rod.....	52
Table 5.1: Effect of bending angle on capillary limit for HP02 in horizontal orientation.....	102

## CHAPTER 1

### HEAT PIPES

#### **1.1 Introduction**

Heat transport has been one of the most difficult and inefficient tasks in thermal management. It often results in costly heat transfer losses and reduced overall efficiencies. Performance of mechanical and electronic components inside automobiles is now governed by the efficiency of cooling system [1]. Heat transfer by heat pipes is one of the fastest and most efficient methods for thermal management. In automobiles, the stress of modern design is on reducing bulk weight and volume of all components. This results in densely packaged components including drive trains and electronic components. The heat pipe is a promising technology that has received significant research interest since early 1950s. The early studies mostly concentrated on heat pipes used in straight configurations. But many practical designs demand heat pipes in contorted shapes [2]. This thesis investigates the feasibility of bendable heat pipes. These heat pipes can be bent after fabrication without affecting their performance.

## **1.2 Heat Pipe**

The heat pipe concept was initially investigated by R.S. Gaugler in 1942 [3]. The remarkable properties of the heat pipe became appreciated and serious development work took place after its independent invention by G. M. Grover in the early 1960's [3].

A heat pipe typically has high conductance, usually an order of magnitude higher than a metal conductor of similar specifications. It transfers heat from a source to a sink by means of cyclic evaporation and condensation of a working fluid. It uses the latent heat of vaporization of the working fluid to transfer heat. The heat pipe does not require any external energy to function and it has no moving parts. For the same heat load, a heat pipe has a very low temperature drop due to its high efficiency. However, unlike a metal conductor a heat pipe has a limit on the amount of heat it can transfer.

## **1.3 Construction**

The basic heat pipe concept can be demonstrated by a simple tubular metal casing with a wick covering the inner surface (Figure 1.1). The wick is made of different materials and has been one of the most investigated aspects of heat pipes. It is usually made of a porous material. A grooved structure can also be used. A working fluid is vacuum-sealed in a pre-determined quantity [4]. The working fluid inside can be any compound that has good wetting characteristics on the wick and is selected on the basis of working temperatures of the heat pipe. If kinetic pressure losses of the vapor and gravitation head losses are neglected the properties of the working fluid can be combined



to form a figure of merit  $M$ . The merit number determines the maximum possible heat transport using the heat pipe.

$$M = \frac{\rho_l \sigma_l L}{\mu_l} \quad 1.1$$

where

$\rho_l$  = density of working fluid in liquid phase

$\sigma_l$  = surface tension of the working fluid

$\mu_l$  = dynamic viscosity of working fluid in liquid phase

$L$  = length of the heat pipe

#### **1.4 Operation**

A heat pipe is broadly divided in three sections namely, evaporator, adiabatic and condenser. A typical heat pipe as shown in Figure 1.1 has one evaporator section that takes heat from a source. The heat absorbed in the evaporator causes change of phase of the working fluid from liquid to vapor. The increased vapor pressure in the evaporator causes the vapor to exit from the evaporator section and travel through the adiabatic section. Traveling through the adiabatic section the vapor reaches the condenser region where condensation rejects the latent heat of the fluid to the sink. The condensed liquid is pumped back against an adverse pressure gradient to the evaporator by a combination of the capillary pumping action and/or bulk forces. This fluid circuit is repeated during the normal operation of the heat pipe and can continue as long as there is sufficient vapor pressure and capillary pressure to support its operation.

At the evaporator end the liquid recedes into the wick pores and hence the menisci in the pores at the vapor interface are highly curved. Whereas the liquid menisci at vapor interface in the condenser end are almost flat. This difference in the interface curvature of the menisci at the vapor interface coupled with the surface tension of the working fluid causes a capillary pressure gradient at the liquid-vapor interface along the length of the pipe. This capillary pressure gradient pumps the working fluid against various pressure losses such as friction, inertia and against bulk body forces [3]. This axial variation of pressure is illustrated in Figure 1.2.

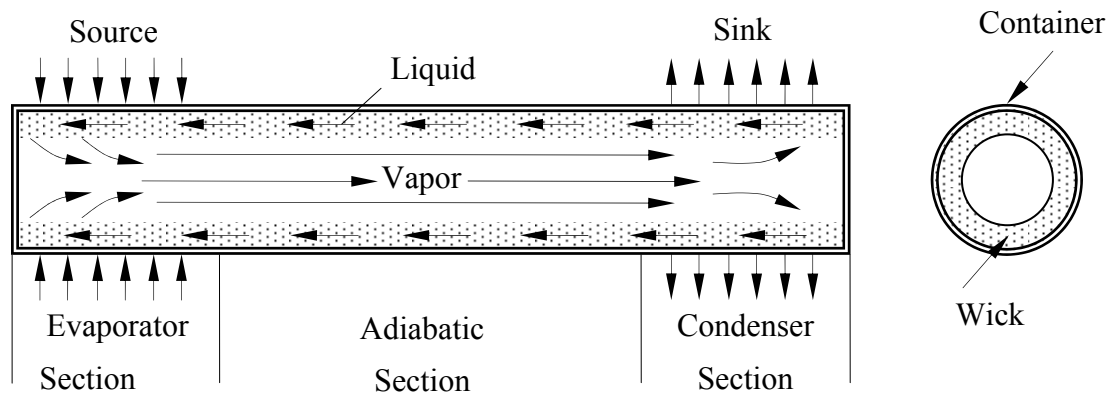


Figure 1.1: Schematic of construction and operation of a typical heat pipe

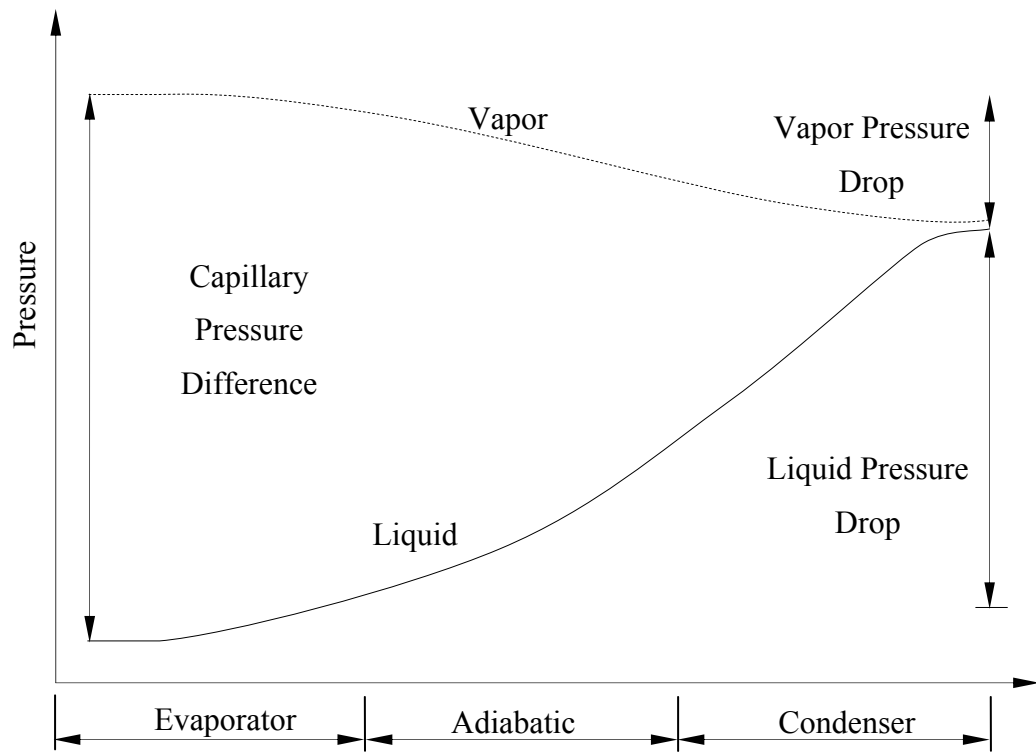


Figure 1.2: Pressure variation along a heat pipe

## **1.5 Operating Limits**

As with any other system, the performance and operation of a heat pipe is limited by various parameters. Physical phenomena that might limit heat transport in heat pipes include capillary forces, choked flow, interfacial shear and incipient boiling. The heat transfer limitations depend on the size and shape of the pipe, working fluid, wick parameters, and operating temperature. The lowest limit among these constraints defines the maximum heat transport limitation of a heat pipe at a given temperature [5].

### **1.5.1 Capillary Limit**

The difference in the capillary pressure across the liquid-vapor interfaces governs the operation of the heat pipes. This is one of the most important parameters that affect the performance and operation of a heat pipe. It is usually a major limiting factor in the working of low-temperature heat pipes. The capillary limit is encountered when the capillary pressure is not sufficient to pump the liquid back to evaporator causing the dry out of the wick of the evaporator end. The physical structure of the wick is one of the most important reasons for this limit and the type of working fluid also affects it. Once limit is encountered, any further increase in heat input may cause serious damage to the heat pipe [5].

When a heat pipe is operating in steady state, there is a continuous flow of vapor from the evaporator section to the condenser section and liquid from the condenser section to the evaporator section through the wick. These flows are possible because of the vapor pressure gradient ( $\Delta p_v$ ) and the liquid pressure gradient ( $\Delta p_l$ ) along the length

of the heat pipe (Figure 1.2). There exists a capillary pressure due to the menisci formed at the liquid-vapor interface; this capillary pressure ( $\Delta p_{cap,max}$ ) is necessary for the flow of liquid back to the evaporator. In addition, there are pressure gradients due to phase change taking place at the evaporator ( $\Delta p_{e,phase}$ ) and the condenser ( $\Delta p_{c,phase}$ ) ends and due to gravity ( $\Delta p_g$ ). The capillary limit is expressed as,

$$\Delta p_{cap,max} \geq \Delta p_l + \Delta p_v + \Delta p_{e,phase} + \Delta p_{c,phase} + \Delta p_g \quad 1.2$$

For the heat pipe to work normally, the capillary pressure should be greater than all the pressure gradients across the liquid-vapor path.

### 1.5.2 Sonic Limit

The evaporator and condenser sections of the heat pipe undergo addition and removal of mass due to the circulation of the working fluid. They act like a nozzle where vapor flows from the adiabatic section into or out of the end sections. The converging-diverging nozzle like nature of the vapor flow path imposes a choking flow condition on the vapor velocity. The velocity at a choke point cannot be greater than the local speed of sound. This is called the sonic limit and the heat transfer can now only increase by increasing the operating temperature of the heat pipe. Although, the operation of a heat pipe under such condition causes a substantial temperature drop across the heat pipe, it is not considered a serious risk [5].

### **1.5.3 Boiling Limit**

A typical cylindrical heat pipe receives heat at the evaporator end where it is transferred to the working fluid radially. When the input flux is sufficient, nucleation sites are formed inside the wick and bubbles are trapped in the wick, blocking liquid return that results in evaporator dry out [6]. As compared to other heat pipe limits, boiling limit is a radial flux constraint and not an axial flux constraint. For liquid-metal heat pipes, the boiling limit is not very common [5].

### **1.5.4 Entrainment Limit**

As liquid and vapor move in opposite directions, the vapor exerts a shearing force on the liquid at the liquid-vapor interface. If this shear force exceeds the surface tension of the liquid, liquid droplets are entrained into the vapor flow and are carried towards the condenser section. The magnitude of this shear force depends on the thermo-physical properties of the vapor and its velocity and if it becomes large enough, it causes dry out of the evaporator [3,5].

### **1.5.5 Viscous Limit**

At low temperatures or low vapor densities, the viscosity of the vapor flow may be dominant as the flow progresses towards the condenser end. If the vapor pressure in the condenser is very low then the heat transfer under such a condition is limited. This usually occurs during the startup phase of a heat pipe [5,7].

### **1.5.6 Condenser Limit**

For proper working of a heat pipe it is necessary that the heat is removed from the condenser end at the same rate as it is being added at the evaporator end. If non-condensable gases are accumulated at the condenser end, they reduce the working length of the condenser end, limiting the heat removing capacity of the condenser. This limit increases the possibility of capillary limit [5].



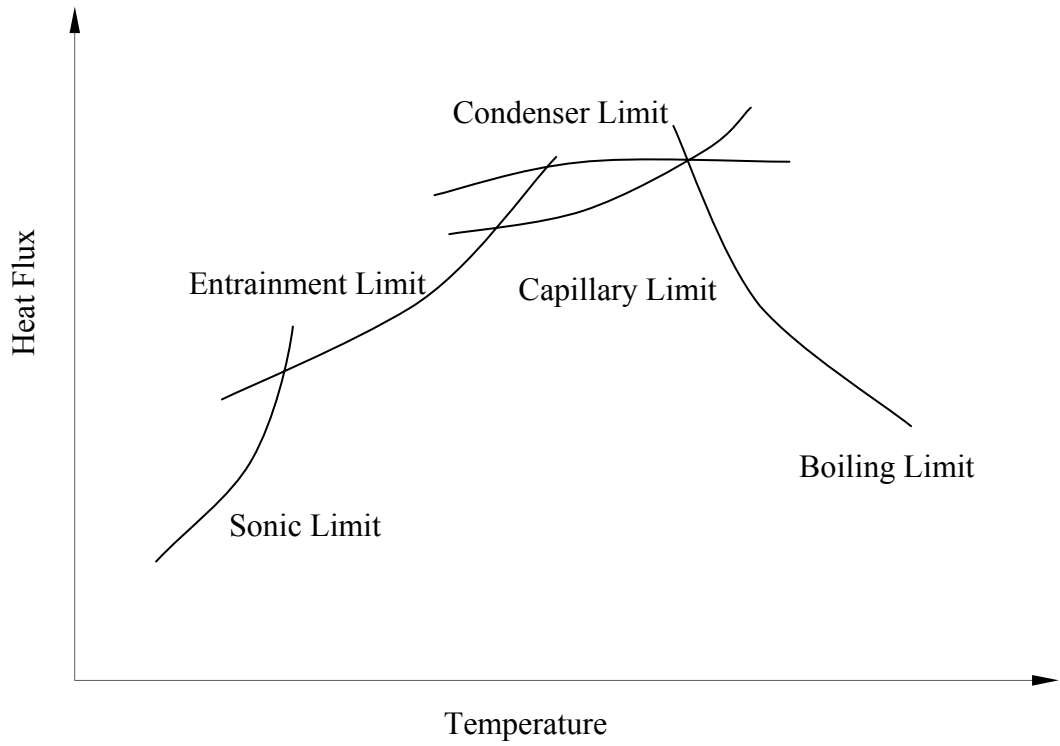


Figure 1.3: Operating limits for a heat pipe

## CHAPTER 2

### BACKGROUND

#### **2.1 Scope of Bendable Heat Pipe**

A capillary pumped heat pipe is one of the most efficient and yet very simple methods of heat transfer. A typical heat pipe is a cylindrical straight pipe which is easy to fabricate and has a low cost of production. But in practice there is seldom any space available that can accommodate a straight heat pipe. The size of a heat pipe usually depends on the heat load it is subjected to. The lack of enough space demands a heat pipe that can be flexed to fit in available pockets of space in a system. Also it allows for compact and flexible overall system design.

Typical applications of heat pipes include desktop and laptop computers, transmission and engine cooling systems in automobiles. Other electronic components like circuit boards, transformers and power supplies are also common applications [7]. The ever-reducing size of computers, electronic instruments and automobiles puts severe restrictions on the physical dimensions of heat pipes. Even when a heat pipe is not required in contorted configurations, the flexibility allows for misalignment between source and sink due to operational vibrations or oscillations.

As with the rest of the heat pipes, flexible heat pipes have received regular attention over the years and not surprisingly many of the problems were put forth by the aerospace industry. A thorough literature review is presented to summarize the previous work done in this area. Also, since the focus of this study is bent heat pipes, only portions pertaining to these types of heat pipes are covered.

## **2.2 Review**

A flexible heat pipe was developed and built by F. E. Bliss, E. G. Clark and B. Stein to analyze its operating characteristics for varying degrees of bend and under vibration in an unbent mode [8]. The purpose of this study was to design a flexible heat pipe capable of being bent or flexed during its operation allowing efficient heat transfer between an oscillating heat source and a stationary sink. The heat pipe was built using a rigid evaporator and condenser sections made from thick drawn copper tubing. A flexible adiabatic section fabricated from a seamless brass bellows connected them. A wick made of four layers of 150 mesh type 304 stainless steel screen, was held against the inside wall using a stainless steel coil spring. It was tested for bends of 0°, 45° and 90° during horizontal operation and also at inclined orientations. The authors noted that the tests for various bends demonstrated an increase in the maximum heat flux associated with wick dry out after each flexing. It was speculated that this was due to the changes in the capillary passage between the layers of screen and wall as the heat pipe was flexed.

One interesting aspect of this study was the internal fins present in the condenser section. It was noted that since the fins significantly reduced the difference between the vapor temperature and the outside temperature of the condenser wall, it had greatly

improved the operating efficiency of the heat pipe. The study concluded that the degree of bending had a minimal effect on the working of the heat pipe and a flexible heat pipe is a feasible idea.

Basiulis and Hummel investigated heat pipe techniques and their applications for electronic component cooling. The various techniques considered were heat pipes, cold plates, gas buffered heat pipes and unidirectional heat pipes. The flexible heat pipes provided relative motion between the heat source and heat sink [7]. This publication steps through the design process starting with the selection of a working fluid. The authors listed various applications for each type of heat pipes studied.

F. Edelstein designed and fabricated a variable conductance heat pipe radiator capable of passively controlling Freon-21 fluid loop temperatures under varying loads [9]. It was made from six grooved heat pipes attached to an aluminum panel. The heat pipes had a flexible section that could bend up to 90°. Tests were carried out with radiator loads up to 800 W.

Saaski and Wright described a proof of concept for a flexible cryogenic heat pipe designed for space operations [10]. This heat pipe was meant for transmitting parasitic heat and generated heat from an infrared sensor on a satellite. In many satellite systems, a U shaped configuration of heat pipes is needed. A 20 W flexible heat pipe designed for operations at 100 K was described. The axial wick structure needed to be considerably flexible to allow bending. A multiple artery structure developed by McDonnell Douglas Astronautics Corporation (MDAC) was chosen due to its considerable capacity for bending. The artery was composed of a tightly wrapped bundle of many fine tubes, each

of which functions independently as an artery to assure redundancy of fluid transport. The composite tube structure allowed for flexibility because each small tube could move independently to some degree. The evaporator and condenser were rigid sections connected by an adiabatic section made from bellows as shown in Figure 2.1. Thermal performance tests were carried out with R-21 at 293 K and methane at 100 K with the heat pipe in horizontal orientation and U shape configuration. The test results for both straight and bent mode were compared and it was concluded that there was no significant effect due to bending.

A comprehensive test program was executed to determine the physical and thermal performance of two flexible cryogenic heat pipes to provide an efficient and flexible thermal link between a detector and a space radiator by Wright et al. at Rockwell International Corp., Space Division [11]. To determine the optimum geometry and materials for the container and the wick, parametric studies were performed and the 100 – 200 K pipe was designed with methane and ethane as the working fluid, with nitrogen and oxygen for the 15 – 100 K pipe. The wick selected was a multi wrap composite, which consisted of a spirally wrapped coarse mesh screen surrounded by a fine mesh outer wrap. V-groove screw threads were machined into the evaporator and condenser whereas a braided flexible bellows made from stainless steel was used for the adiabatic section. This flexible section together with the spiral multi wrap wick demonstrated good flexibility and compatibility with methane as the working fluid. The authors concluded that overall this configuration worked well as a highly flexible link between the source and the sink and had good potential for high power transport scenarios.

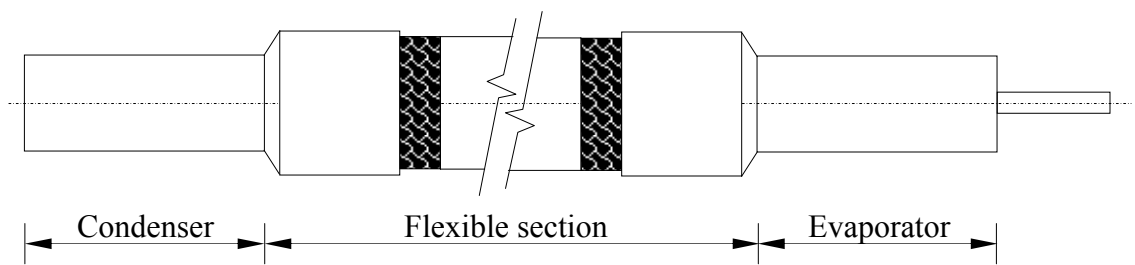


Figure 2.1: Flexible cryogenic heat pipe [10]

H. Koch, H. Kreeb and M. Perdu developed a modular axial grooved heat pipe system for an operating temperature range of 100 – 400 K intended for typical space applications [12]. Various tests were performed to evaluate the performance as a function of temperature or inclination angle, start up, operating life, working fluid and of bended heat pipes.

Munzel et al. conducted an experiment for the European Space Research and Technology that consisted of two bendable artery heat pipes which were flown aboard a rocket Centre as a part of the International Heat Pipe Experiment [13]. It consisted of two aluminum heat pipes having a length of about 90 cm with an outer diameter of 0.7cm. The wick and artery systems were made from 160 mesh stainless steel screen and ammonia was the intended working fluid. The two arteries were positioned to lie in the same diametric plane so that the pipes could be bent with no reduction in the heat transport capability. The experiment was supposed to test two heat pipes; one straight and one bent into a z-shape. The bent heat pipe was later replaced with a straight one due to priming problems.

There is growing interest in heat pipe thermal diodes and thermal switches for space applications. A thermal diode can protect electronic components from overheating during mission critical periods like pre launch operations, vehicle maneuvers and reentry into the earth's atmosphere [15]. Similarly, a thermal switch can be used for transport of heat from a source to one of several heat sinks depending on the operating conditions. Development work was undertaken for near room temperature applications of a thermal diode for spacelab by M. Groll et al. The focus of this study was to predict the transient shutdown of the thermal diode using a mathematical model and experimental results,

both of which were in good agreement. It was noted that bendability is no serious constraint for all three designs, though in the case of complex artery structures, e.g. modular artery with 4 or 5 webs, the bend radius has to be relatively large to avoid performance degradations.

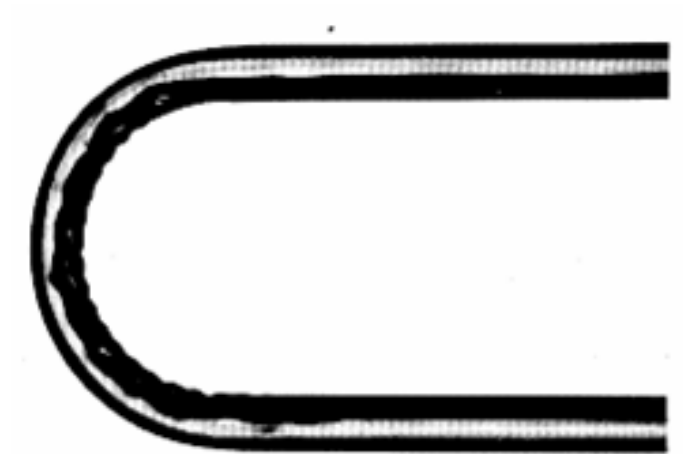
Three variable conductance heat pipes were fabricated by M. E. Peeples and L. D. Calhoun in order to investigate the effect of tight radius bends in the adiabatic section on the heat pipe performance [16]. Analytical studies were conducted to evaluate the geometry and performance requirements of candidate heat pipe designs. The heat pipes were bent in the adiabatic section to make a J or L shape with a very small bend radius. There was a probability that capillary pumping could be reduced due to deformation of internal structure in the bent area, resulting in performance degradation. Two pipes were fabricated from a thin wall stainless steel with a multi-tube central artery and a wall screen wick. Freon 21 was the working fluid. The third pipe was made of aluminum with an axially grooved wick and ammonia was used as the working fluid. All the pipes were bent using a conventional pipe bender and it was found using a radiograph image (Figure 2.2-a), that in the bent area the deformation of the artery lowered the permeability of artery, effectively reducing the heat transfer capacity of the pipe due to inadequate flow of condensate from condenser to evaporator. The corrugations in the inner bend surfaces of the heat pipe tube, and local separation of the wall wick, caused unpredictable voids and it also made it difficult to determine the exact charge of the working fluid required. In order to circumvent these problems, the heat pipes were fabricated in such a way that the heat pipe tube was bent before inserting the wick structure and also wick in the bent



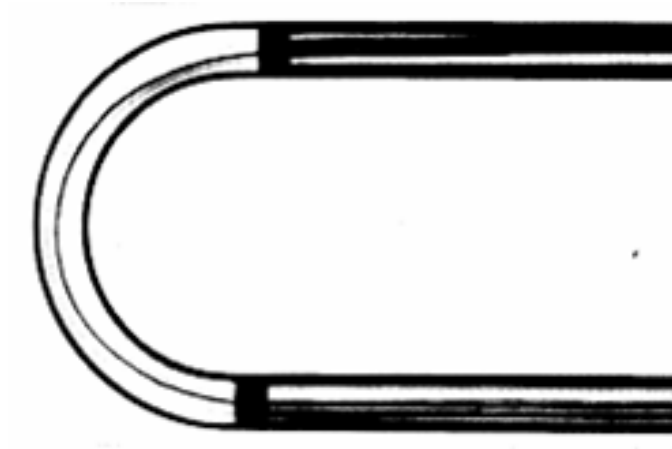
area was removed to minimize cavities caused. The radiograph in Figure 2.2-b clearly shows the improvement in the fabrication quality of the heat pipes.

A bendable gas controlled variable conductance heat pipe was developed and made entirely from stainless steel with ammonia as working fluid and a homogeneous wick as capillary system [17]. Designed by Mathieu et al., it presented an excellent potential for high performance because of its heat transport capability of 100 W through a 1 cm diameter tube. There were performance requirements to transport a minimum of 100 Wm, in zero gravity and in the presence of control gas (variable conductance) and, the heat pipe should not lose any performance when curved in U-shape with a radius of curvature of 10 cm.

Meier et al. designed a heat pipe for use in a space reactor where it was required to bend around the reactor core in two approximately 90° bends on a 180 mm radius and have design lifetime of 7 years [18]. Because of this lifetime requirement and working temperature of 1400 K, molybdenum was the material chosen for the container with sodium as the compatible working fluid. It employed a non-concentric screen annular sintered wick. Before fabrication of the heat pipe, a series of bending experiments were carried out to finalize proper bending procedure and temperature so that no cracks or breaks were generated. A bending test when conducted on an unsupported wick at 353 K that showed the compression side of the bent wick was severely buckled. The buckles caused a reduction of 17% in the vapor flow area and an increase in pore size was also observed at the sharp corners, which would lead to significant reduction in performance. The conclusion was that bending on an unsupported wick would not produce satisfactory



(a) Conventional wick structure



(b) Modified wick structure

Figure 2.2: Heat pipe bends [16]

results. Another bending test with a steel tube mandrel to prevent buckling of the wick was performed, but large tears were generated on the tension side. Finally, a stainless steel heat pipe was completely filled with sodium at 1070 K. When the pipe was bent at 365 K (highest attainable temperature to provide required ductility for molybdenum but still low enough to keep the sodium mandrel in solid state), the results were successful with no tears in the tension side and very little buckling on the compression side with a very minute change in porosity.

D. M. Ernst in a report to NASA JPL for a heat pipe heat rejection system and demonstration model for the nuclear electric propulsion (NEP) spacecraft evaluated and redesigned prototype heat pipe components, and then further fabricated and tested them [19]. The evaluation demonstrated the validity of several complicated geometries and wick structures including bends in the heat pipe. Two types of heat pipes with 30° bends at each end of the adiabatic section were tested for several wick designs. A heat pipe with four wraps of 325 mesh wick was found as a good design with respect to performance and mass. It transferred 3800 W over a temperature drop of 117.9°C.

Merrigan et al. demonstrated in a 1984 publication that flexible sodium/stainless steel heat pipes can be fabricated and operated at temperatures up to 1100 K with an axial heat flux of 1950 W/cm<sup>2</sup> [20]. The relevance of this publication to the work in this thesis is the study of the effect of bend angle on the heat pipe temperature distribution. There was a requirement for high power, flexible heat pipe capable of bending through angles of up to 180° and working temperatures of both cold and high temperatures. Therefore, as a demonstration flexible heat pipe employing sodium as working fluid and using stainless steel wick and tube was fabricated and tested. “This device has been flexed repeatedly

through angles of  $180^\circ$ , both at room temperature with the sodium working fluid frozen and at temperatures to 1000 K while radiating heat to a room temperature environment". A 100 mesh stainless steel screen wrapped in 3 layers in alternating directions was used to make the wick. The adiabatic section was made from a standard high vacuum flexible line section. The heat pipe was tested at a temperature of 1000 K in the horizontal orientation. Then the condenser end was elevated upward through an arc up to a bend of  $180^\circ$  in the vertical plane. The heat pipe operation was visually verified during this bending experiment.

Later to determine the effect of bending on the performance, the heat pipe was operated in the horizontal position and tested in three positions of  $0^\circ$ ,  $90^\circ$  and  $180^\circ$ . During testing axial temperatures were recorded against input power to the heat pipe. Figure 2.3 shows the results of these experiments. While the data indicates a significant increase in axial temperature drop, there was no loss of heat pipe function due to bending even under test loads up to  $1950 \text{ W/cm}^2$ . Repeated startup tests were conducted from below the freezing point of sodium (working fluid) with no apparent effect due to bending. The authors concluded that this heat pipe could be bent up to  $180^\circ$  even when under load.

R. M. Shaubach and N. J. Gernert worked on a project to develop and demonstrate flexible heat pipes for transport of heat from stationary to translating sections of spacecraft [21]. Previous flexible heat pipes concepts employed flexible bellows with a screen wick that allowed bending. Such heat pipes are typically low power devices due to the high flow resistance of the screen wick structure.

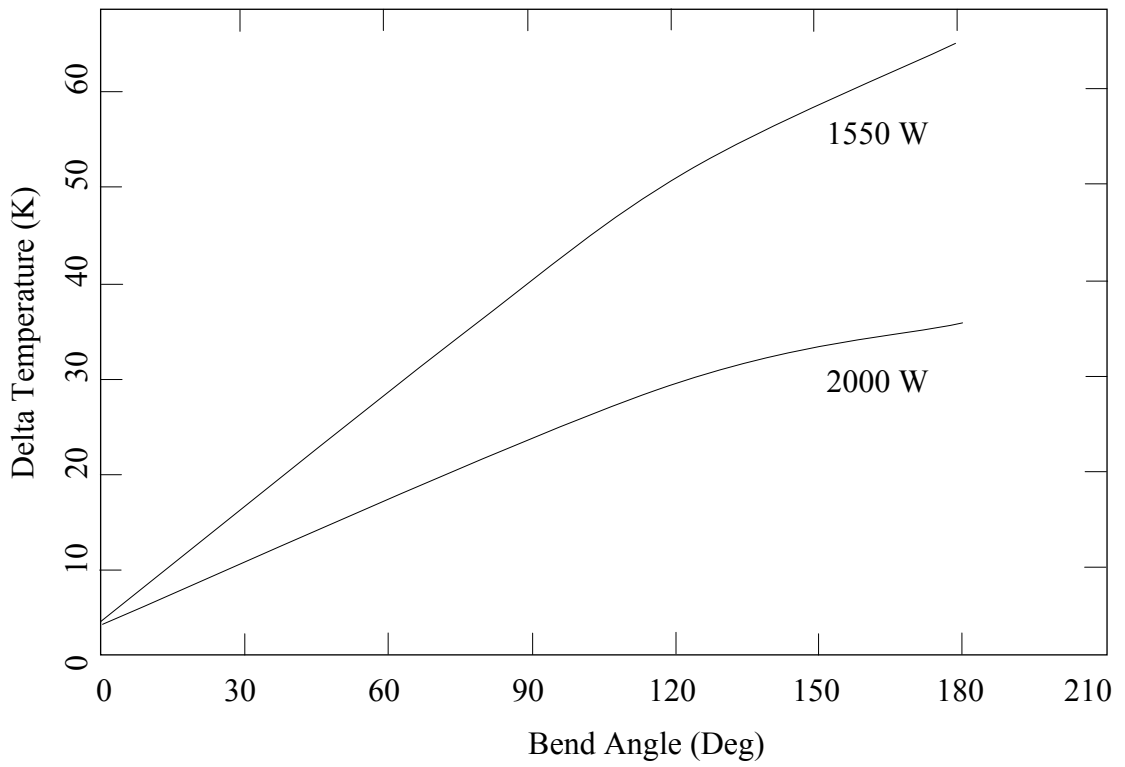


Figure 2.3:  $\Delta T$  between evaporator exit and end of condenser versus bend angle of heat pipe [26]

Flexible heat pipes with high power capacity are made possible by using flexible screen wicks, which can be made from several different alloys and mesh sizes. These flexible screen wicks are integrated with high performance circumferential distribution wicks in an envelope that is flexible in the adiabatic section. Three heat pipes identical in all respects except that the wicks were built using screens, powder metal and spiral “V” grooves were tested. A computer program developed at Thermacore Inc. was used to estimate the performance of each heat pipe; these calculations showed that for the same power the lowest  $\Delta T$  was predicted for the heat pipe with the microgrooves followed by the sintered powder metal and the wrap screen, whereas the sintered powder metal wick had the highest predicted heat transport capability followed by the wrapped screen wick and then the microgrooves. The microgrooves design was dropped due to difficulties faced in fabrication. The better performance obtained with sintered powder wicks as compared to the screen wicks was attributed to the bonding of wick structure to the heat pipe wall. A screen wick has empty clearances between the layers and gap between the screen and the heat pipe wall. These clearances are filled with a comparatively low thermal conductivity working fluid that increases the thermal resistance of the heat pipe and consequently causes increase in the temperature drop. This difference causes an increase in performance by a factor of 3 in sintered powder wicks.

Hwangbo and Joost developed a variable conductance heat pipe with a flexible joint for temperature control of high power electronics using a space radiator [23]. The design requirements for this pipe mandated that a 0.5” O.D. heat pipe should be able to sustain loads up to 3500 W-inch at a vapor temperature of 80 °F. The design consisted of a sintered screen axial slab made by a 20 mesh screen sandwiched between two 100

meshscreens. This benefited from the increased permeability due to the 20 mesh screen as well as better capillary pumping by the 100 mesh screens. An analytical model was developed and several operating conditions were simulated to demonstrate the feasibility of this design with ammonia as working fluid.

G. P. Peterson [24] developed a bellows heat pipe using analytical and computer modeling for cooling of electronic components. This study first developed an analytical model that was used to build a computer model. Since the design of the heat pipe was governed by the evaporator temperature i.e. temperature of electronic component, the source heat flux was not specified in the model. The results from the computer model were benchmarked against previous work in this field and were found to agree with the results obtained by others. This computer model was then used for designing and optimizing a bellows heat pipe, which was designed to maintain the heat source at a constant temperature of 40°C. It is noted that this heat pipe was capable of transporting 45 W with a thermal resistance of 0.47°C/W.

A flexible loop heat pipe cold plate was developed by N. J. Gernert and J. Brown [28], which was very similar to the work done earlier by Gernert et al. [26]. The major difference is that this prototype operates in any orientation. It sustained a heat load of 45 W over a temperature drop of 20 °C.

The Advanced Camera for Surveys (ACS) is an instrument containing two CCD cameras. It operates at temperatures below -80 °C. The camera was cooled by using two thermo-electric coolers, which transported the heat from the cameras to heat pipes, which in turn transported it to the sink. The heat pipes were chosen since they are frequently

used in space applications for passive heat transport to remotely and awkwardly located radiator panels. Since the location and alignment of the CCDs were important, the heat pipes were designed with a flexible section to minimize the thermal induced structural loads. This work by R. B. Schweickart and M. M. Buchko [32] discussed the design and testing of these heat pipes. The flexible heat pipes used ammonia as working fluid and a rolled screen mesh wick supported by screen mesh web. Both the evaporator and condenser were 316L stainless steel and the flexible section was made from Swagelok® flexible stainless steel hose. As the flexible sections of the heat pipes were pre-formed after the wicks were inserted, additional bending of the flexible section posed little risk of wick damage. Thermal performance testing showed that both pipes exceeded their minimum required heat transport capacity by a wide margin.

In an effort to build a flexible heat pipe that can provide for bending, twisting, oscillating and deforming that is typically required in compact electronics, Lu Shaoning and Li His-Shang designed and built prototypes of a mini flexible heat pipe with a vacuum grade transparent plastic tube [2]. The heat pipes were small in diameter, typically few millimeters, so as to accommodate mobile computers. New wick structures were designed to make internal two-phase flow visible while providing the required capillary pumping action. The evaporator and condenser of the heat pipes were made of brass tubes and a transparent polyurethane tube was used for the flexible adiabatic transport section. Transparent wick structures were built from copper wire spring with a spring-braid wick and helical mesh stripe. This work however only discussed results from spring wick heat pipe that made good contact with the heat pipe container and flexibility



was maintained in any bent position. The spring was made from copper wire and water was used as working fluid.

Ultra-high-molecular-weight (UHMW) film wicks and formed UHMW wicks with Kapton and aluminized Mylar containers were used to design, fabricate and test flexible heat pipes by Glass et al. [33]. The heat pipes used methanol as the working fluid and tests were carried out at steady state. The authors note “The successful fabrication and operation of the heat pipe demonstrated that flexible polymeric heat pipes are feasible. From preliminary design studies, it appears that the design of a wick such that capillary and boiling limits are satisfied is the primary challenge”.

The following references are given for the reader interested in further studies.

Test results for lifetests of heat pipes used in a telecommunications satellite are discussed with the test setup by W. D. Muenzel in a report for ESA [14]. Four bendable artery heat pipes 7 mm in diameter were subjected to lifetests under a variety of operating conditions, both stationary and accelerated as well as under thermal shocks.

Ernst and Eastman studied designs for liquid metal heat pipes for space and terrestrial applications for high temperature heat recovery [22]. The design criterion and several wick designs like sintered powder wick/arteries, sintered axial grooves and flexible screen arteries were discussed.

R. S. Bhatti and S. Vanoost [25] considered A95 stainless steel heat pipes with ammonia as working fluid for all possible cases of space applications. Different bend configurations and lengths were also included in the study.

A flexible heat pipe cold plate technology was developed by Gernert et al. for aircraft thermal control [26]. Four such heat pipes were built for a variety of difficult aircraft cooling situations. In each case, a cold plate transferred the source heat to the most convenient heat sink by an integrally connected flexible heat pipe. This permitted relative motion between the electronics package to be cooled and the heat sink and it also allowed cooling system access in awkward places.

A method was suggested by Gus'kov et al. for calculating the thermal resistance and constraints on the load for an arterial flexible heat pipe working in cryogenic and low temperature modes [27]. It permitted prediction of the heat pipe operation with various working fluids and different design variations; one such result for propylene heat pipe was presented.

A report of joint activities of various Russian organizations aimed at the development of a flexible heat pipe and its modified version intended for thermal management of spacecraft instrumentation was presented by Zelenov et al [29]. A flexible heat pipe increased reliability of units moving, folding and opening in space in addition to a reduction in power consumption of the thermal control system. Different heat pipes were developed as an outcome of experimental and theoretical studies of various configurations of the evaporator, condenser and adiabatic zones. It was shown that the principal performance characteristics of these pipes were comparable to other flexible heat pipes' performance.

Quasi steady state operating characteristics of a flexible copper-water heat pipe were obtained experimentally by investigating its thermal performance under varying acceleration loading by S. K. Thomas and K. L. Yerkes [30,31].

Ozaki et al. designed a bent aluminum looped heat pipe as a part of a graphite faceskin panel on a deployable radiator panel [34].

A summary of the literature reviewed is presented in Table 2.1 and Table 2.2.

Table 2.1: Summary of published work on flexible heat pipes

Reference	Wick Type	Working Fluid	Flexible/Bends	Load	Operating Temperature
F. Edelstein [9]	Grooved	–	Up to 90	800 W	–
E. W. Saaski and J. P. Wright [10]	Tightly wrapped fine screen	Methane	–	20 W	100 K
		R-21	–	20 W	293 K
J. P. Wright, P. J. Brennan and C. R. McCreight [11]	Spiral coarse mesh screen encapsulated by fine mesh outer wrap	Methane, ethane	–	110 W	100-200 K
W. D. Muenzel, C. J. Savage, A. Accensi and B. G. M. Aalders [13]	160 mesh stainless steel screen	Ammonia	Z shaped	30 W	303 K
M. E. Peeples, L. D. Calhoun [16]	Multi-tube central artery, wall screen wick	Freon-21	U Bend	20 W	293 K
	Axial grooves	Ammonia	U Bend	20 W	293 K
J. P. Mathieu, B. Moschetti and C. J. Savage [17]	Homogeneous wick	Ammonia	U Bend	100 W.m	293 K
K. L. Meier, H. E. Martinez and J. E. Runyan [18]	Non-concentric screen annular sintered wick	Sodium	Two 90° bends	15000 W	1400 K
D. M. Ernst [19]	325 mesh stainless steel	Sodium	Two 30° bends	3800 W	923 K
M. A. Merrigan, E. S. Keddy, J. T. Sena and M. G. Elder [20]	Stainless steel wick	Sodium	90°, 180°	1950 W/cm <sup>2</sup> axial flux	1000 K

Table 2.2: Summary of published work on flexible heat pipes

Reference	Wick Type	Working Fluid	Flexible/Bends	Load	Operating Temperature
R. M. Shaubach and N. J. Gernert [21]	Spiral grooves	Acetone	Flexible	135 W	333 K
	Screen	Acetone	Flexible	690 W	333 K
	Powder metal	Acetone	Flexible	2350 W	333 K
H. A. N. Hwangbo and T. E. Joost [23]	Sintered screen axial slab	Ammonia	–	3500 W-in	300 K
G. P. Peterson [24]	5 layer 100 mesh stainless steel screen	Ammonia	Flexible	45 W	313 K
N. J. Gernert and J. Brown [28]	Porous polymer	Methanol	Flexible loop heat pipe	45 W	$\Delta T$ of 20 K
R. B. Schweickart and M. M. Buchko [32]	Rolled screen mesh	Ammonia	Flexibility required for misalignment	30 W	249 – 273 K
				20 W	249 K
				30 W	273 K
Shaoning Lu and His-Shang Li [2]	Copper spring	Water	Flexible	–	–

## CHAPTER 3

### FACTORS AFFECTING DESIGN AND PERFORMANCE

#### **3.1 Introduction**

As described before, the basic components of a heat pipe are the working fluid, the container and the capillary structure. During the construction of a heat pipe a number of factors control the type of materials that can be used. Also, it is obvious that there will be some conflicting combinations that will not work when used in a heat pipe [3].

#### **3.2 Working Fluid**

Every heat pipe is designed for a particular operating temperature range. The selection of the working fluid mainly depends on this range of temperatures. Some of the commonly used working fluids in AuTherMML are listed in Table 3.1 along with their related thermo physical properties and useful ranges. The useful range of a working fluid extends from the point where the saturation pressure is greater than 0.1 atm and less than 20 atm [5].

Within the operating temperature range, a variety of possible fluids can be used. In order to determine the best working fluid, a number of characteristics must be examined. The main characteristics are discussed in following pages [3].

Table 3.1: Thermo physical properties of working fluids used at AuTherMML [3]

<b>Working Fluid</b>	<b>Melting Point, K at 1 atm</b>	<b>Boiling Point, K at 1 atm</b>	<b>Useful Range, K</b>
Water	273.1	373.1	303 – 473
Methanol	175.1	337.8	283 – 403
R134a	172.0	246.4	208 – 343

### **3.2.1 Compatibility with Wick and Container**

Chemical compatibility of the heat pipe container metal and the working fluid is important. The working fluid and the container might work as a galvanic cell in tandem with other parts of the heat pipe. Any such reaction may generate non-condensable gases degrading the overall performance of the heat pipe [3,5].

### **3.2.2 Thermal Stability**

At working temperatures that are typically higher than room temperatures, the container metal may act as a catalyst in decomposition of the working fluid. Some organic fluids break down into different compounds necessitating the need to keep the film temperature below certain temperatures [3,5]. This is not a problem for inorganic fluids.

### **3.2.3 Wetting of Wick and Container**

Any fluid can be used in a conventional heat pipe provided it has good wetting characteristics with the wick and container wall material. The capillary pressure generated in the wick is subject to wettability of the fluid with the wick structure. Also, the superheat required to initiate boiling can be increased by good wetting. When a fluid does not have good wetting characteristic, it can be improved by surface treatments. To improve wetting characteristics, the copper containers were oxidized during fabrication of the heat pipes used in this research [36].



### **3.2.4 High Latent Heat and Thermal Conductivity**

The heat transport through the heat pipe is a direct function of the latent heat of the working fluid. The performance of the heat pipe is directly proportional to the latent heat. Also, a higher latent heat allows for good heat transfer at lower temperatures. Thermal conductivity of the working fluid is of major concern at the condenser end. The condensed liquid has a comparatively lower conductivity and increased thermal resistance.

### **3.3 Container**

The function of the container is to provide a hermetically sealed enclosure for the working fluid. It is necessary to avoid any diffusion of air into the heat pipe. The type of the heat pipe and its application decides the shape of the container. The desired characteristics are, wick type & material and working fluid compatibility, strength to weight ratio, thermal conductivity, ease of machining and wettability.

Degradation of the container material leads to chemical reaction with the working fluid. In addition to generating non-condensables, these reactions tend to corrode the internal surfaces of the container, increasing the thermal resistance and also reducing the surface tension and wetting angle. Such chemical reactions also cause pitting of the inside wall that promotes formation of enhanced nucleation sites which leads to premature boiling of the working fluid [6].

Apart from the chemical compatibility, a heat pipe container is necessarily a pressure vessel and hence careful attention is required for selection of material grade.

Also, it is required to make a leak proof seal and structural integrity must be ensured for the entire working pressure range of the heat pipe [6].

### **3.4 Capillary Structure**

The capillary wick structure in a heat pipe provides a mechanism by which the working fluid returns to the evaporator and evenly distributes the liquid film over the evaporator surface on the inside. Since the capillary force is of premier importance to sustain the working of heat pipes, the wick pores must be small. Smaller pores provide for greater capillary pumping pressure but also increase resistance to liquid flow through the wick, thereby increasing the overall liquid pressure drop across the wick. The wick covers the entire inner surface of the heat pipe and hence, the heat must travel through heat pipe container walls and wick to evaporate the liquid. The radial temperature drop due to this is dependent on the thickness of the wick and its thermal conductivity. For a higher thermal conductivity the wick must have lower porosity but this conflicts with the need for lower liquid pressure gradient [3,5,6].

The wick structures are broadly classified into two categories as discussed in following sections.

#### **3.4.1 Homogeneous Wicks**

Homogeneous wicks are constructed from a single material that has a uniform cross section. The common materials used include metal screens, sintered metal felts, sintered metal powders and axially grooved wicks (Figure 3.1). Each type of wick made

from these materials has its own advantages and limitations, and a detailed discussion on this topic is beyond the scope of this work.

### **3.4.2 Composite Wicks**

A composite wicking structure is built using two or more materials described in section 3.4.1 thus taking advantage of their respective strengths. A composite wick typically handles the two main functions of capillary pumping and liquid transport in different sections of the wick. A typical example is a screen wick covering the axially grooved wick structure as shown in Figure 3.2.

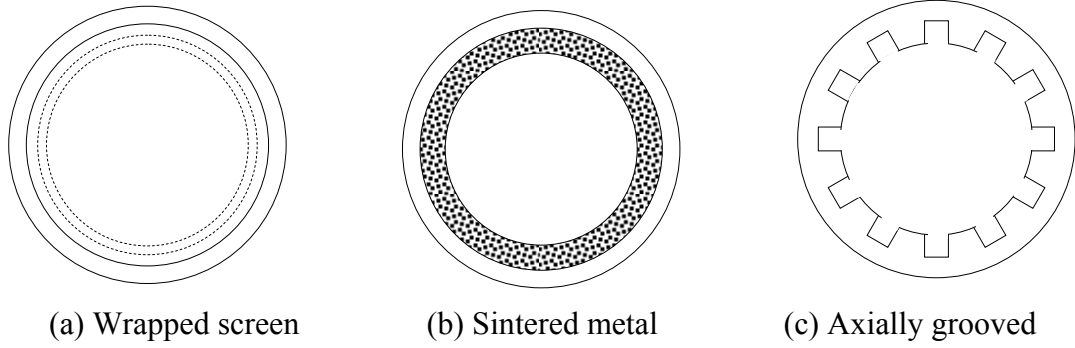


Figure 3.1: Homogeneous wicks

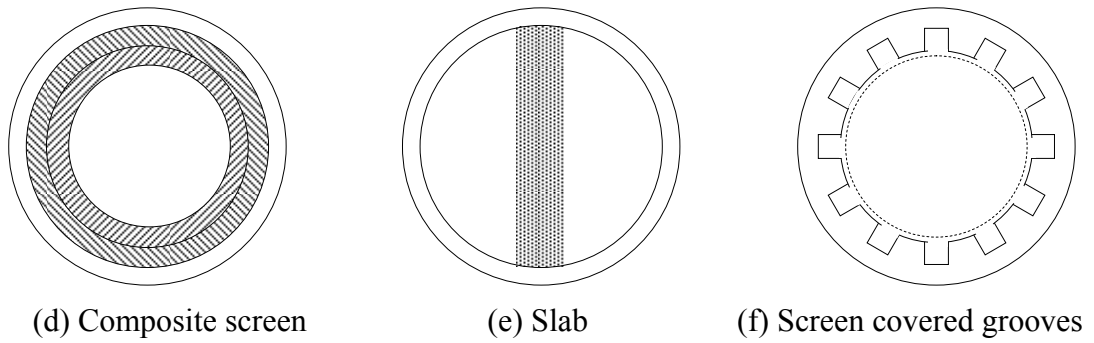


Figure 3.2: Composite wicks

## CHAPTER 4

### TESTING AND PERFORMANCE EVALUATION

#### 4.1 Performance Evaluation

The performance evaluation of a heat pipe is a necessary step that has to be often repeated in order to characterize many factors such as working temperature and maximum heat transfer capacity (as described in Section 1.5). The heat pipe performance is usually defined in terms of the temperature drop across the working length of heat pipe at a given power level. Lowering the temperature drop between the evaporator and condenser is the goal of a heat pipe. The electrical circuit analogy can be easily used to explain this.

The heat pipe is like an electrical conductor. The heat flowing (current) across is reduced by losses (resistance - mainly frictional pressure drop) causing a temperature drop (voltage drop) across evaporator-condenser circuit. In this way the heat pipe performance is quantified for a lower resistance or a higher conductance value. If  $Q$  is the heat load on the system and  $\Delta T$  is the temperature drop across the heat pipe then the thermal resistance  $R$  is given by,

$$R = \frac{\Delta T}{Q} \quad 4.1$$

The relation shown in the above equation is a derivative of the classic conduction equation,

$$Q = \frac{K \cdot A \cdot \Delta T}{L} \quad 4.2$$

It is clear that resistance  $R$  is defined as,

$$R = \frac{L}{K \cdot A} \quad 4.3$$

During this work the heat pipe performance was measured in terms of Conductance, which is a reciprocal quantity of Resistance as defined above. In a way this measured quantity is similar to material thermal conductivity.

#### **4.1.1 Testing Procedure**

The testing procedure devised was based on the same principle. The heat pipe was subjected to a heat load across its working length. The evaporator is connected to a heat source, typically a heater block. This heater block was powered by cartridge heaters whose power input was controlled by a regulated power supply. Heat was extracted from the condenser end by a water circulator that has a supply of constant temperature water from a chiller. The setup is shown in Figure 4.1. A record of temperatures at different power levels was kept using two thermocouples mounted on the evaporator and condenser end as indicated.

The chiller was started first and allowed to attain a steady 20°C bath temperature. The heat pipe was also allowed to attain a steady state temperature of 20°C to assure a common starting point for all the tests performed. The power was then supplied to the heater in uniform increments and the heat pipe temperatures were observed until steady

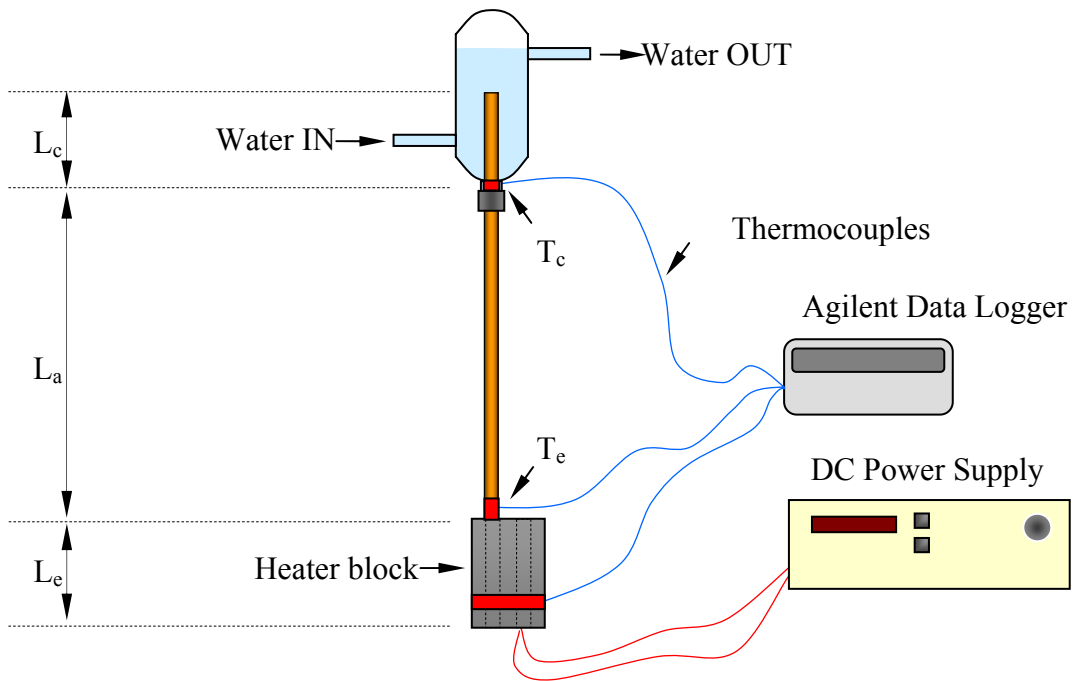


Figure 4.1: Heat pipe test setup for conductance measurement

state was reached and maintained for at least fifteen minutes. The ambient temperature was maintained between 20-23°C to keep the parasitic losses at approximately the same levels for all tests. A sample graph is shown in Figure 4.2. At this point, a note of all the readings was taken and used for further analysis.

#### **4.1.2 Conductance**

The temperatures of the evaporator and condenser at steady state were recorded and a temperature gradient was calculated. With the known power input, the heat pipe's performance at that load was measured in terms of conductance  $G$  as defined below,

$$G = \frac{Q}{\Delta T} = \frac{K \cdot A}{L} \quad 4.4$$

The unit of conductance is W/°C or W/K. Thus for a heat pipe with a steady state heat load of 12W and  $\Delta T$  of 0.72°C (Figure 4.2) the conductance was 16.8 W/K. The heat pipe performance was then plotted as a graph of conductance against input power. A sample graph is shown in Figure 4.3.

#### **4.2 Copper Equivalence**

As mentioned above, this measurement technique converts the heat pipe into a quasi solid material. As shown in Equation 4.4, the thermal conductivity is expressed in the form of thermal conductance. However, unlike a solid, the heat pipe's conductivity depends on many factors due to the complexity of two phase heat transfer and flow that occurs inside the heat pipe as described in Section 1.4. The location of temperature measurement chosen during testing is a major factor influencing the thermal conductivity reported.



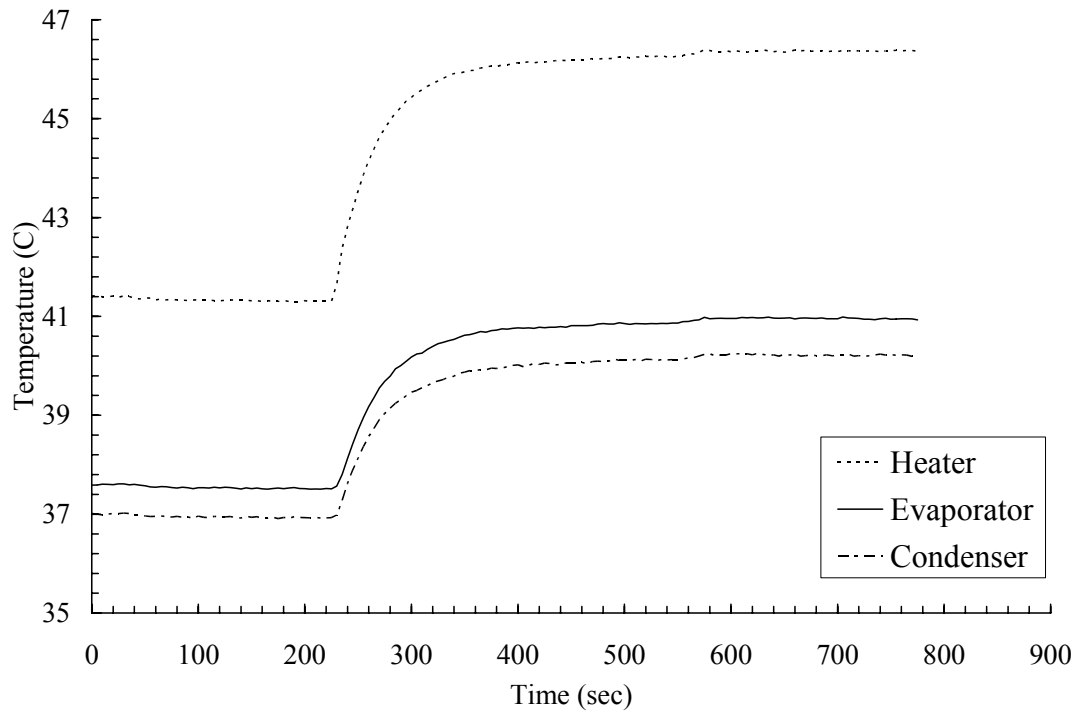


Figure 4.2: Steady state temperature curves during testing

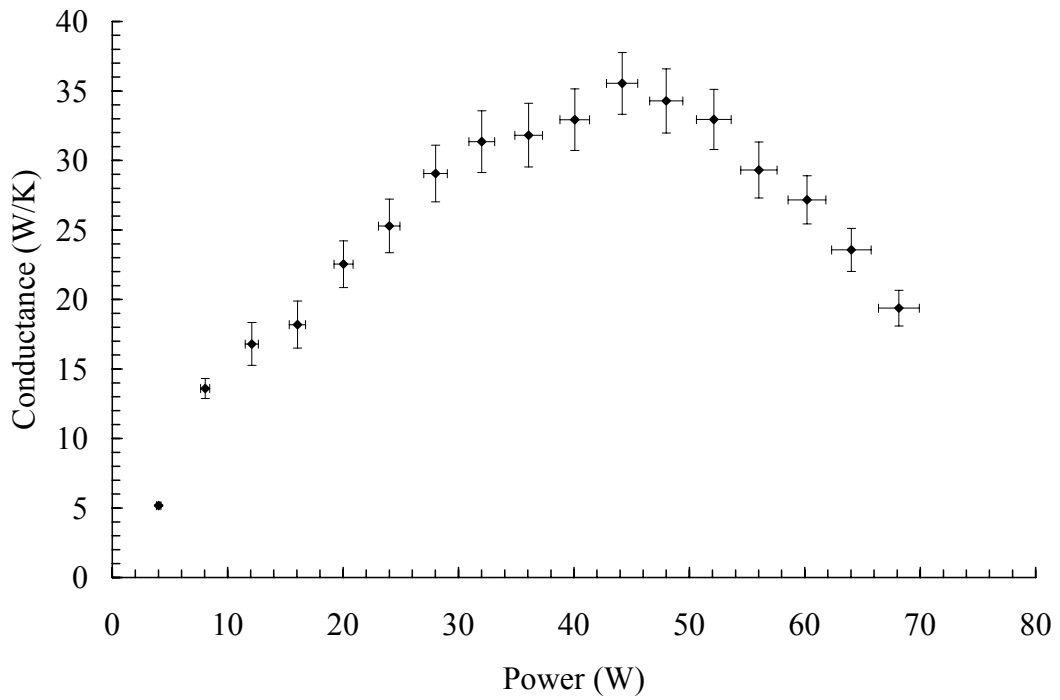


Figure 4.3: Heat pipe conductance against input power applied

### 4.2.1 Measurement Errors and Losses

The measurement of thermal conductance is complicated by a number of other parameters not related to the physical state of the material. The nature of the test setup affects the data reduction due to various losses and leakages of the applied heat load. Thermal contact resistance is one of the major causes of heat loss in a test setup. It depends on factors such as pressure, surface roughness and hardness etc [35]. Contact resistance comes into importance at two points in the setup, the contact between electrical heaters and heater block and the contact resistance between heater block and the test subject.

The heat is transmitted across the interfacial contacts by conduction, through the air trapped in the gaps and via radiation [35]. Thermal resistance is caused by oxidation of contacting surfaces, gaps between interfacial surfaces, and radiation heat transfer between microscopic voids due to surface roughness. Additionally, heat loss through the insulation also adds to the parasitic losses in the system. The heat supplied by the heaters,  $Q$ , is split into,

- $Q_{\text{Heater block}}$  = heat dissipated by the heater block
- $Q_{\text{Insulation}}$  = heat loss through the insulation
- $Q_{\text{Adiabatic}}$  = heat loss through the adiabatic section of the heat pipe
- $Q_{\text{Condenser}}$  = heat rejected to circulating water

$$Q = Q_{\text{Heater block}} + Q_{\text{Insulation}} + Q_{\text{Adiabatic}} + Q_{\text{Condenser}} \quad 4.5$$

Assuming that the condenser rejects all the heat to circulating water,  $Q_{\text{Condenser}}$  is the actual heat transferred through the heat pipe and all others are lost through the system. As shown in Equation 4.5, since all of these are included in the evaluation of heat pipe conductance (Equation 4.4), it introduces a corresponding error in recording of data.

The other factors that indirectly contribute to heat loss include errors in the measurement of input power and recorded temperatures. Also the variation in the temperature of cooling water is unpredictable. The changes in surrounding conditions increase or decrease the heat loss to the environment.

It is obvious that a number of such systematic errors are present in testing and that any reporting of thermal conductance of the heat pipe is subjective to the viewpoint of the person conducting test. Under such conditions, there is a possibility of disagreement in the results and trends for tests conducted at different periods of time on the same test subject using the same test setup. All such factors can be termed as a ‘system bias’ towards the reliability of the test results. The literature is full of measurements and performance estimates reported by different sources, and they are affected by the same problem i.e. it is difficult to gauge the system bias and compare the results of tests conducted by separate entities. The absence of any standards based testing method makes it impossible to evaluate all literature on a common basis.

#### **4.2.2 Parasitic Losses**

The data obtained during testing includes heat loss as described in the previous section. To estimate parasitic losses during each test, a separate test was carried out on each heat pipe where the water circulator was removed and the condenser end of heat

pipe was insulated. Then, the heat input was arranged similar to normal testing conditions. Since there is no cooling, once the heat pipe comes to steady state the power input corresponding to the evaporator temperature is the parasitic loss at that particular temperature. In the absence of cooling, to protect the heat pipe from damage, the applied heat loads during such tests were typically very low. The power losses for higher range of evaporator temperature were then extrapolated from this data. It was observed that this method resulted in a linear relation between the parasitic heat loss and the evaporator temperature. A typical plot is shown in Figure 4.5.

After each test, the power applied for heat load was corrected using this relation for parasitic loss. A graph of power vs. conductance (Figure 4.6) showing the original and corrected conductance values is included to demonstrate the concept. All similar plots always show only corrected conductance values thereby excluding parasitic losses unless otherwise specified.

### **4.2.3 Benchmarks**

As mentioned in section 1.1, efficient heat removal is critical to many devices and the steady increase in energy density means that solid metal conductors can no longer be used to transfer the high amount of heat flux produced. However heat pipes can be compared with the high thermal conductivity metals like Copper (401 W/m.K),

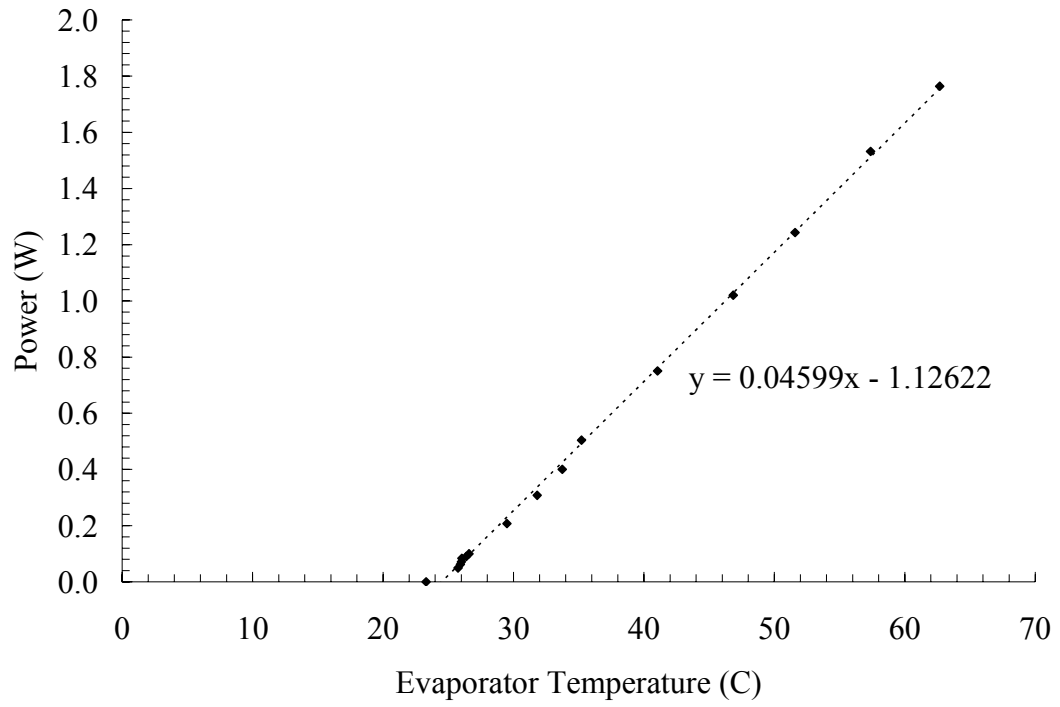


Figure 4.4: Estimation of parasitic losses

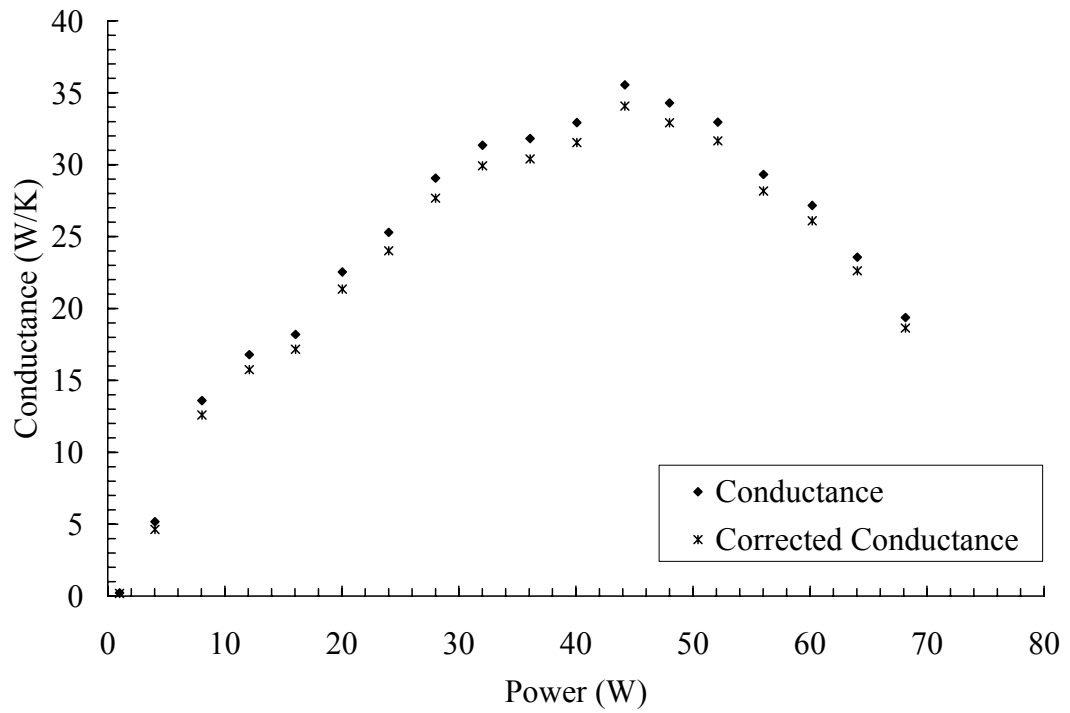


Figure 4.5: Conductance corrected to account for parasitic losses

Silver (429 W/m.K) and Aluminum (237 W/m.K). These well-established values provide an easy way of benchmarking any test setup that measures thermal conductivity by verifying these material conductivities. Since all the heat pipes used for this project were made of copper, use of copper as a benchmark was a natural choice. Oxygen free copper was used in all the tests and the dimensions were chosen to match that of the heat pipe.

#### **4.2.4 Concept of Copper Equivalence**

There is a need for a quick and easy method to record performance characteristics of heat pipes using parameters that are reproducible. As shown in Section 4.2.1 the measurement of thermal conductivity is a fairly complicated process which involves many parameters that can influence the data and ultimately cause deviation in the final result.

A simple approach is adopted to tackle this problem. Once a heat pipe is ready for testing and a corresponding test setup is designed, a solid copper rod of known thermal conductivity of the same dimensions as the heat pipe is prepared. This copper rod is now the benchmark for all tests done on that heat pipe. The copper rod is then tested in the same setup and a dataset of its conductance is recorded. Since the copper rod is of the same physical shape and size, once it is replaced with the heat pipe, everything remains the same in the test setup including the insulating material. This means that both the test subjects undergo performance testing under exactly similar conditions.

The data with such test for two completely different test objects now includes a common system bias, which covers all parasitic losses and contact resistances. The

conductance of the heat pipe is usually very high as compared to that of the copper rod, therefore the copper equivalence  $CE$  is defined as,

$$CE = \frac{G_{heat\ pipe}}{G_{copper\ rod}} \quad 4.6$$

Once a  $CE$  value is recorded for a heat pipe, it effectively neutralizes the discrepancies due to system bias and since a standard copper alloy is used for evaluation, it is used to compare performance of heat pipes from different sources. The standard benchmark also enables a comparison between different types of heat pipes which otherwise cannot be directly matched due to the differences in physical and operational characteristics.

#### **4.2.5 Why Copper Equivalence Works?**

The vast amount of past work on heat pipes shows that there is a tendency to study performance of heat pipes in terms of its heat transfer limits and the temperature and pressure profiles along its length. Although this data is important, for most applications it is imperative to explore all available heat pipe variations. A data pertaining to heat transfer limits, pressure and temperature profiles can do little in providing a common ground for comparison. Theoretical models, both analytical and numerical are complicated and time consuming to develop. These models typically require a lot of assumptions to allow a solution and hence may not be directly comparable. This is where copper equivalence greatly helps because of its straightforward application and procedure. By comparing results with a standard copper rod on the same test setup this

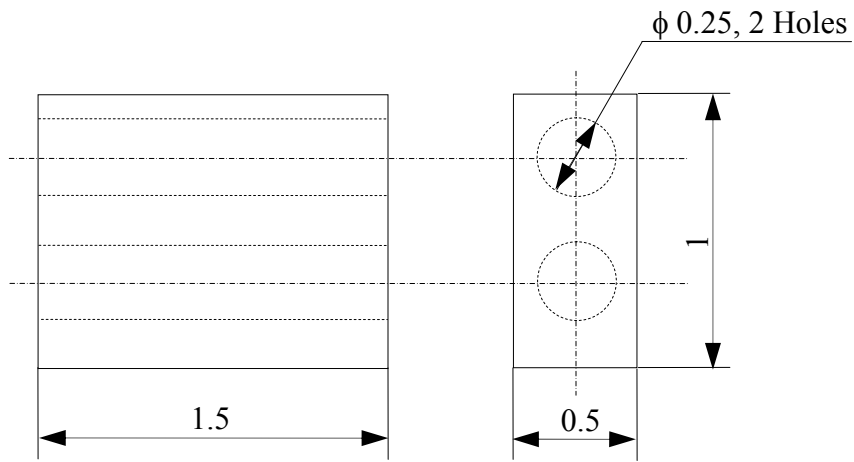
method effectively eliminates a large number of unknowns (Equation 4.5), which are difficult to evaluate due to the complexity of the various modes of heat transfer involved.

#### **4.2.6 Application**

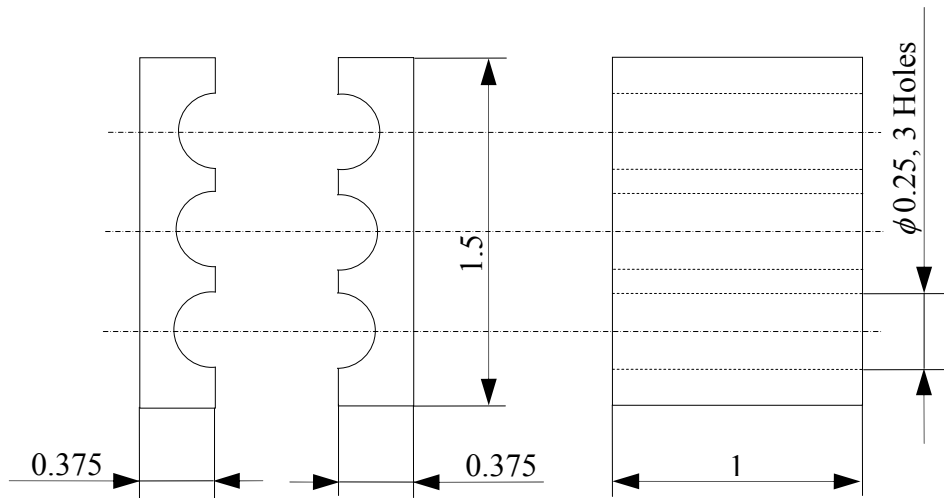
The application of copper equivalence was advantageous during the testing phase of this thesis. The first test setup, shown in Figure 4.1, was later modified and a new heater block was designed that used two heaters on either side of the heat pipe. It used a split design and allowed minor variation in pipe diameter, which also helped reduce the contact resistances (Section 4.2.1) as there was a tighter integration between heaters, heater block and the heat pipe. Both heater blocks are shown in Figure 4.6. But it was clear that this changed the parasitic losses associated with the setup and hence it was not possible to directly compare the results obtained with different heat pipes. Thus the copper equivalence was really useful for studying the results described in this thesis.

A comparative study of copper 101 rod on both heater blocks showed that the conductance values for heater block 02, although followed the same trend, were on an average 9% lower than those for heater block 01. Since all the other parameters were constant, this indicated that the test setup using heater block 02 had lower parasitic losses. The relevant data is included in Table 4.1.





(a) Heater block 01 used with HP01



Not to scale

All dimensions in inches

(b) Split heater block 02 used with HP02

Figure 4.6: Schematic of heater blocks used

Table 4.1: Conductance values of copper 101 rod

Heater Block 01		Heater Block 02	
Power (W)	Conductance (W/K)	Power (W)	Conductance (W/K)
0.50	0.0698	0.51	0.0578
1.00	0.0761	1.01	0.0671
1.49	0.0790	1.50	0.0699
2.01	0.0820	2.04	0.0761
3.08	0.0850	3.04	0.0789
3.99	0.0845	4.03	0.0806
5.14	0.0884	5.02	0.0814
6.01	0.0865	5.99	0.0824

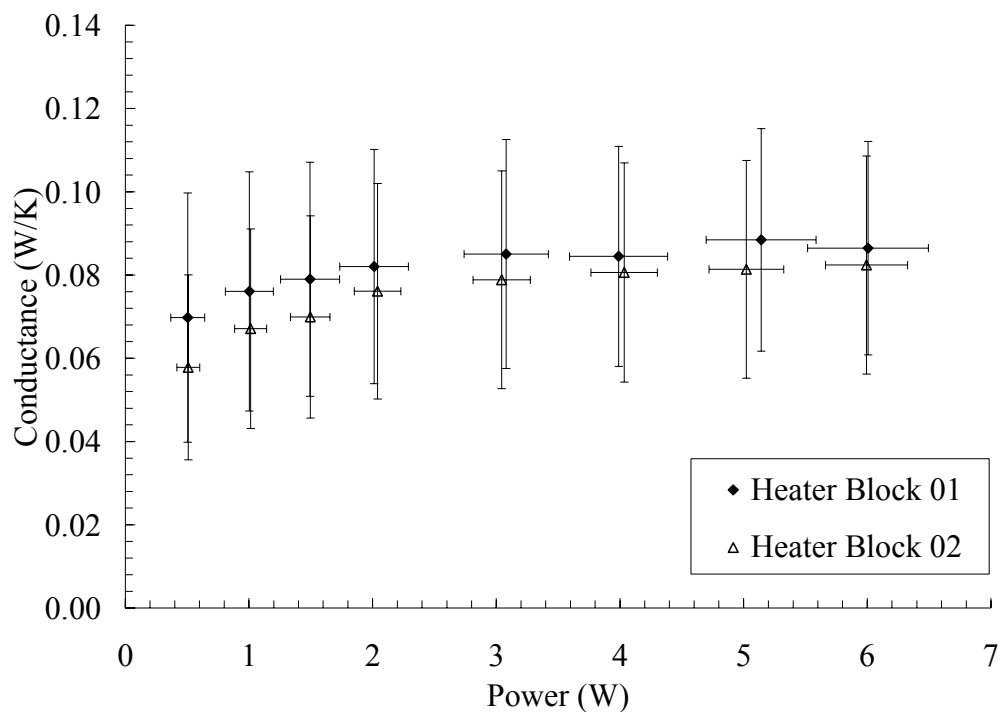


Figure 4.7: Comparison of copper rod data on heater blocks

## CHAPTER 5

### BENDABLE HEAT PIPES

#### **5.1 Introduction**

As discussed in Chapter 2, flexible heat pipes have garnered significant research interest in the past due to their obvious advantages. Flexible heat pipe designs include flexible sections made from bellows or bendable tubing. These types of heat pipes are usually designed to be fabricated in a particular shape. Fabrication techniques were developed to make bended heat pipes in required shapes and in some cases wicks were totally removed from the flexible sections to avoid potential problems with deformed wicks.

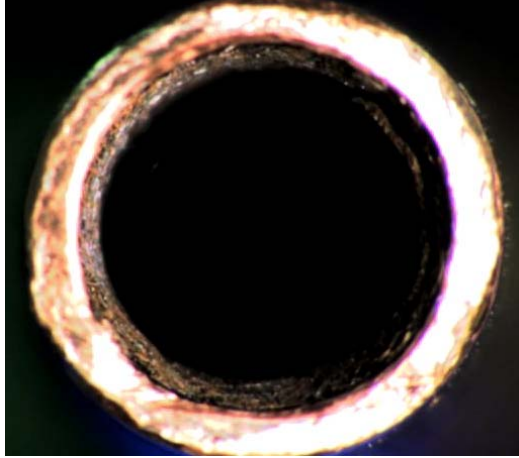
It is observed that there are no references in the literature for heat pipes that can be bent into a contorted shape after fabrication. This thesis documents the evaluation and testing of bendable copper-water heat pipes made using sintered copper felt wicks. Once fabricated, this heat pipe can be twisted to fit into the available space or reach narrow spaces.

#### **5.2 Bendable Wicks**

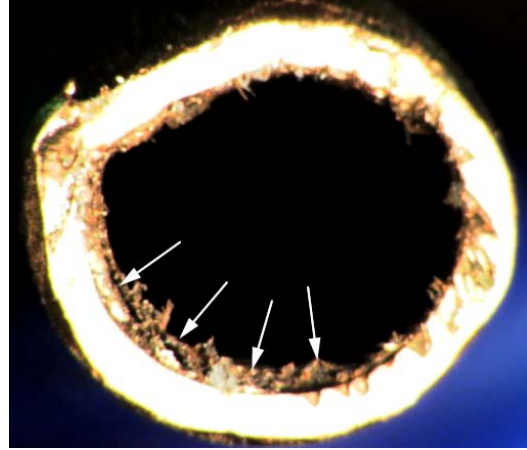
Only certain types of wicks can be used in bendable heat pipes. And wick will have a tendency to separate from the container walls under bending. This separation has

two adverse effects, a reduction in the vapor core area that reduces heat transfer capacity and a disruption in the path of liquid flowing back to the evaporator. If the bending angle is severe, the wick can crumple [16] and even tear off in extreme cases. The sintered copper felt wick provides a very flexible wick material that does not crack after bending as well. However, a wick made from sintered metal powder will crack under bending. Although other wicks made from metal screens may also work with supporting springs, this work is a continuation of ongoing work on metal felt heat pipes at AuTherMML [37]. The heat pipe was bent in only one location to reduce the complexities in testing. After successful tests on such heat pipes further studies on multiple bends could be carried out. Several bending angles ( $15^\circ$ ,  $30^\circ$ ,  $45^\circ$ ,  $60^\circ$  and  $90^\circ$ ) with a constant bending radius of 18.18mm (pipe axis) were tested.

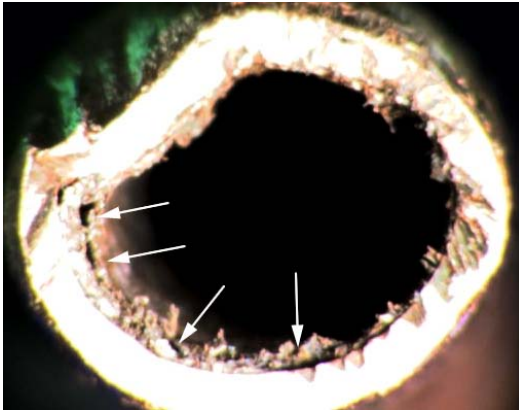
A series of photographs of the heat pipe cross section after bending were taken for various bent configurations and expectedly separation of wick was observed. However, it was noted (Figure 5.1) that the separation from the wall slowed down after  $45^\circ$ . Also a  $90^\circ$  bend was cut and, it was observed that the wick was not damaged due to stretching and crumpling at outer and inner walls as shown in Figure 5.2 (a) & (b). It can be seen in Figure 5.2 (c)-(e) that the inner and outer walls of the curved part of the heat pipe had deformed due to crumpling and stretching respectively. The working fluid gets trapped in the gaps created by the separation of the wick from the container walls. This film of working fluid has a lower conductivity as compared to that of the wick and it reduces the heat transfer to the heat pipe. Therefore, deformation is acceptable only in the adiabatic section and not in the condenser section and the evaporator section.



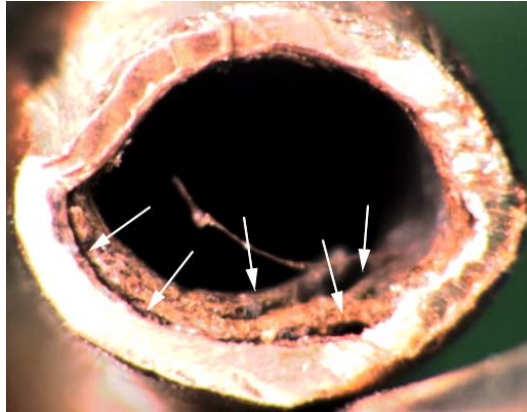
(a) Straight Heat Pipe  
(10x magnification)



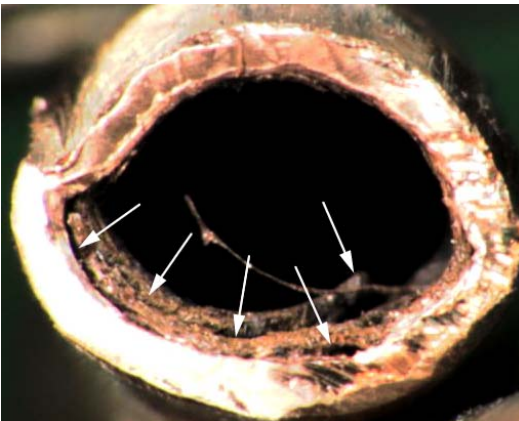
(b) 15° Bend  
(10x magnification)



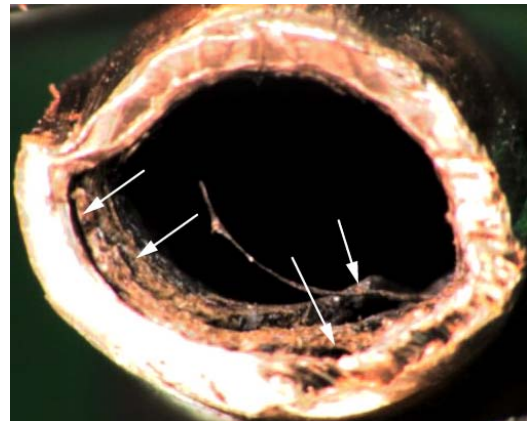
(c) 30° Bend  
(10x magnification)



(d) 45° Bend  
(10x magnification)



(e) 60° Bend  
(10x magnification)

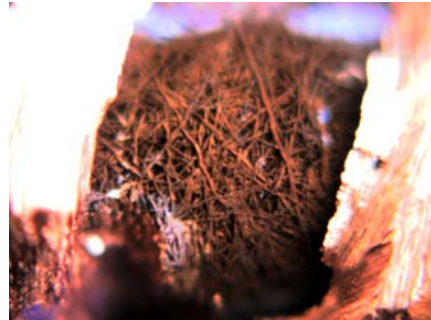


(f) 90° Bend  
(10x magnification)

Figure 5.1: Wick separation near heat pipe wall due to bending



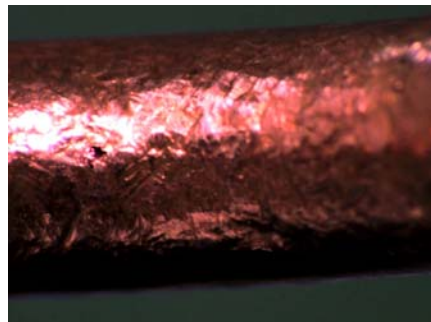
(a) No damage to wick due to bending  
(90°)  
(10x magnification)



(b) No damage to wick due to bending  
(90°)  
(10x magnification)



(c) Straight heat pipe wall texture  
(5x magnification)



(d) Bended heat pipe inner wall  
(5x magnification)



(e) Bended heat pipe outer wall  
(5x magnification)

Figure 5.2: Bending effects on heat pipe wall and wick

### 5.3 Performance Limit

As discussed in Section 1.5, a heat pipe has various performance limits. However, when the heat pipe has a single bend at the center, the only limit affected is the capillary limit. As shown in Equation 1.2, the vapor pressure drop and liquid pressure drop will be affected due to bending as the flow paths are altered. Low fluid velocities typically characterize the liquid flow and bending effects can be neglected [5]. Therefore, at steady mass flow, the vapor velocities are very high and the flow is laminar or turbulent depending on working temperature and heat load.

#### 5.3.1 Vapor Pressure Drop

A detailed analysis of vapor flow by C. A. Busse [5,38] was used to study bending effects on the capillary limit.

The capillary limit is given by,

$$\Delta p_{cap,max} \geq \Delta p_l + \Delta p_v + \Delta p_{e,phase} + \Delta p_{c,phase} + \Delta p_g \quad 1.2$$

The maximum capillary head is given by,

$$\Delta p_{cap,max} = \frac{2\sigma}{r_{eff}} \quad 5.1$$

where  $r_{eff}$  is the effective capillary radius and  $\sigma$  is the surface tension. Busse assumed that the vapor flow was laminar and the heat pipe was isothermal, so density was constant. Also the axial pressure gradient was assumed constant over the heat pipe cross section.

The two dimensional steady flow of the incompressible vapor is represented by the conservation equations for mass and momentum (Figure 5.3),

r momentum equation:

$$v \frac{\partial v}{\partial r} + w \frac{\partial v}{\partial z} = -\frac{1}{\rho} \frac{\partial p}{\partial r} + \nu \left[ \frac{\partial}{\partial r} \left( \frac{1}{r} \frac{\partial}{\partial r} (rv) \right) + \frac{\partial^2 v}{\partial z^2} \right] \quad 5.2$$

z momentum equation:

$$v \frac{\partial w}{\partial r} + w \frac{\partial w}{\partial z} = -\frac{1}{\rho} \frac{\partial p}{\partial z} + \nu \left[ \frac{1}{r} \frac{\partial}{\partial r} \left( r \frac{\partial w}{\partial r} \right) + \frac{\partial^2 w}{\partial z^2} \right] \quad 5.3$$

Continuity equation:

$$\frac{1}{r} \frac{\partial}{\partial r} (rv) + \frac{\partial w}{\partial z} = 0 \quad 5.4$$

Boundary conditions:

$$\text{At } r = 0 \quad \frac{\partial w}{\partial r} = 0, v = 0 \quad 5.5$$

$$\text{At } r = R_v \quad w = 0, v = \begin{cases} v_\delta, & 0 < z < L_e \\ 0, & L_e < z < L_e + L_a \\ -v_\delta, & L_e + L_a < z < L_t \end{cases} \quad 5.6$$

A radial Reynolds number  $Re_r$  is defined as vapor velocity distributions are related to interfacial velocity  $v_\delta$ ,

$$Re_r = \frac{\rho_v v_\delta R_v}{\mu_v} \quad 5.7$$

This is related to the rate of mass flow per unit length by,

$$Re_r = \frac{1}{2\pi\mu_v} \frac{dm_v}{dz} \quad 5.8$$



To solve these equations, Busse proposed an approximate expression for the axial velocity profile,

$$w(r, z) = 2\bar{w}(z) \left( 1 - \frac{r^2}{R_v^2} \right) \left[ 1 + a(z) \left( \frac{r^2}{R_v^2} - \frac{1}{3} \right) \right] \quad 5.9$$

where  $a(z)$  is an arbitrary function for the correction to the parabolic Poiseuille velocity profile that was found by assuming that the average pressure gradient over the cross section equals the axial pressure gradient at the center [5]. The values of  $a(z)$  for various values of radial Reynolds numbers are shown in Figure 5.4. This gives results for the pressure drops in all three sections [5].

Evaporator:

$$\Delta p_e = -\frac{8\mu_v Q_e}{\pi\rho_v R_v^4 h_{fg}} \frac{L_e}{2} \left[ 1 + Re_r \left( \frac{7}{9} - \frac{8A}{27} + \frac{23A^2}{405} \right) \right] \quad 5.10$$

Adiabatic:

$$\Delta p_a = -\frac{8\mu_v Q_e}{\pi\rho_v R_v^4 h_{fg}} L_a \left[ 1 + \frac{Re_z R_v}{8L_a} \left( \frac{8(A-a)}{27} + \frac{23(A^2 - a^2)}{405} \right) \right] \quad 5.11$$

Condenser:

$$\Delta p_e = -\frac{8\mu_v Q_e}{\pi\rho_v R_v^4 h_{fg}} \frac{L_c}{2} \left[ 1 + Re_r \left( \frac{7}{9} - \frac{8a}{27} + \frac{23a^2}{405} \right) \right] \quad 5.12$$

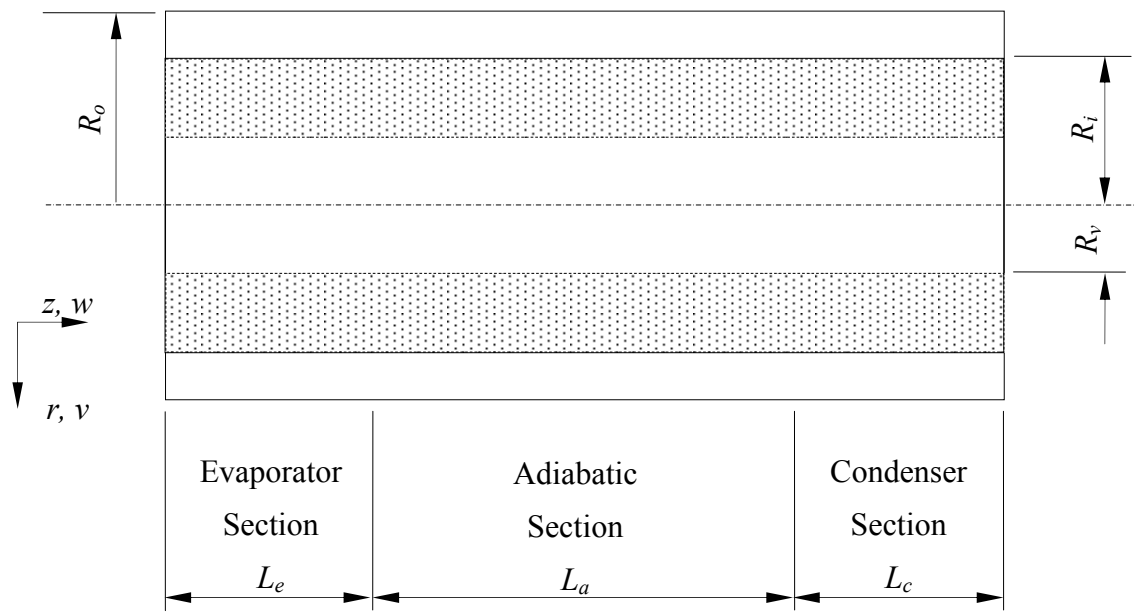


Figure 5.3: Heat Pipe Nomenclature

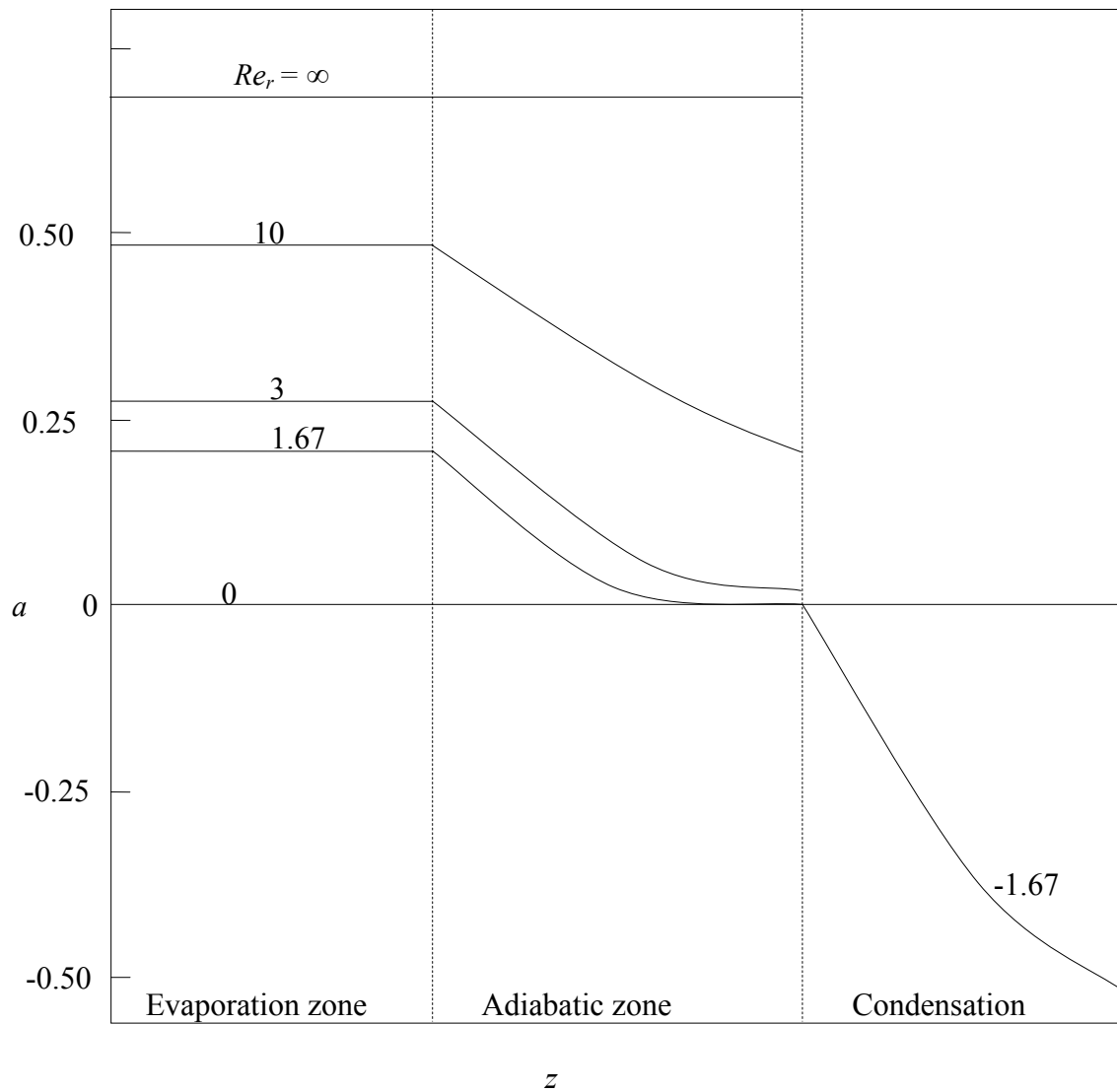


Figure 5.4: The correction function  $a(z)$  [38]

Where  $Re_z$  is the axial Reynolds number,

$$Re_z = \frac{2R_v \bar{w}_a \rho_v}{\mu_v} \quad 5.13$$

and A is

$$A = \frac{15}{22} \left[ 5 + \frac{18}{Re_r} - \sqrt{\left( 5 + \frac{18}{Re_r} \right)^2 - \frac{44}{5}} \right] \quad 5.14$$

For the case, when the wet point is near the condenser end cap (Figure 1.2) the pressure drop in the entire heat pipe is found by adding Equation 5.10, Equation 5.11 and Equation 5.12,

$$\Delta p_v = - \frac{(fRe_z) \mu_v}{2R_v^2 A_v \rho_v h_{fg}} Q_e L_{eff} \quad 5.15$$

where  $L_{eff}$  is the effective length of heat pipe,

$$L_{eff} = \frac{L_e}{2} + L_a + \frac{L_c}{2} \quad 5.16$$

### 5.3.2 Other Pressure Drops

The liquid pressure drop is given by

$$\Delta p_l = \frac{\mu_l}{KA_w \rho_l h_{fg}} Q_e L_{eff} \quad 5.17$$

where  $K$  is the wick permeability and is given by an empirical relation [5],

$$K = \frac{A(X^2 - 1)}{X^2 + 1} \quad 5.18$$

$$X = 1 + \frac{Bd^2\phi^3}{(1-\phi)^2}$$

$$A = 6 \times 10^{-10} \text{ m}^2$$

$$B = 3.3 \times 10^7 \text{ m}^{-2}$$

$d$  = diameter of copper felt strand

The pressure drops due to phase change at the evaporator,  $\Delta p_{e,\delta}$ , and the condenser,  $\Delta p_{c,\delta}$ , are very small and can be neglected [6]. The hydrostatic pressure drop has two components, normal hydrostatic pressure drop  $\Delta p_{\perp}$  and axial hydrostatic pressure drop  $\Delta p_{\parallel}$ .

$$\Delta p_{\perp} = \rho_l g D_v \sin \phi \quad 5.19$$

$$\Delta p_{\parallel} = \rho_l g L_t \cos \phi \quad 5.20$$

Depending on the inclination  $\phi$  of heat pipe the axial pressure drop either assists or works against the capillary pumping pressure [6].

### 5.3.3 Capillary Limit

Combining Equation 5.15, Equation 5.17, Equation 5.19 and Equation 5.20 the expression for capillary limit 1.2 is given by [5],

$$\frac{2\sigma}{r_{eff}} = \left( \frac{\mu_l}{KA_w \rho_l h_{fg}} + \frac{(fRe_z)\mu_v}{2R_v^2 A_v \rho_v h_{fg}} \right) Q_e L_{eff} \pm \rho_l g L_t \cos \phi + \rho_l g D_v \sin \phi \quad 5.21$$

Let the liquid and vapor frictional coefficients be respectively defined as,

$$F_l = \frac{\mu_l}{KA_w \rho_l h_{fg}} \quad 5.22$$

$$F_v = \frac{(fRe_z)\mu_v}{2R_v^2 A_v \rho_v h_{fg}} \quad 5.23$$

therefore the capillary heat input limit is given by,

$$Q_{cap} = \frac{\frac{2\sigma}{r_{eff}} \pm \rho_l g L_t \cos \phi - \rho_l g D_v \sin \phi}{L_{eff} (F_l + F_v)} \quad 5.24$$

This is the base relation for a straight cylindrical heat pipe that has inclination  $\phi$  with respect to the vertical. It should be noted that since this heat pipe uses a wick, which allows circumferential communication of liquid, the normal hydrostatic pressure drop term has to be accounted for in the capillary limit [6].

When the heat pipe is in the horizontal position,  $\phi$  is  $90^\circ$  and the axial pressure drop is eliminated, therefore the capillary limit is given by,

$$Q_{cap, horizontal} = \frac{\frac{2\sigma}{r_{eff}} - \rho_l g D_v}{L_{eff} (F_l + F_v)} \quad 5.25$$

Similarly in the vertical orientation, the inclination is zero and there is no normal pressure drop term,

$$Q_{cap, vertical} = \frac{\frac{2\sigma}{r_{eff}} \pm \rho_l g L_t}{L_{eff} (F_l + F_v)} \quad 5.26$$

When the heat pipe is in gravity assisted mode of operation, the axial pressure drop term is positive in Equation 5.26 otherwise when the evaporator is on the top and the heat pipe is working against the gravity, it has a negative sign.

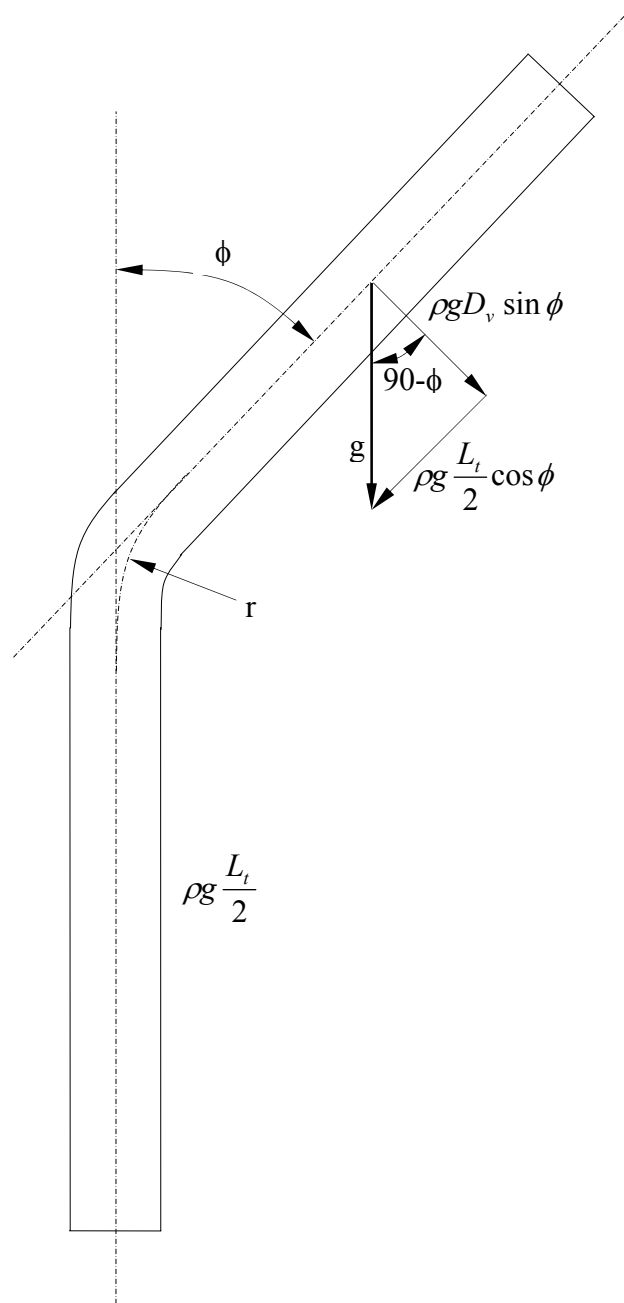


Figure 5.5: Hydrostatic pressure drops in a bended heat pipe

### 5.3.4 Other Limits

In addition to the capillary limit, other performance limits were also calculated to check if they could be responsible for heat pipe failure. The relations required for these limits were used from available literature [5,6] and are listed below,

- Sonic Limit 
$$Q_{sonic} = 0.474 A_v \rho_v h_{fg} \left[ \frac{\gamma_v R_v T_0}{2(\gamma_v + 1)} \right]^{\frac{1}{2}} \quad 5.27$$

- Entrainment Limit 
$$Q_{entrainment} = A_v h_{fg} \left[ \frac{\sigma \rho_v}{2R_{h,s}} \right]^{\frac{1}{2}} \quad 5.28$$

- Boiling Limit 
$$Q_{boiling} = \frac{2\pi L_e k_{eff} T_v}{h_{fg} \rho_v \ln(r_i/r_v)} \left( \frac{2\sigma}{r_n} - \Delta p_{cap,max} \right) \quad 5.29$$

### 5.3.5 Bend Loss

When a pipe is bended, there is an additional pressure drop caused primarily due to result of secondary flow and is usually represented by an equivalent length of a straight pipe [39]. The secondary flows are rotating motion, normal to the pipe axis and are superimposed on the main flow in the direction of the axis. The friction at the pipe walls and the centrifugal force combine to produce these rotations [40]. The bend loss can be accounted for as a function of dynamic pressure of the vapor,

$$\begin{aligned} \Delta p_{bend} &= K_b \frac{\rho w^2}{2} \\ &= K_b \frac{Q_e^2}{2\rho A_v^2 h_{fg}^2} \end{aligned} \quad 5.30$$



Most of the available data in the literature relate this loss to the relative radius of the curvature,  $\frac{R_v}{r}$  or the Dean number,  $De$  and account for the bend angle in terms of the length of the curvature. The technical paper No. 410 by the Crane company [40] provides a relation for calculating bend loss coefficients,  $K_b$ . The relation provided by the Crane company [40] is for turbulent flows in bends of  $90^\circ$ . Also the published work on evaluating bend losses is for losses in pipelines and their joints and fittings for turbulent flows. The work available on laminar flow is very limited and the only reported study included experimental results for a loss factor  $K_b$  as a function of the Reynolds number [41]. The data is available for some limited radii ratios of 4.52, 6.08, 13.06 and 23.42. The data indicates that as the Reynolds number increases the friction factor for the bend decreases.

H. Ito [42] and Misra et al. [43] have published results of their work on the laminar flows in curved pipes. Both of them have produced similar relations for the relative friction factor of a curved pipe in terms of the Dean number.

Where the Dean number is defined as

$$De = Re \sqrt{\frac{R_v}{r}} \quad 5.31$$

The relation by Ito [42] is

$$\frac{f_b}{f_s} = 0.1033 De^{\frac{1}{2}} \left[ \left( 1 + \frac{1.729}{De} \right)^{\frac{1}{2}} - \frac{1.315}{\sqrt{De}} \right]^{-3} \quad 5.32$$

Misra et al. [43] have presented following relation

$$\frac{f_b}{f_s} = 0.6341628 De^{\frac{1}{2}} \left[ \left( 1 + \frac{6.1154102}{De} \right)^{\frac{1}{2}} - \frac{2.4729355}{\sqrt{De}} \right]^{-3} \quad 5.33$$

For laminar flow through a bend of angle  $\phi$ , the bend loss is a sum of the pressure drops due to bend and frictional pressure drops in a straight pipe of an equivalent length. This results in a relation between friction factor  $f_b$  for bends and friction factor  $f_s$  for the straight sections.

$$\Delta p_b = K_b \frac{w^2}{2} + \Delta p_s \quad 5.34$$

or

$$\frac{f_b L_b w^2}{4R_v} = K_b \frac{w^2}{2} + \frac{f_s L_b w^2}{4R_v} \quad 5.35$$

where,  $K_b$  is bend loss coefficient and  $L_b$  is length of bend.

For a bended pipe with a curvature radius  $r$  and angle  $\phi$  the length  $L_b$  is given by  $r\phi$ . Therefore Equation 5.35 becomes,

$$\frac{f_b r \phi}{2R_v} = K_b + \frac{f_s r \phi}{2R_v} \quad 5.36$$

$$f_b = \frac{2R_v K_b}{r \phi} + f_s \quad 5.37$$

$$K_b = \frac{r \phi f_s}{2R_v} \left( \frac{f_b}{f_s} - 1 \right) \quad 5.38$$

### 5.3.5.1 Bend Loss Coefficient for Vapor Flow

It's relation from Equation 5.32 was selected for calculating the bend pressure loss in this study. From Equations 5.32 and 5.38,

$$K_b = \frac{r\phi_s}{2R_v} \left\{ 0.1033De^{\frac{1}{2}} \left[ \left( 1 + \frac{1.729}{De} \right)^{\frac{1}{2}} - \frac{1.315}{\sqrt{De}} \right]^{-3} - 1 \right\} \quad 5.39$$

A plot of  $K_b$  vs  $De$  is shown in Figure 5.6. The above relation was directly used in the calculations for the capillary limits reported in the following section.

### 5.3.6 Capillary Limit for Bended Heat Pipe

It was proposed in the last two sections that the effect of the bending angle can be accounted for by representing the bending losses as a function of the axial velocity. Due to various possible orientations of a bended heat pipe, expressions for the capillary limit in various orientations are given below [5].

- Heat pipe oriented horizontally

$$Q_{cap, horizontal} = \frac{\frac{2\sigma}{r_{eff}} - \rho_l g D_v - \left( K_b \frac{Q_e^2}{2\rho A_v^2 h_{fg}^2} \right)}{L_{eff} (F_l + F_v)} \quad 5.40$$

- Heat pipe in a vertical gravity assisted orientation

$$Q_{cap, vertical, gravity} = \frac{\frac{2\sigma}{r_{eff}} + \rho_l g \frac{L_t}{2} (1 + \cos \phi) - \rho_l g D_v \sin \phi - \left( K_b \frac{Q_e^2}{2\rho A_v^2 h_{fg}^2} \right)}{L_{eff} (F_l + F_v)} \quad 5.41$$

- Heat pipe in a vertical adverse gravity orientation

$$Q_{cap, vertical, adverse} = \frac{\frac{2\sigma}{r_{eff}} - \rho_l g \frac{L_t}{2} (1 + \cos \phi) - \rho_l g D_v \sin \phi - \left( K_b \frac{Q_e^2}{2\rho A_v^2 h_{fg}^2} \right)}{L_{eff} (F_l + F_v)} \quad 5.42$$

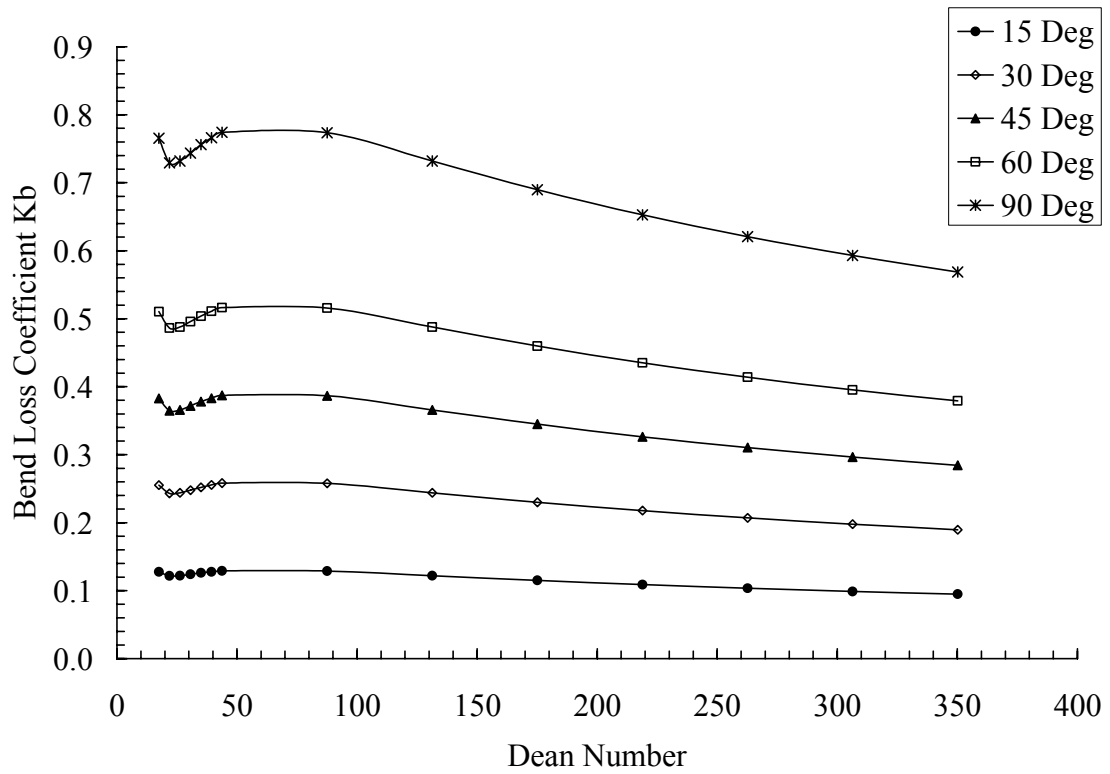


Figure 5.6: Resistance to flow with Dean number

In Equations 5.41 and 5.42, the axial hydrostatic pressure loss is divided into two parts. The cosine component accounts for reduction in the axial drop due to bending. These relations were used along with the temperature and power data taken from the operation of the bent heat pipes to study the change in the capillary limit due to bending.

#### **5.4 Testing and Evaluation**

Two heat pipes were tested for studying the concept of bendable heat pipes. The heat pipes tested consisted of a wick made from the sintered copper felt with water as the working fluid. The two heat pipes were designated as HP01 and HP02. The first set of tests were carried out on HP01 and included testing in horizontal, vertical gravity assisted and bended in the vertical gravity assist orientation for the angles of 15°, 30°, 45°, 60° and 90° with a constant bending radius of 18.18mm.

For HP02, additional tests were carried out for bended heat pipes in both the horizontal and the adverse gravity orientation for the same series of angles. This allowed for the elimination of the effects caused by the axial hydrostatic pressure drop. The axial hydrostatic pressure drop is a significant component in the total capillary pumping pressure in the vertical gravity assisted position. Testing in the horizontal and vertical adverse gravity orientation meant that the heat pipe was working solely on the capillary pumping pressure. A schematic of bended configurations is shown in Figure 5.7

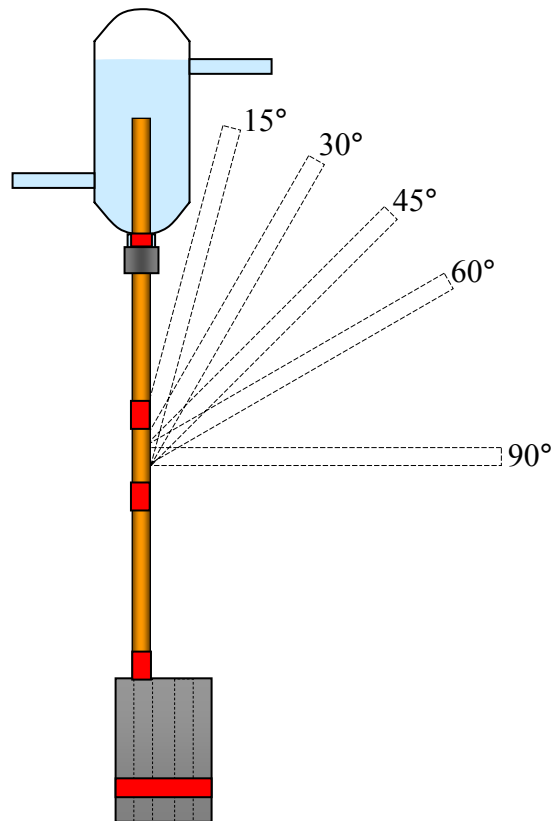


Figure 5.7: Schematic of bending configurations for HP01

#### 5.4.1 Specifications of HP01

• Container outer diameter (D)	–	6.35 mm
• Working length (L)	–	276.2 mm
• Evaporator length ( $L_e$ )	–	38.1 mm
• Condenser length ( $L_c$ )	–	38.1 mm
• Adiabatic section length ( $L_a$ )	–	200 mm
• Sintered metal felt wick thickness	–	0.3175 mm
• Porosity ( $\phi$ )	–	87%
• Length of metal felt strands	–	10 mm
• Diameter of metal felt strands	–	$3.5 \times 10^{-2}$ mm
• Charge	–	1.3g
• Permeability	–	$442.76 \mu\text{m}^2$

#### 5.4.2 HP01 Bending Test Results

The results are presented in the graphical format due to the large number of readings for each test. The charts are included for input power against copper equivalence for following cases:

- Straight horizontal and vertical
- $15^\circ$  bended vertical

- 30° bended vertical
- 45° bended vertical
- 60° bended vertical
- 90° bended vertical

Vertical refers to gravity assisted operation.

Finally a graph showing measured increase in  $\Delta T$  with the bending angle is included. It was noticed that in all tests the copper equivalence vs power plots showed a similar trend. A peculiar bell shaped curve was observed for all tests for HP01. As the power was increased, the copper equivalence went up till it reached a maximum value and then it came down. The test was stopped when the heat pipe either stopped working or the temperatures did not attain a steady state.

It was noticed that the tests for 45° and 90° bends produced abnormally high conductance values and it is not possible to relate this behavior to any particular cause. These tests were repeated two and four times respectively with similar outcomes.



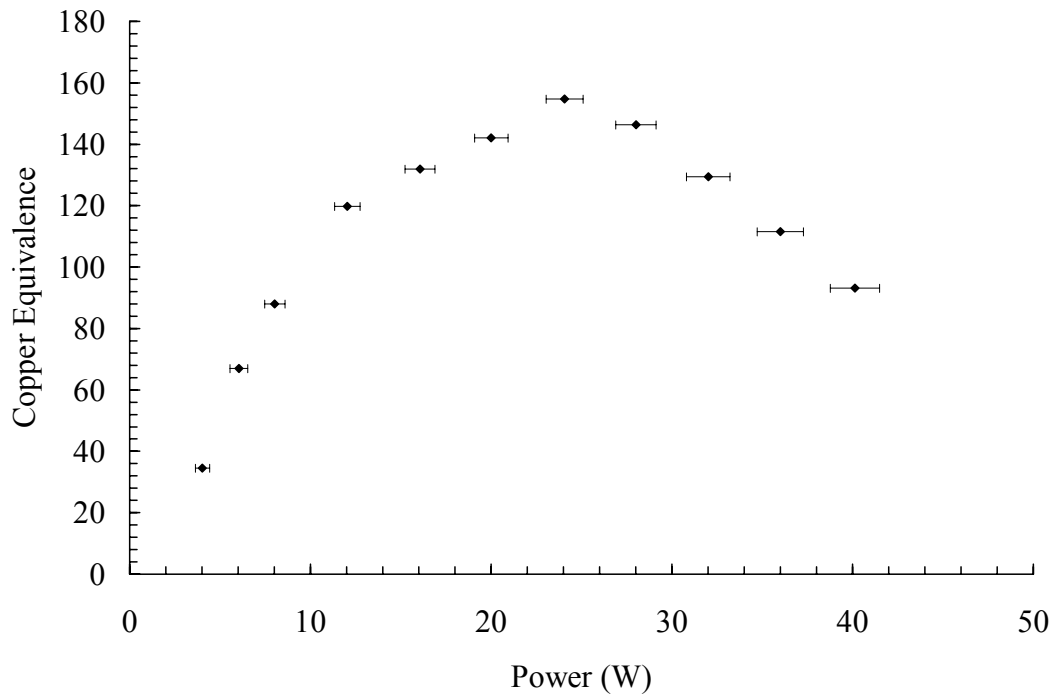


Figure 5.8: Test results for HP01 in straight horizontal position

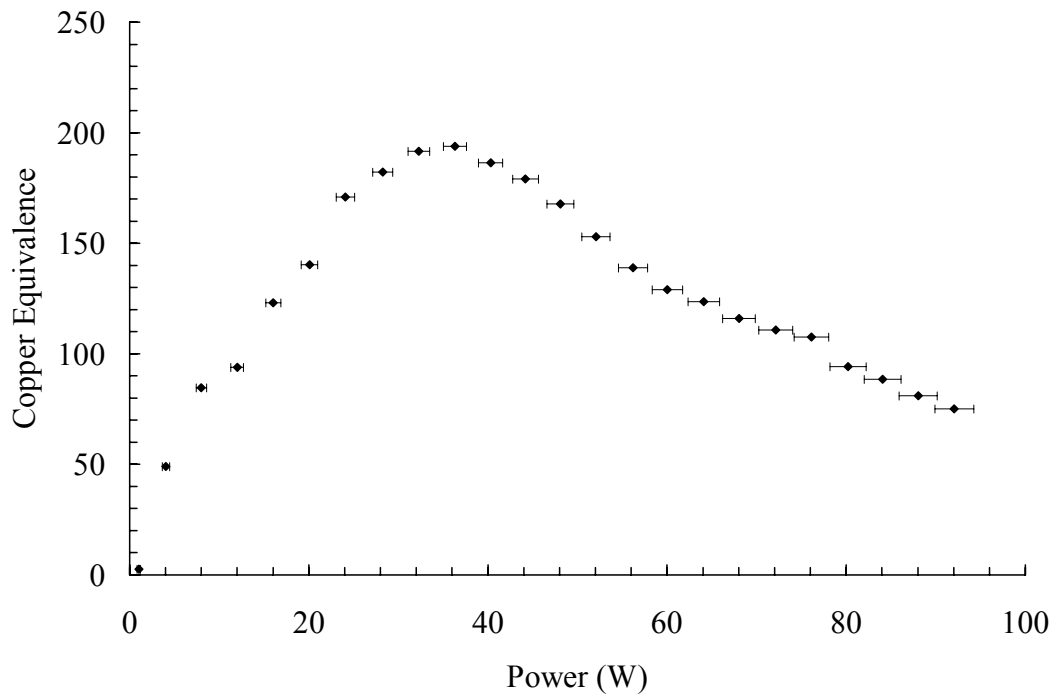


Figure 5.9: Test results for HP01 in straight vertical gravity assist position

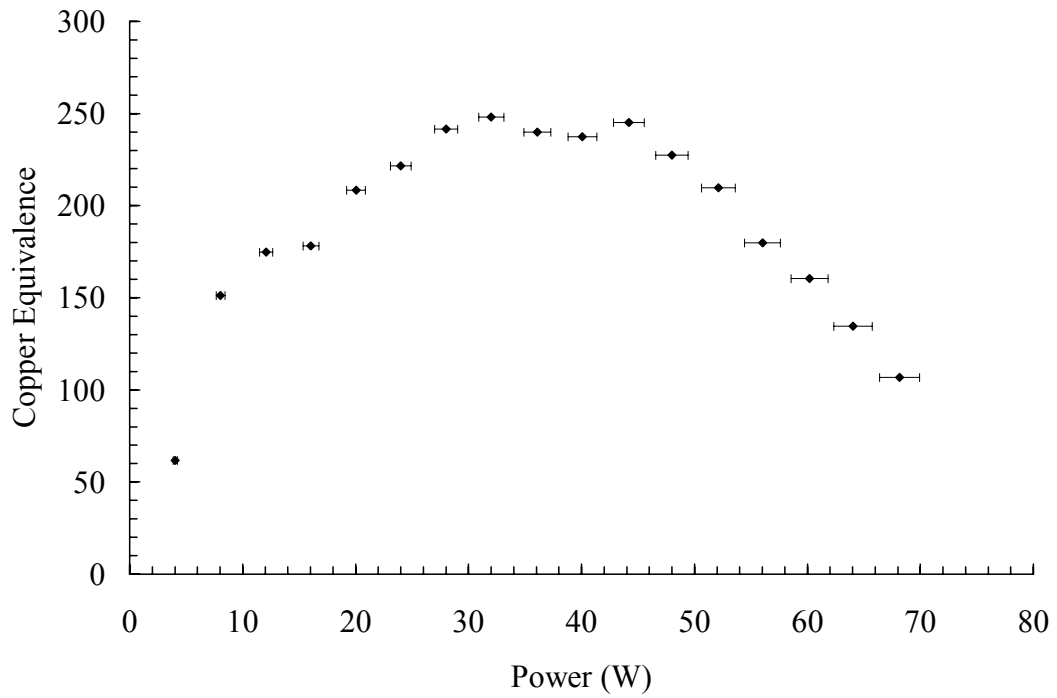


Figure 5.10: Test results for HP01 in 15° bended vertical gravity assist position

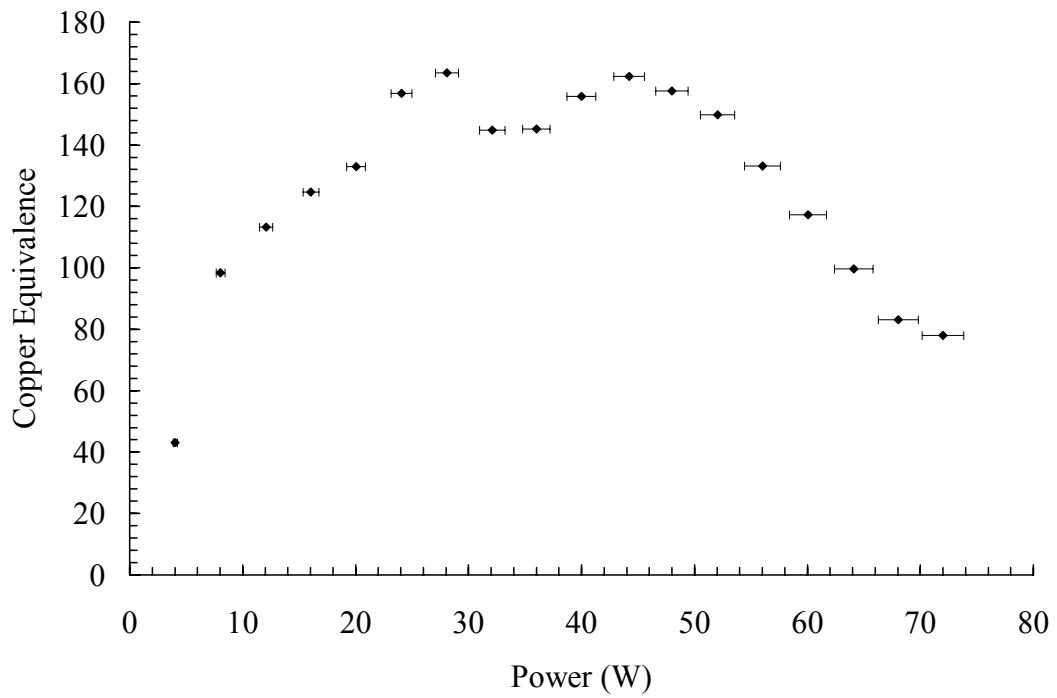


Figure 5.11: HP01 Test results for HP01 in 30° bended vertical gravity assist position

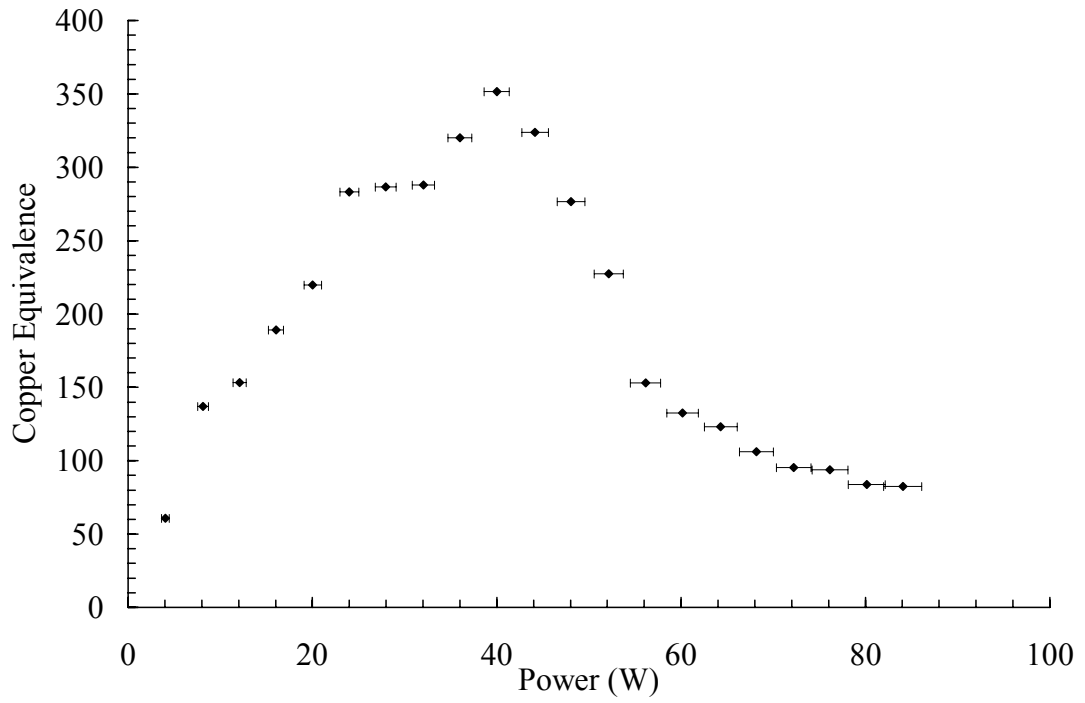


Figure 5.12: Test results for HP01 in 45° bended vertical gravity assist position

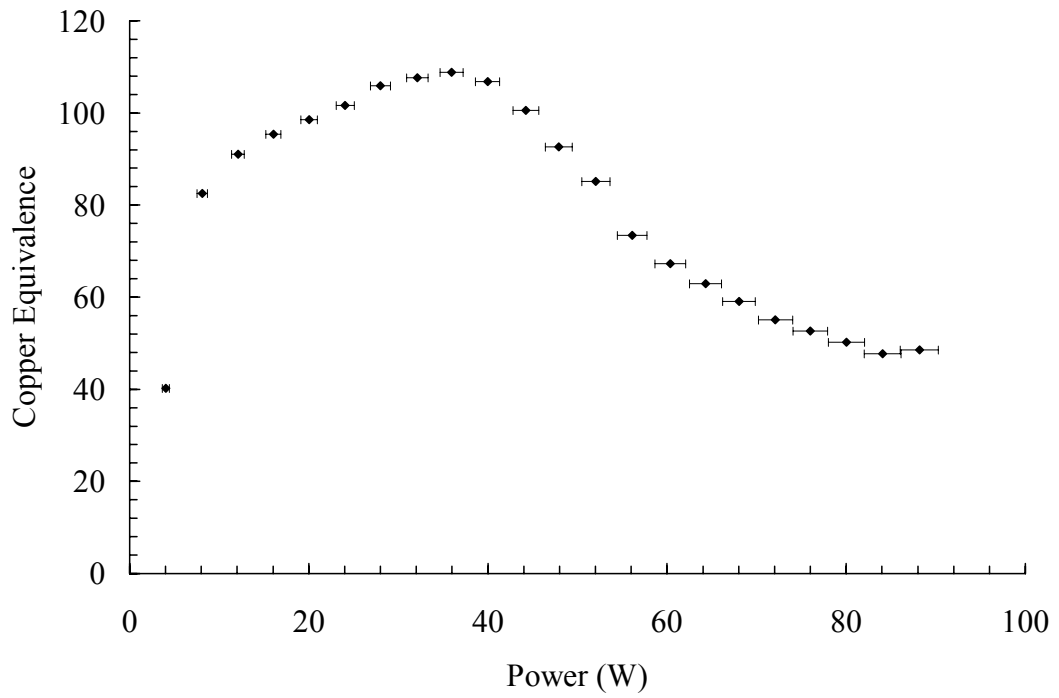


Figure 5.13: Test results for HP01 in 60° bended vertical gravity assist position

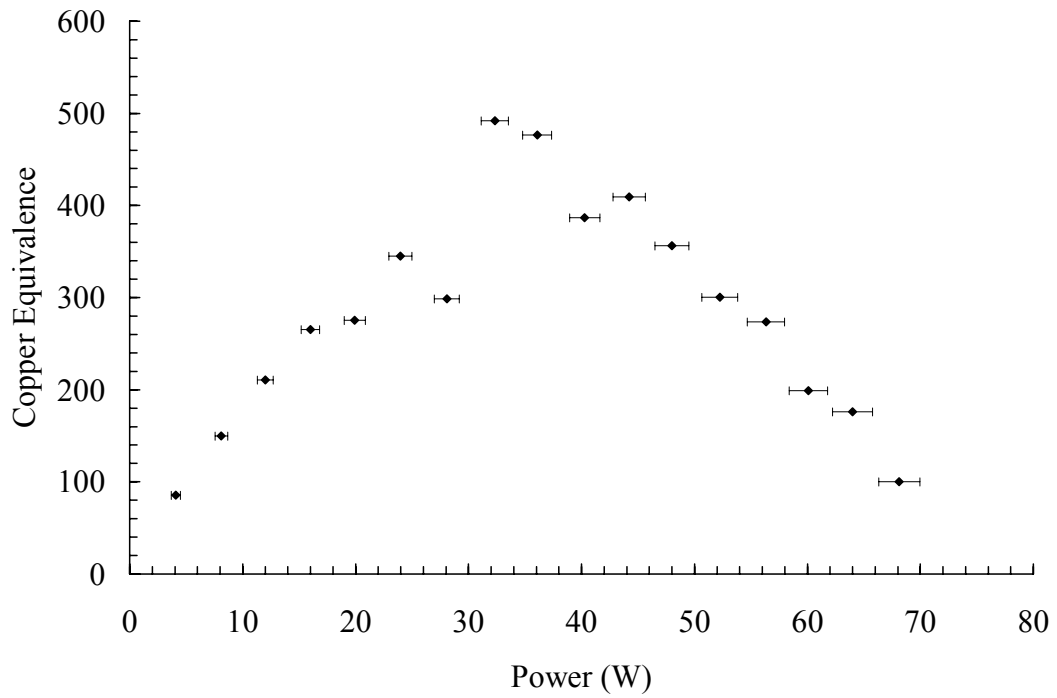


Figure 5.14: Test results for HP01 in 90° bended vertical gravity assist position

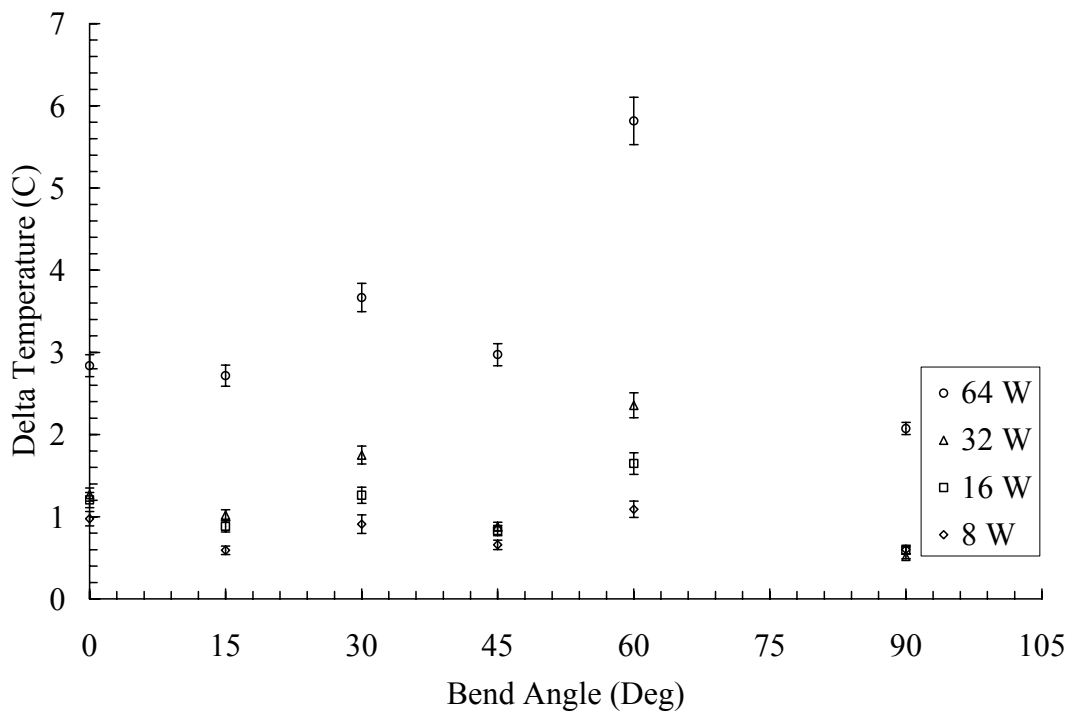


Figure 5.15:  $\Delta T$  across HP01 for various bend angles

### 5.4.3 Capillary Limits for HP01

The capillary limit was calculated using the equations presented in Section 5.3.3. Since a heat pipe typically has a very low temperature gradient over its length, the temperature measured at the evaporator end was used as the operating temperature for the heat pipe. This temperature was used for the thermo physical properties of the water vapor. Also, whenever any of the other performance limits was lower than the capillary limit, it was included on the chart.

The capillary limit charts are presented for following cases,

- Straight horizontal and vertical
- 15° bended vertical
- 30° bended vertical
- 45° bended vertical
- 60° bended vertical
- 90° bended vertical

Vertical refers to gravity assisted operation.

Each chart also shows steady state heat input from the tests described in previous section.

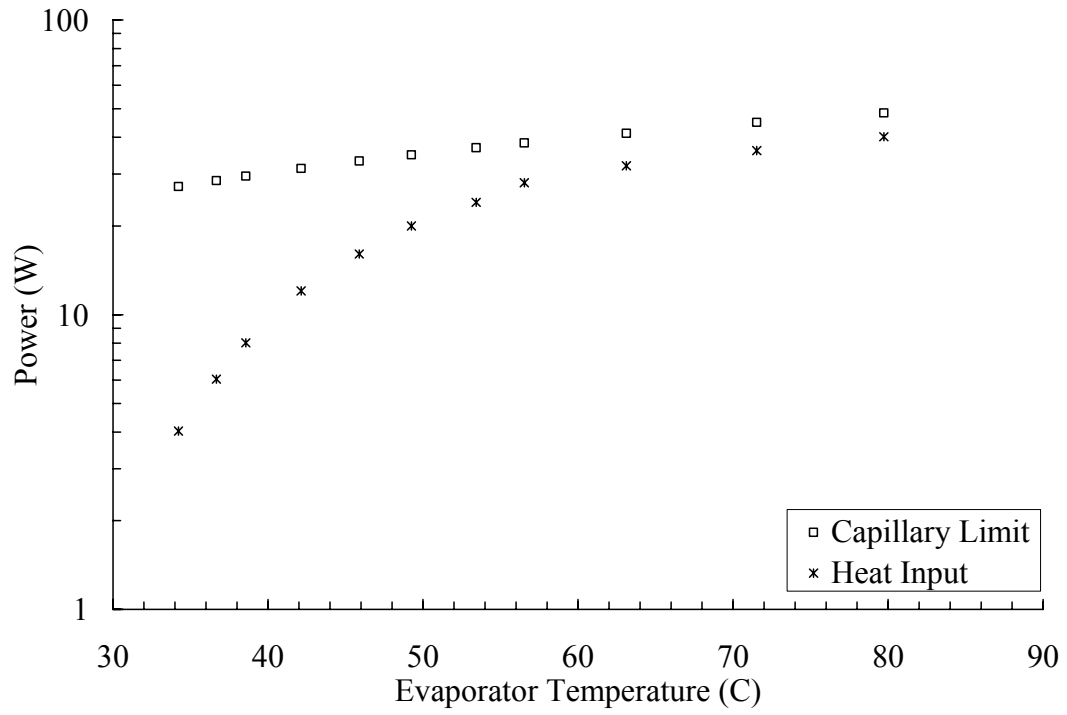


Figure 5.16: Capillary limit for HP01 in straight horizontal orientation

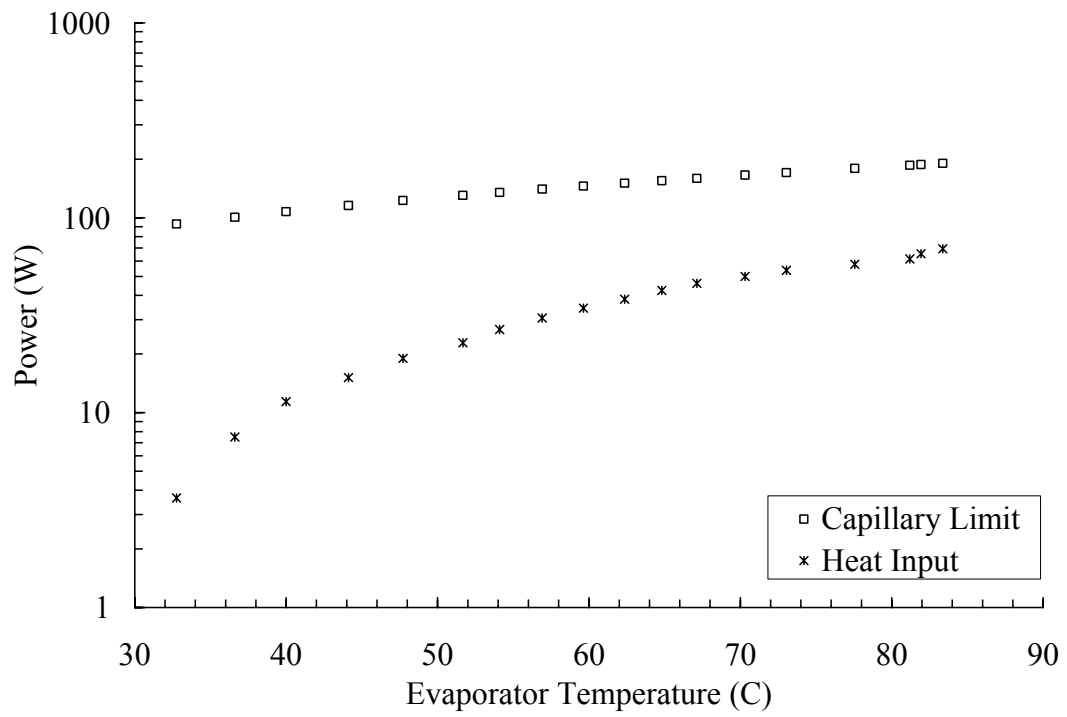


Figure 5.17: Capillary limit for HP01 in straight vertical orientation

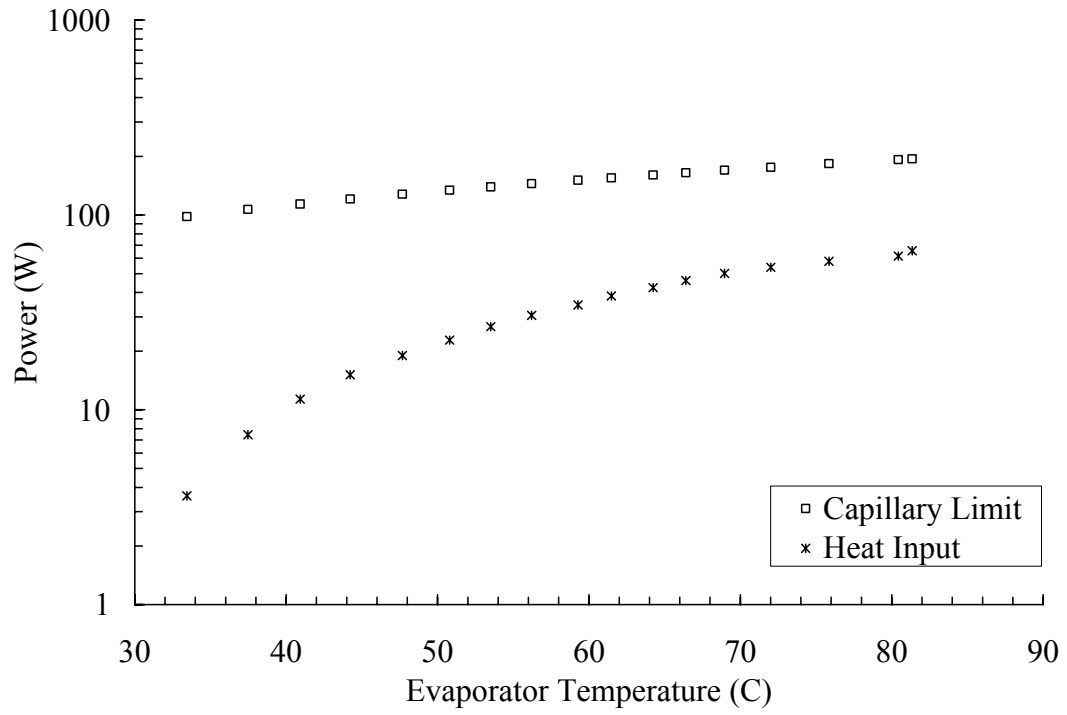


Figure 5.18: Capillary limit for HP01 in 15° bended vertical orientation

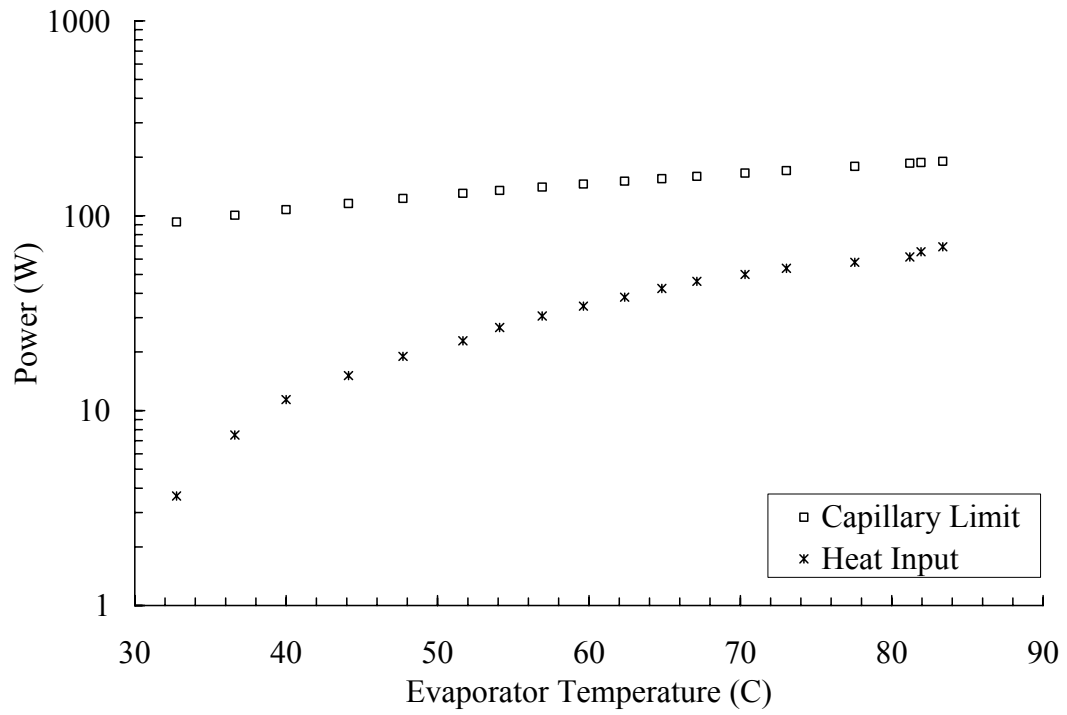


Figure 5.19: Capillary limit for HP01 in 30° bended vertical orientation

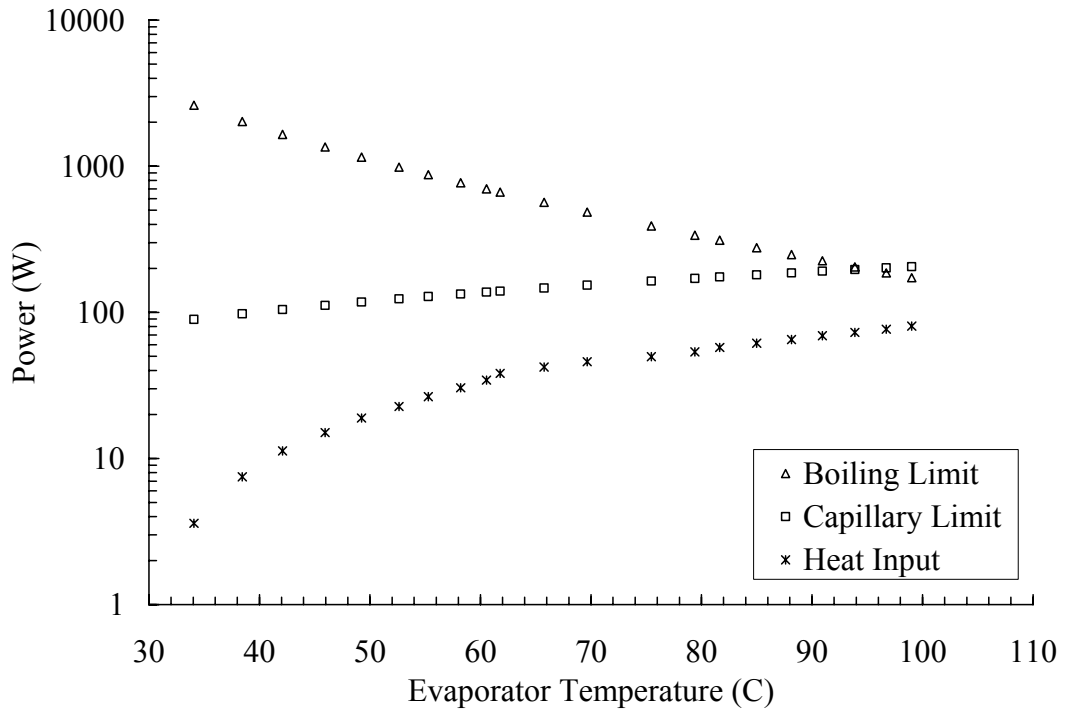


Figure 5.20: Capillary limit for HP01 in 45° bended vertical orientation

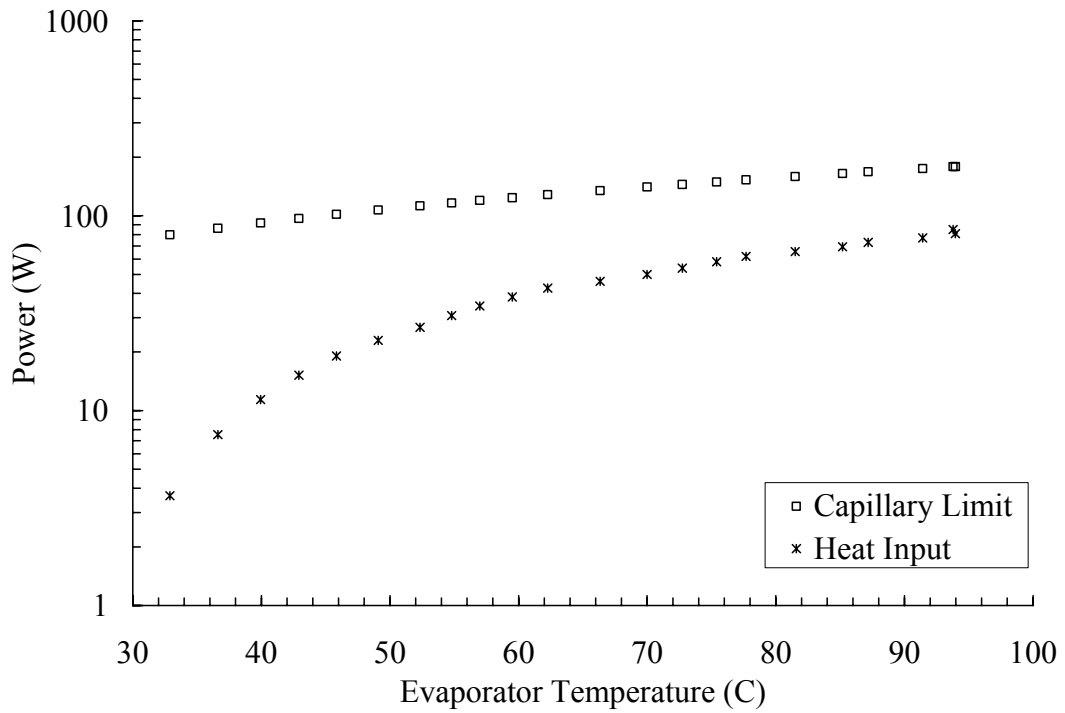


Figure 5.21: Capillary limit for HP01 in 60° bended vertical orientation



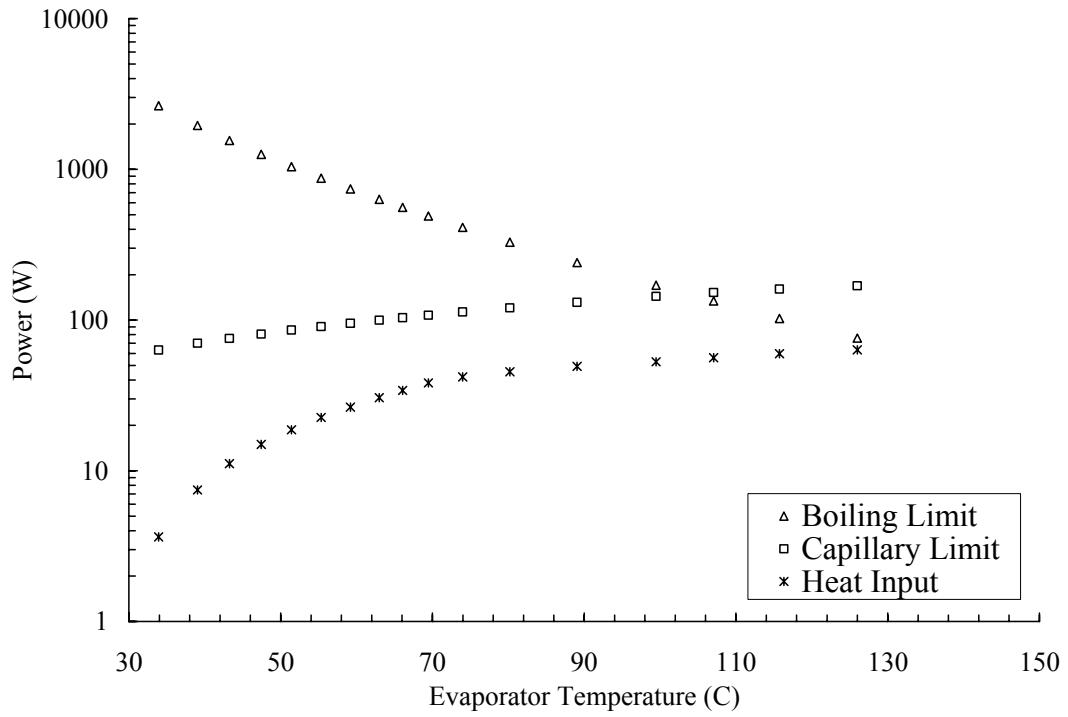


Figure 5.22: Capillary limit for HP01 in 90° bended vertical orientation

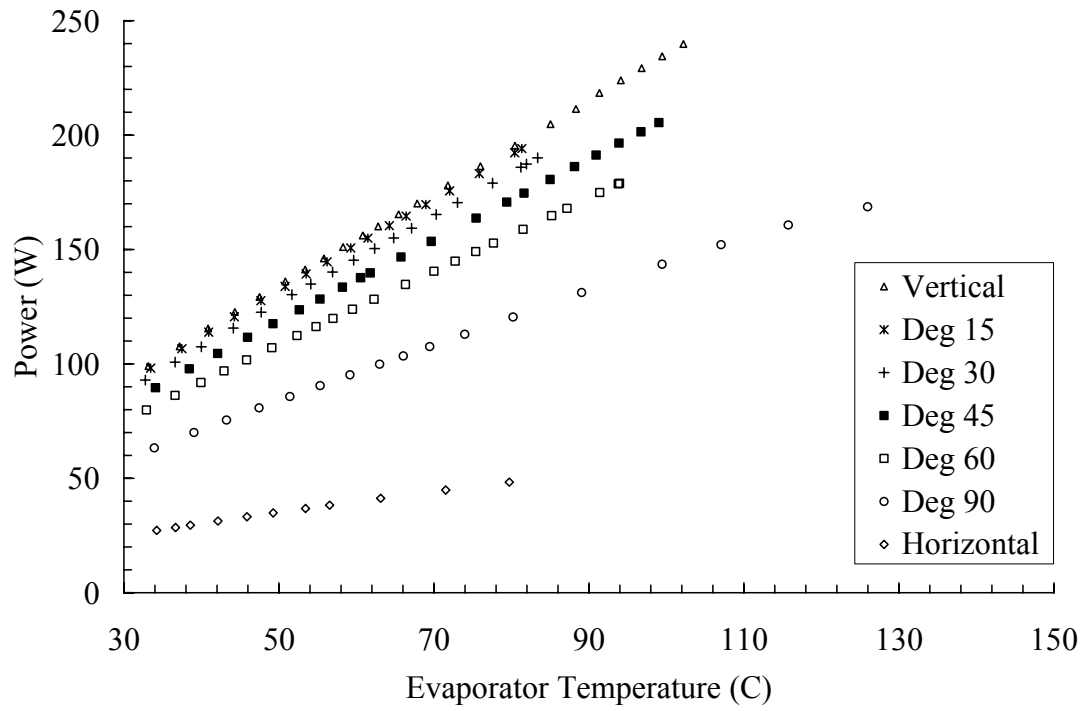


Figure 5.23: Effect of bending angle on capillary limit for HP01

From these charts it is evident that as the bending angle increases, the capillary limit decreases, mainly due to the decrease in the axial hydrostatic pressure drop. The loss due to the bending itself was not significant and is almost negligible compared to the loss in the axial hydrostatic pressure drop. Also for vertical, 45° and 90° configurations, the boiling limit was approached (Figure 5.20 and Figure 5.22) due to the high temperature and input heat flux during the later part of the operating range. Therefore, even though the conductance values for 45° and 90° were doubtful, it can be seen that the imminent dry out due to boiling limit coincided with the lack of steady state. This gives confidence in the results obtained.

#### 5.4.4 Specifications of HP02

HP02 was identical to HP01 in all aspects; the only differences were in the geometric dimensions and the quantity of working fluid used.

- Working length (L) – 274.1 mm
- Evaporator length ( $L_e$ ) – 25.4 mm
- Condenser length ( $L_c$ ) – 48.65 mm
- Adiabatic section length ( $L_a$ ) – 200 mm
- Charge – 1.26g

#### 5.4.5 HP02 Bending Test Results

During the testing of HP01, it was noticed that the hydrostatic pressure drop in the axial direction made all other pressure drops insignificant. Hence, testing was extended to

include bending in the horizontal orientation as well. In this orientation, only the normal hydrostatic pressure drop is effective and it is very small in comparison to the axial hydrostatic pressure drop.

Results are included for following cases,

- Straight horizontal and vertical
- 15° bended horizontal and vertical
- 30° bended horizontal and vertical
- 45° bended horizontal and vertical
- 60° bended horizontal and vertical
- 90° bended horizontal and vertical

Vertical refers to gravity assisted operation.

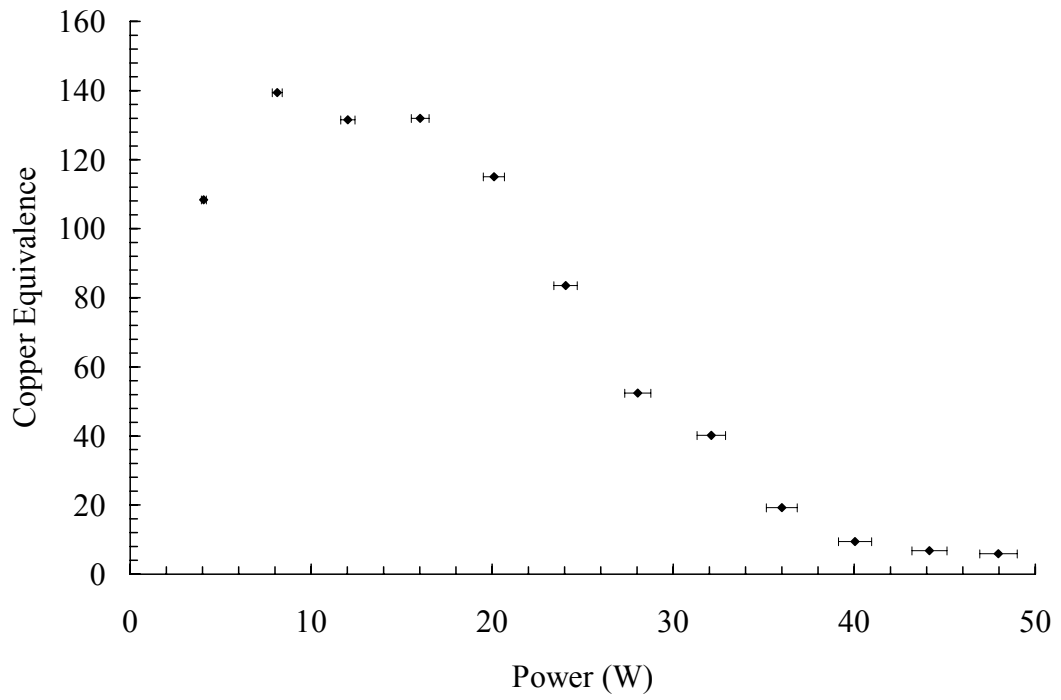


Figure 5.24: Test results for HP02 in straight horizontal orientation

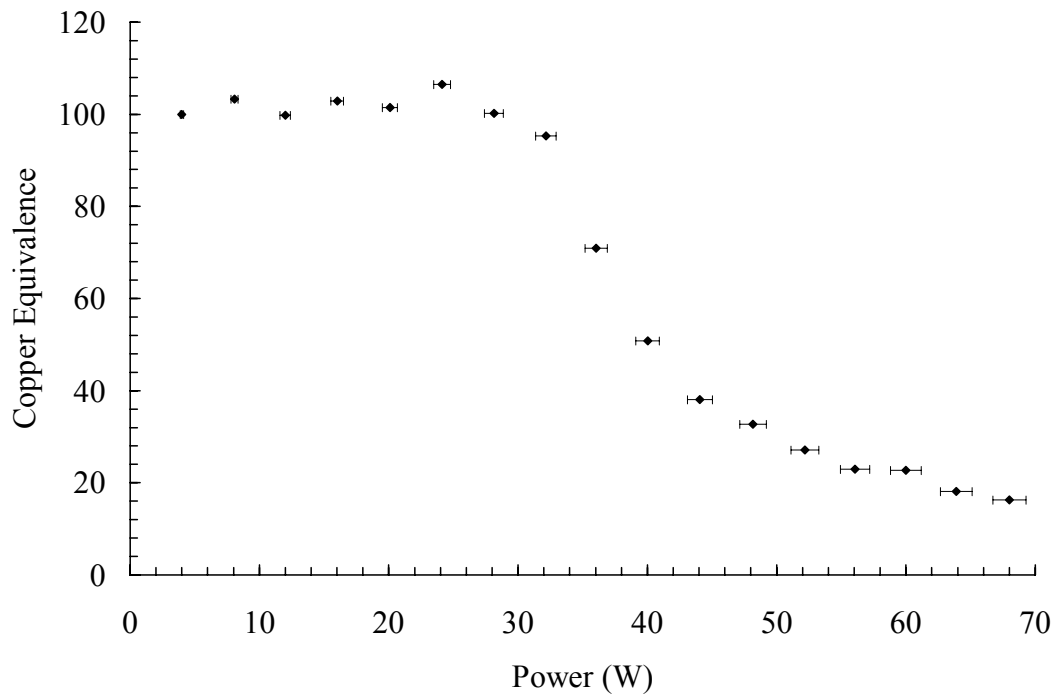


Figure 5.25: Test results for HP02 in straight vertical orientation

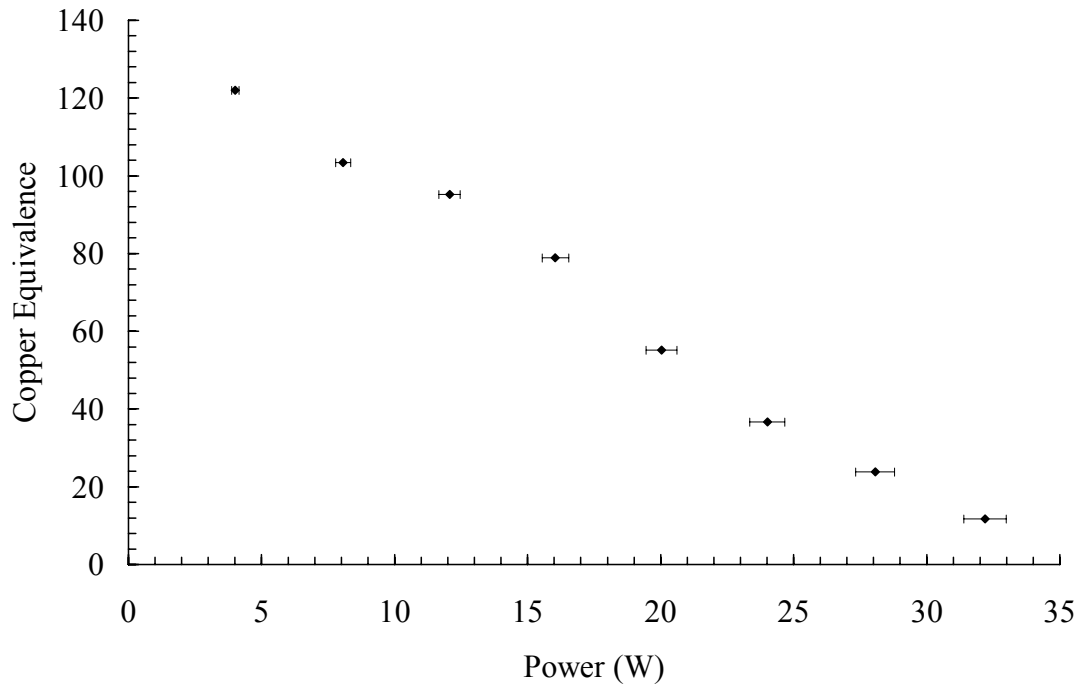


Figure 5.26: Test results for HP02 in 15° bended horizontal orientation

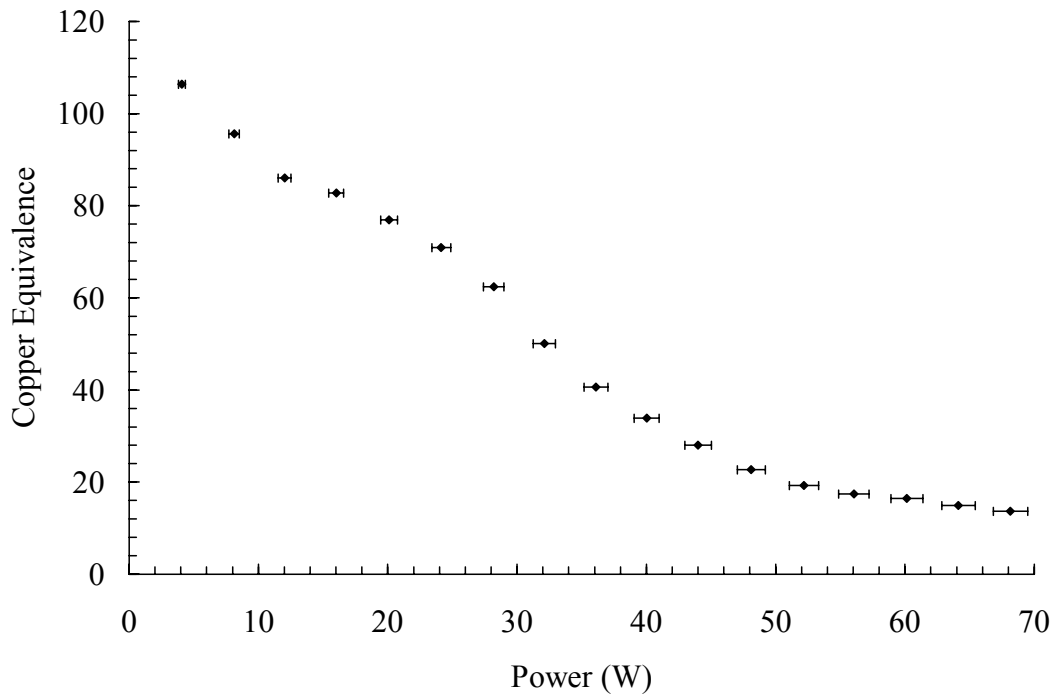


Figure 5.27: Test results for HP02 in 15° bended vertical orientation

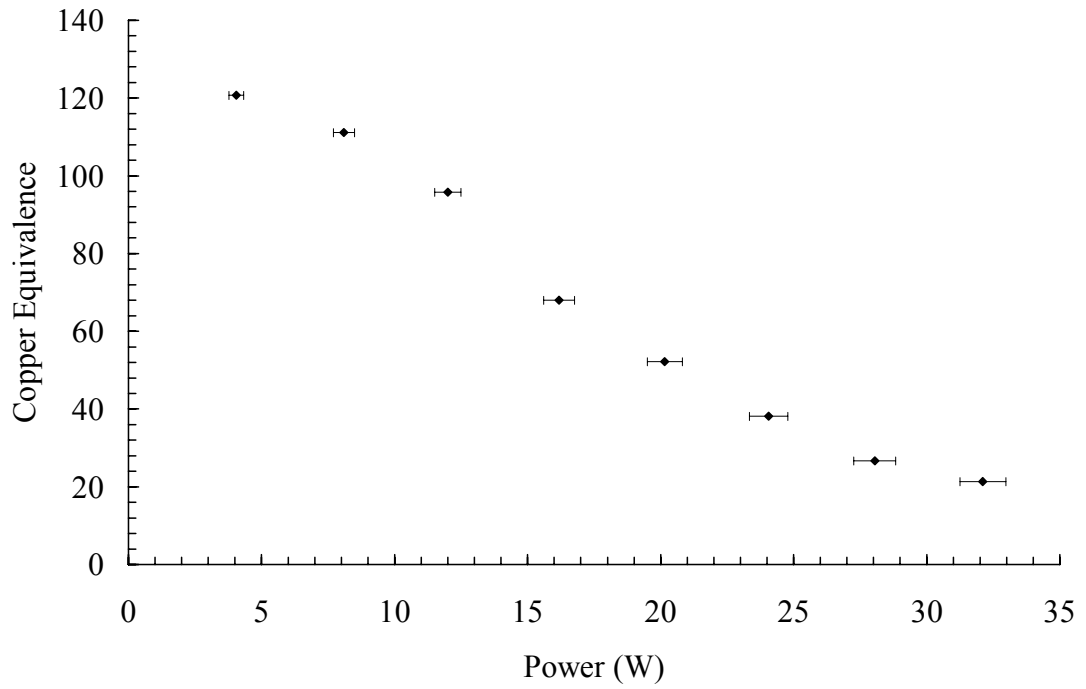


Figure 5.28: Test results for HP02 in 30° bended horizontal orientation

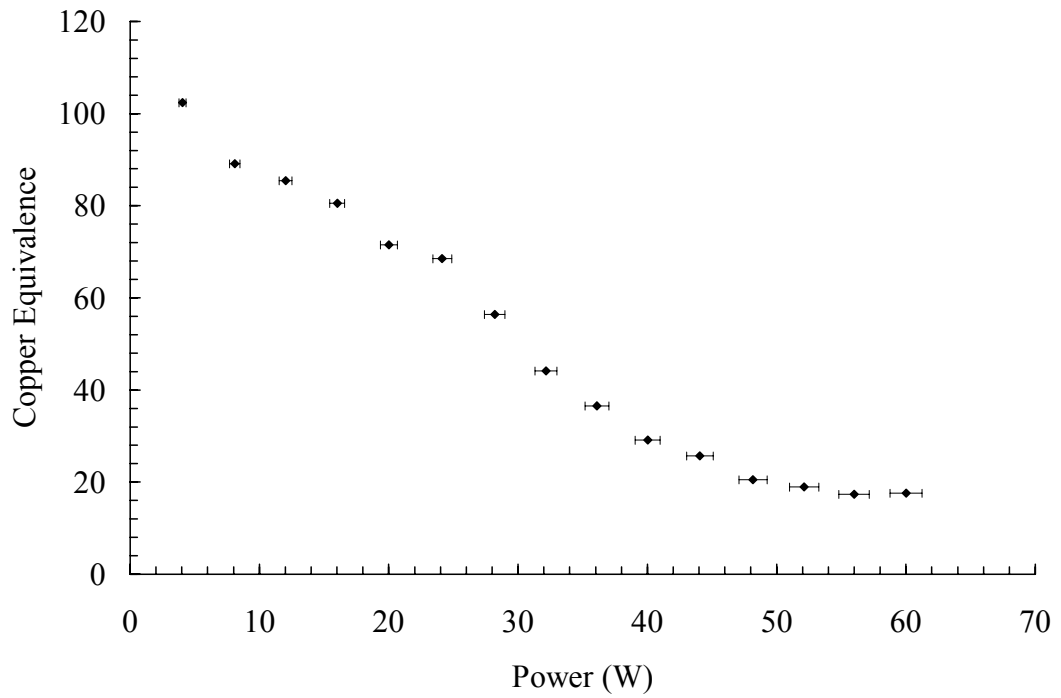


Figure 5.29: Test results for HP02 in 30° bended vertical orientation

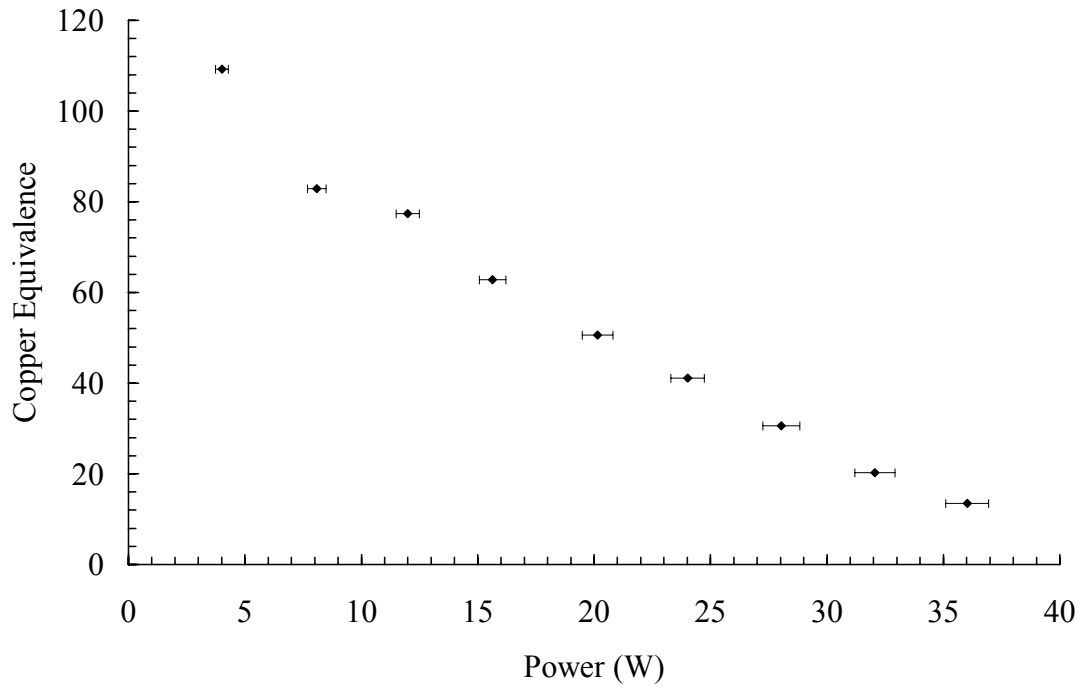


Figure 5.30: Test results for HP02 in 45° bended horizontal orientation

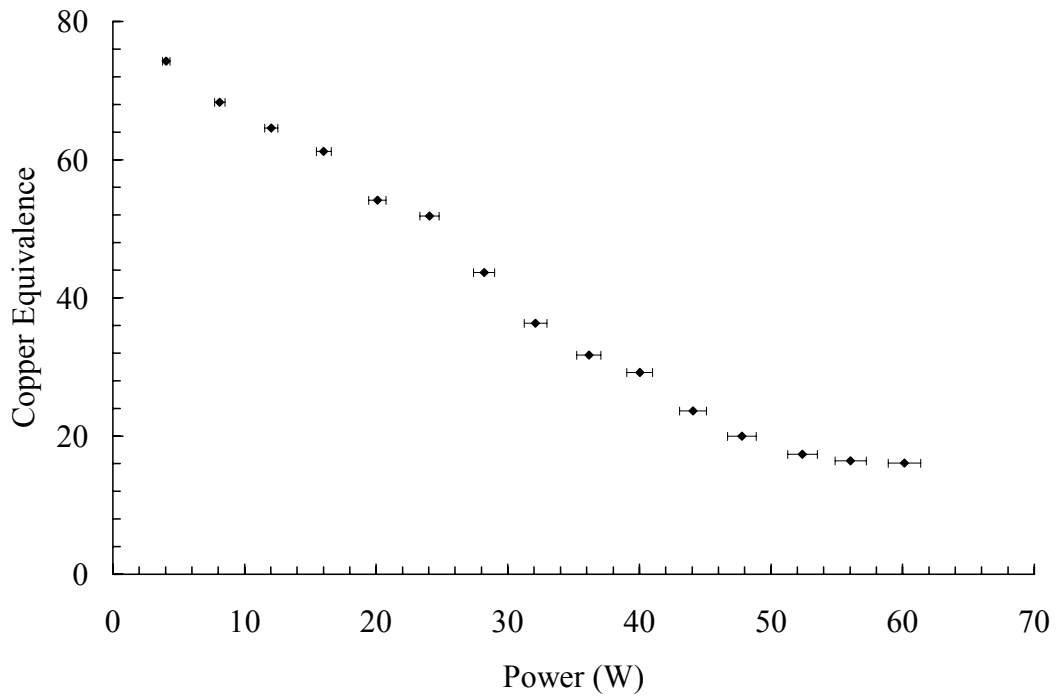


Figure 5.31: Test results for HP02 in 45° bended vertical orientation

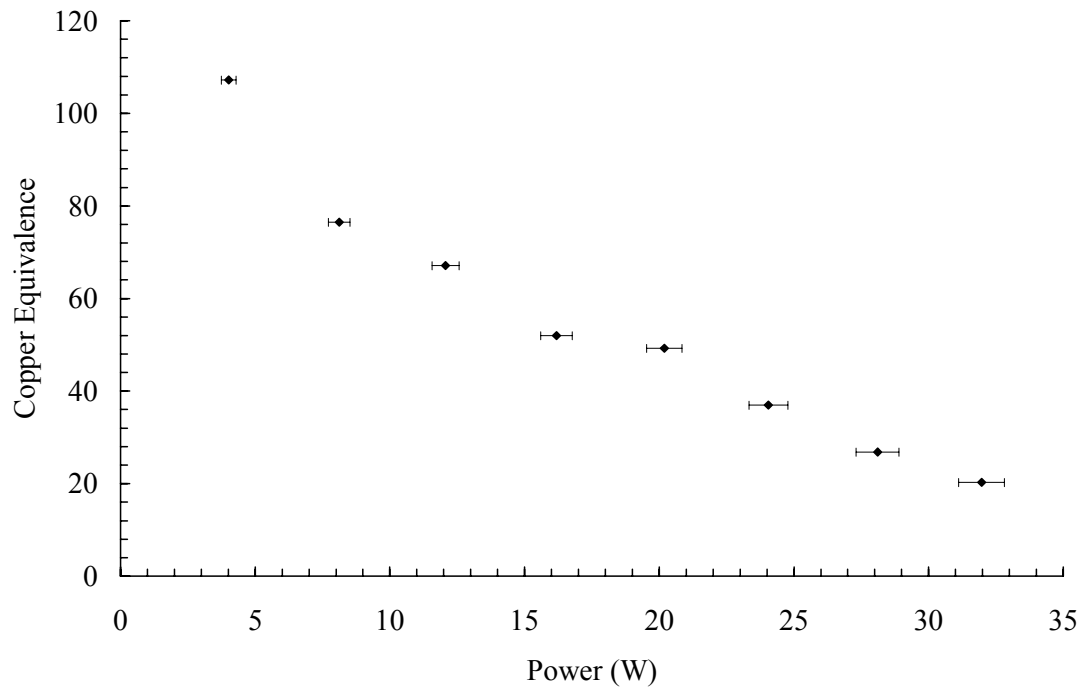


Figure 5.32: Test results for HP02 in 60° bended horizontal orientation

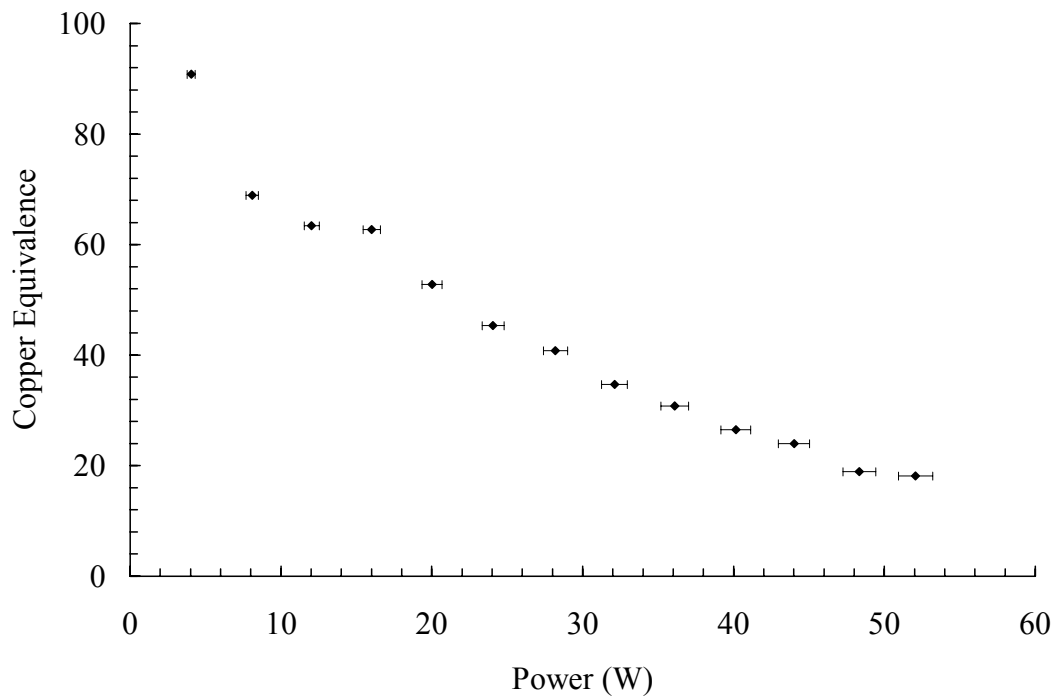


Figure 5.33: Test results for HP02 in 60° bended vertical orientation



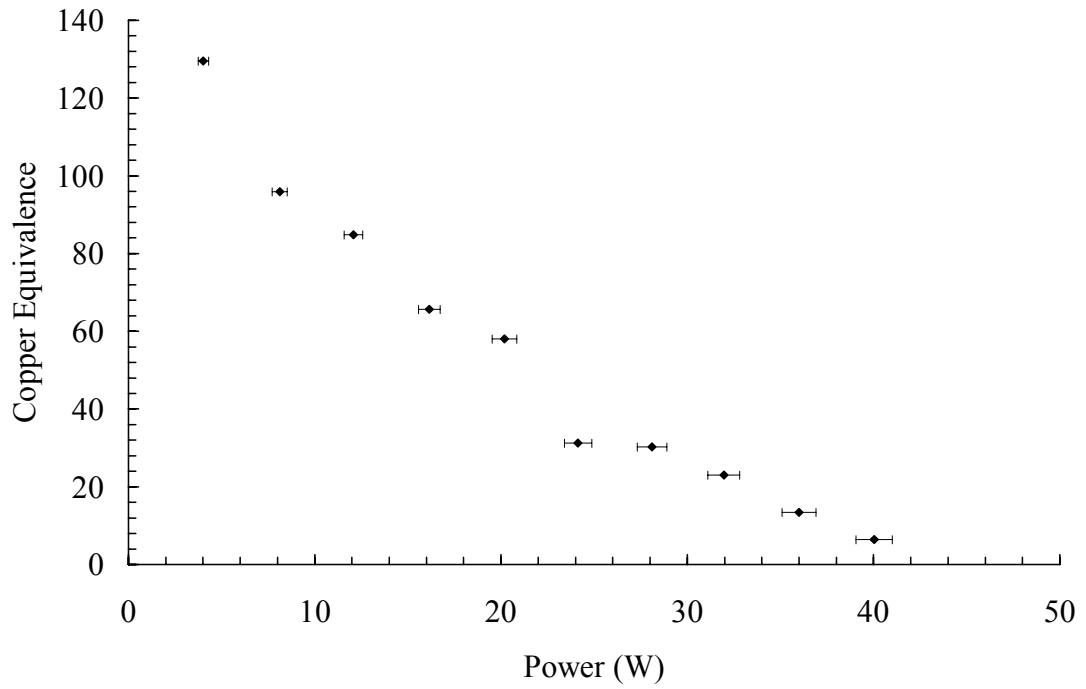


Figure 5.34: Test results for HP02 in 90° bended horizontal orientation

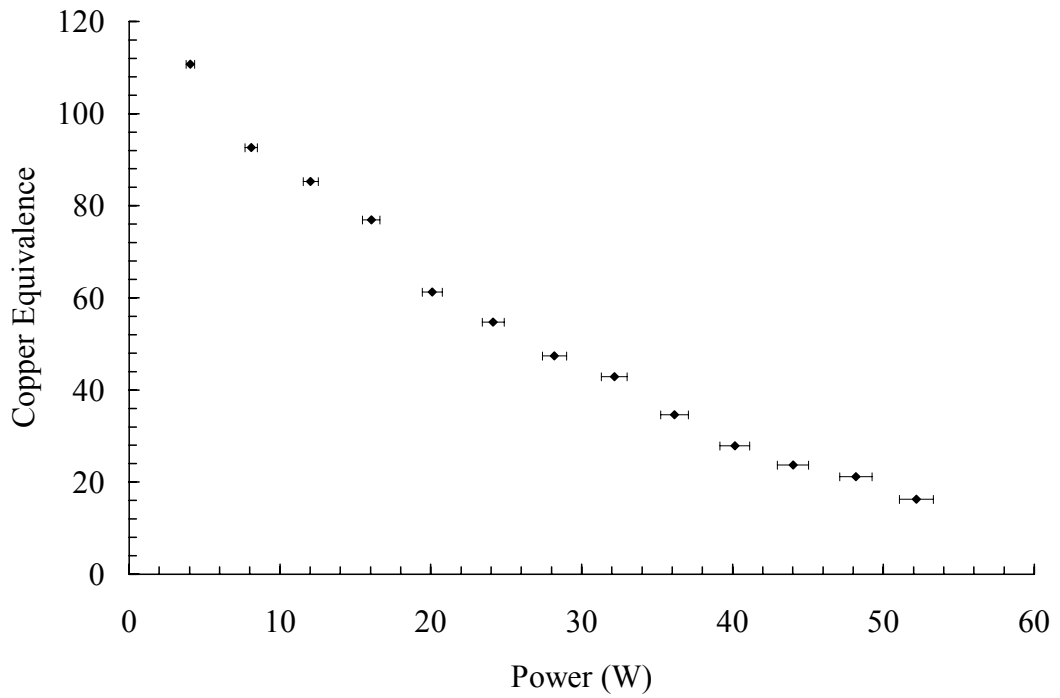


Figure 5.35: Test results for HP02 in 90° bended vertical orientation

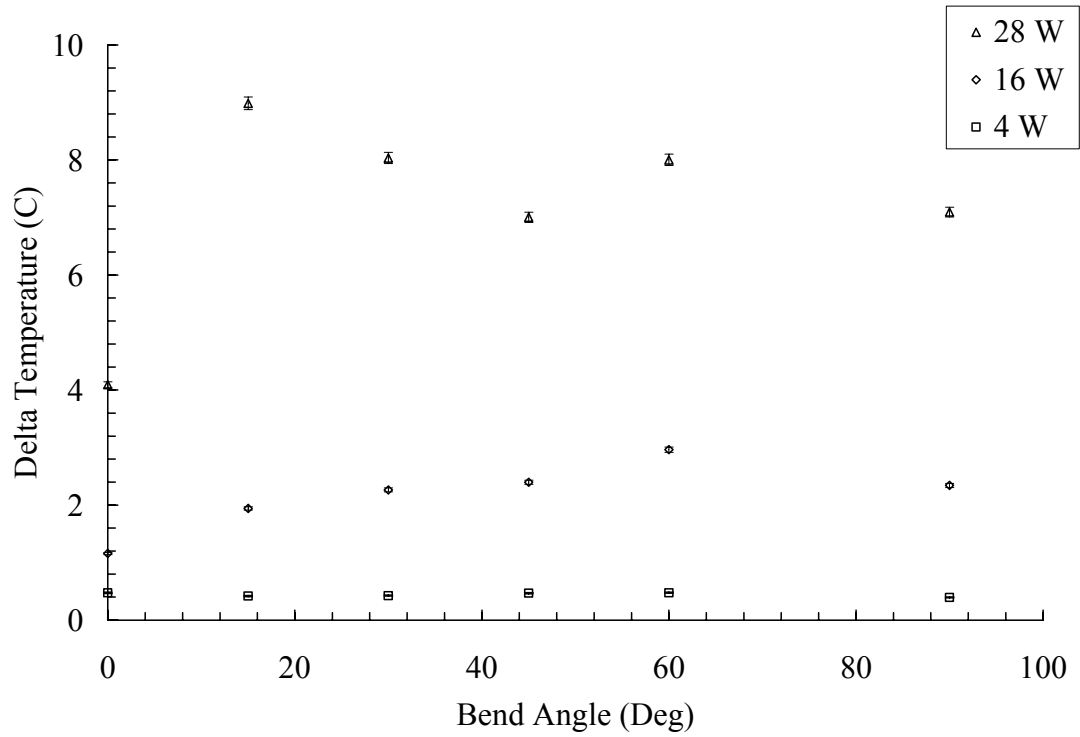


Figure 5.36:  $\Delta T$  across HP02 for various bend angles in horizontal orientation

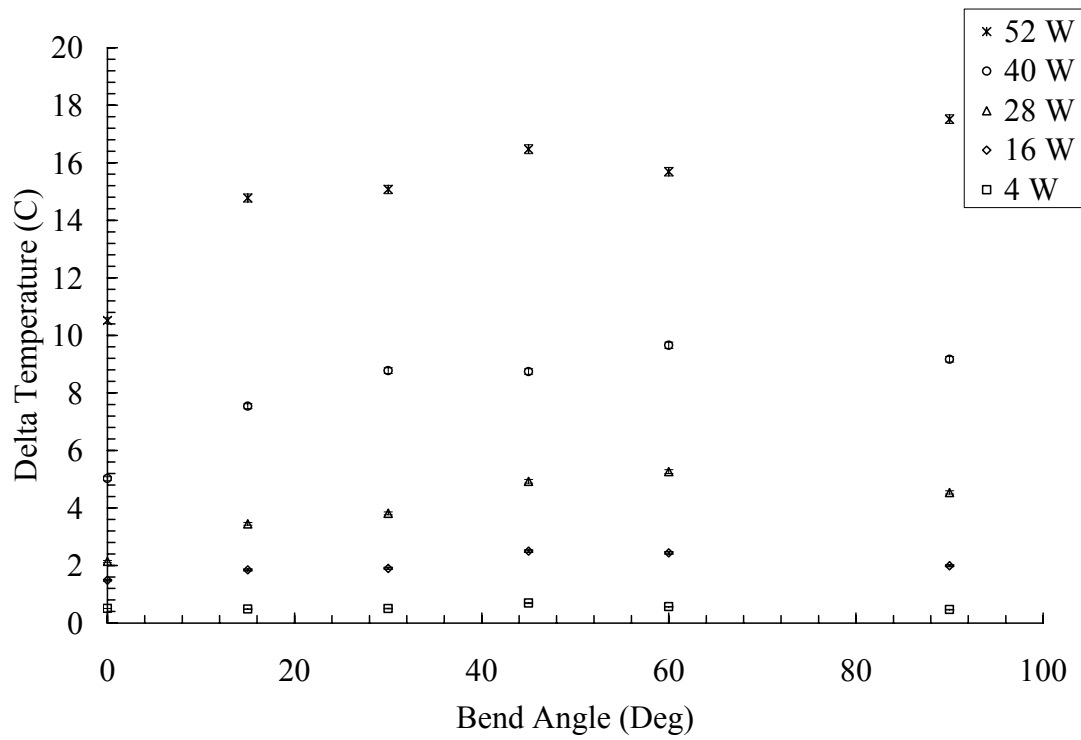


Figure 5.37:  $\Delta T$  across HP02 for various bend angles in vertical orientation

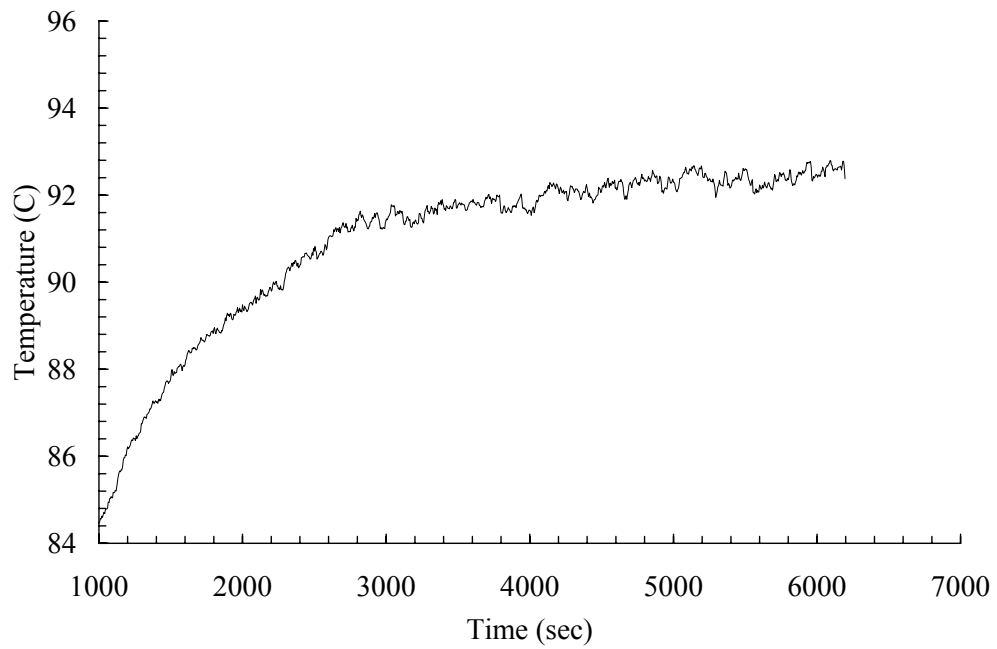


Figure 5.38: Evaporator of HP02 could not attain steady state at 40W power input in 90°  
bended vertical orientation

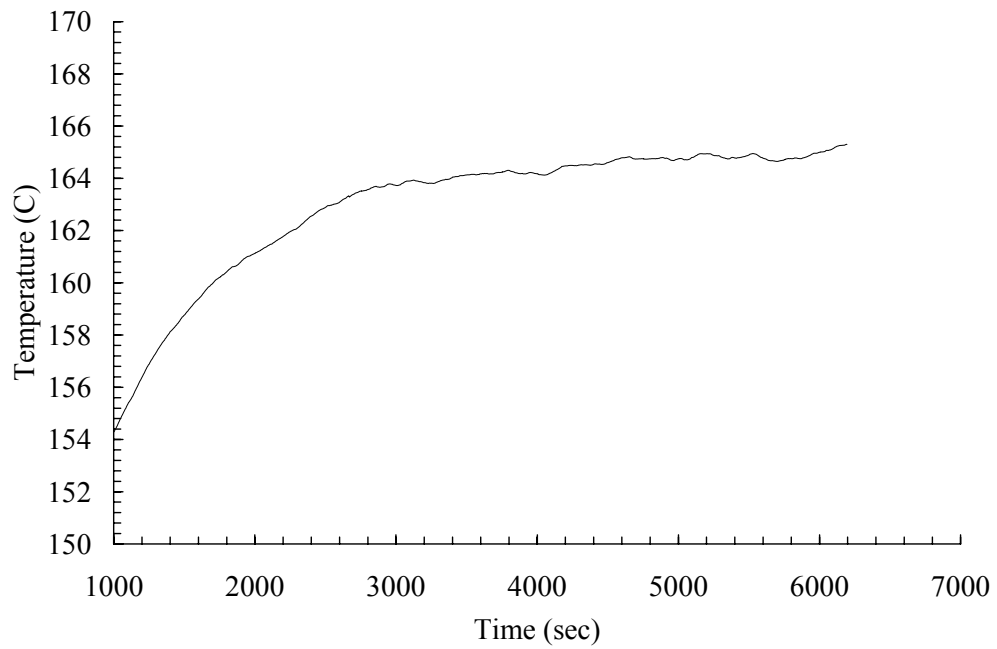


Figure 5.39: Heater of HP02 could not attain steady state at 40W power input in 90°  
bended vertical orientation

#### **5.4.6 Capillary Limits for HP02**

Capillary limit was calculated using the equations presented in Section 5.3.3. The procedure followed was similar to the one used for HP01 in Section 5.4.3.

The capillary limit charts are presented for following cases,

- Straight horizontal and vertical
- 15° bended horizontal and vertical
- 30° bended horizontal and vertical
- 45° bended horizontal and vertical
- 60° bended horizontal and vertical
- 90° bended horizontal and vertical

Vertical refers to gravity assisted operation.

Each chart also shows steady state heat input from the tests described in previous section.

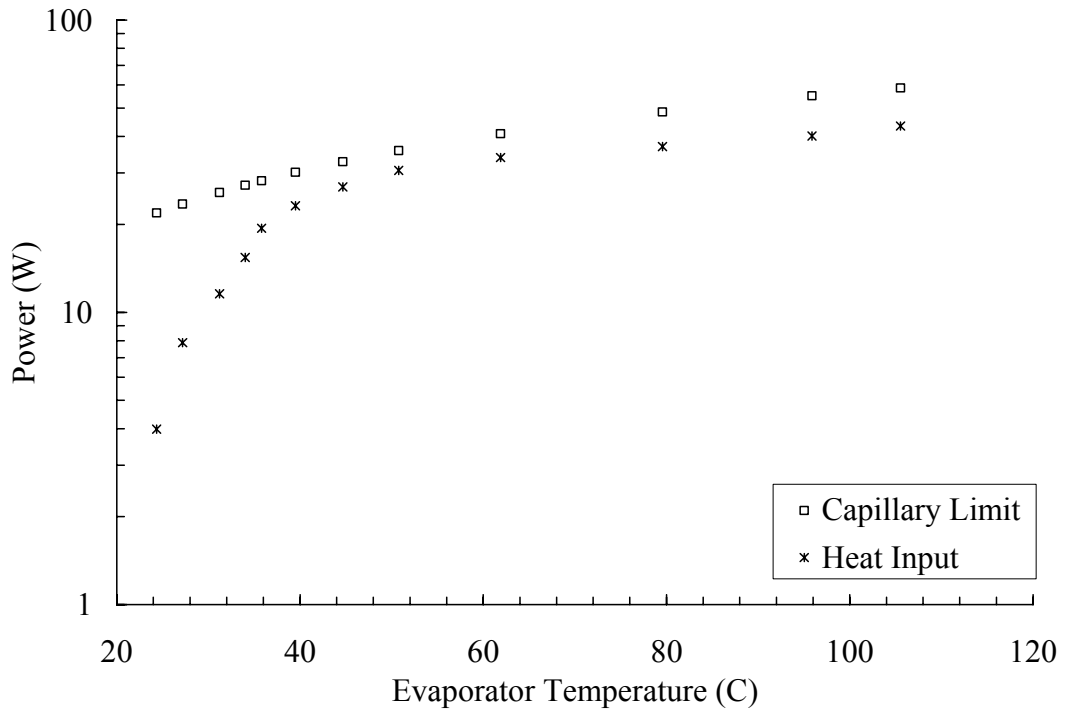


Figure 5.40: Capillary limit for HP02 in straight horizontal orientation

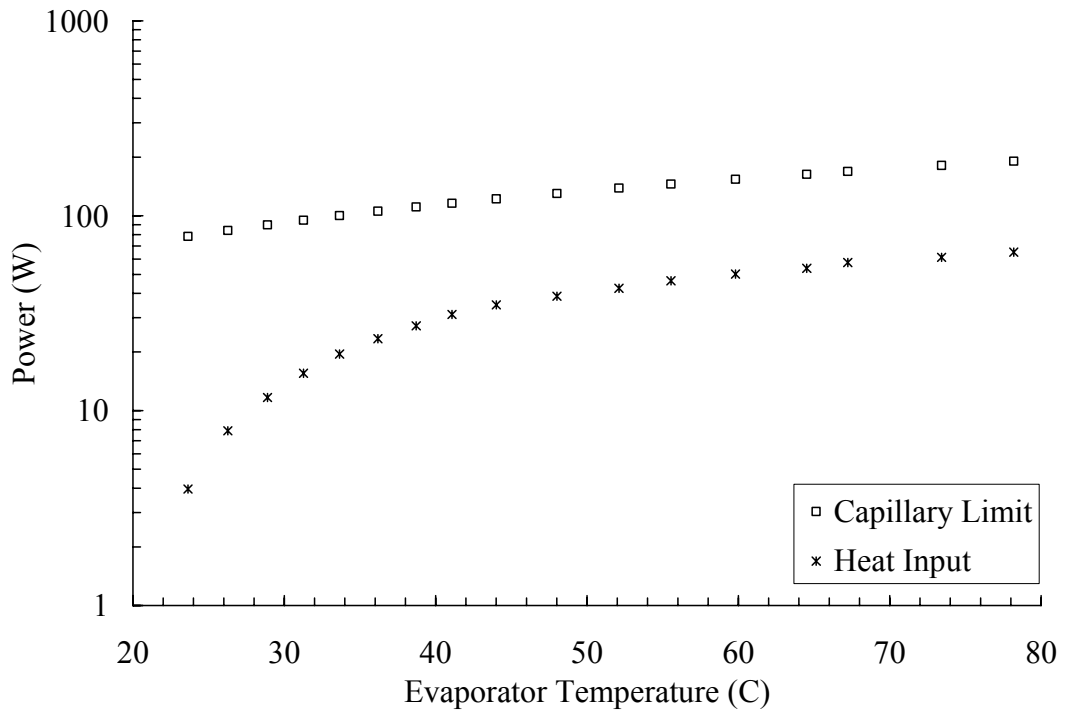


Figure 5.41: Capillary limit for HP02 in straight vertical orientation

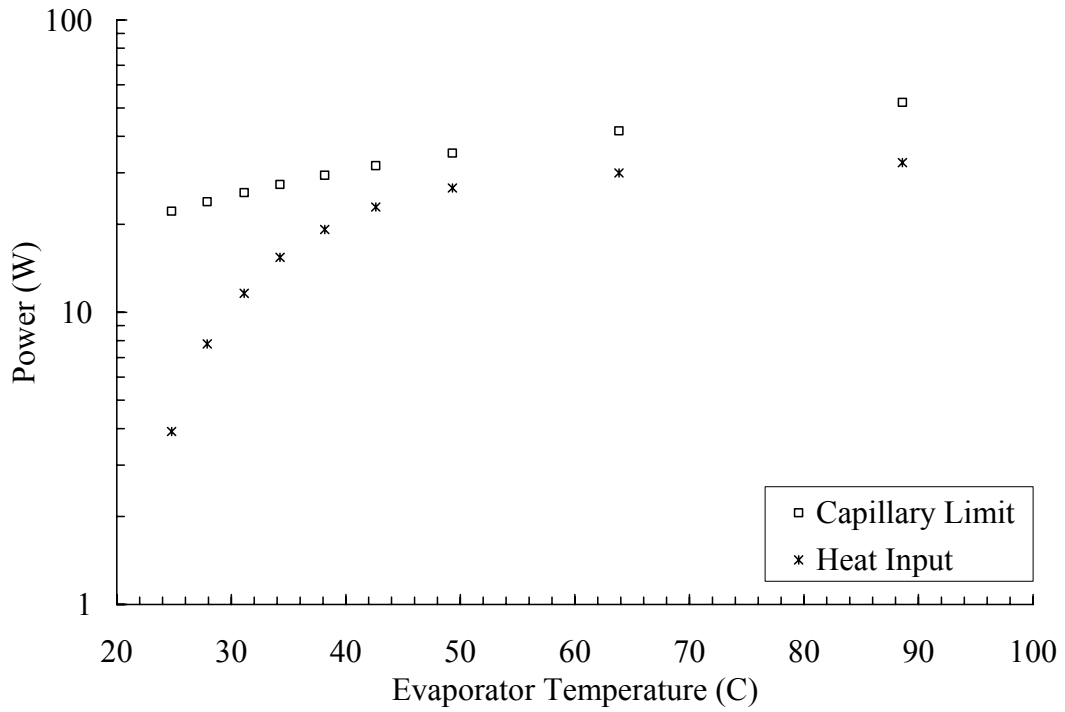


Figure 5.42: Capillary limit for HP02 in 15° bended horizontal orientation

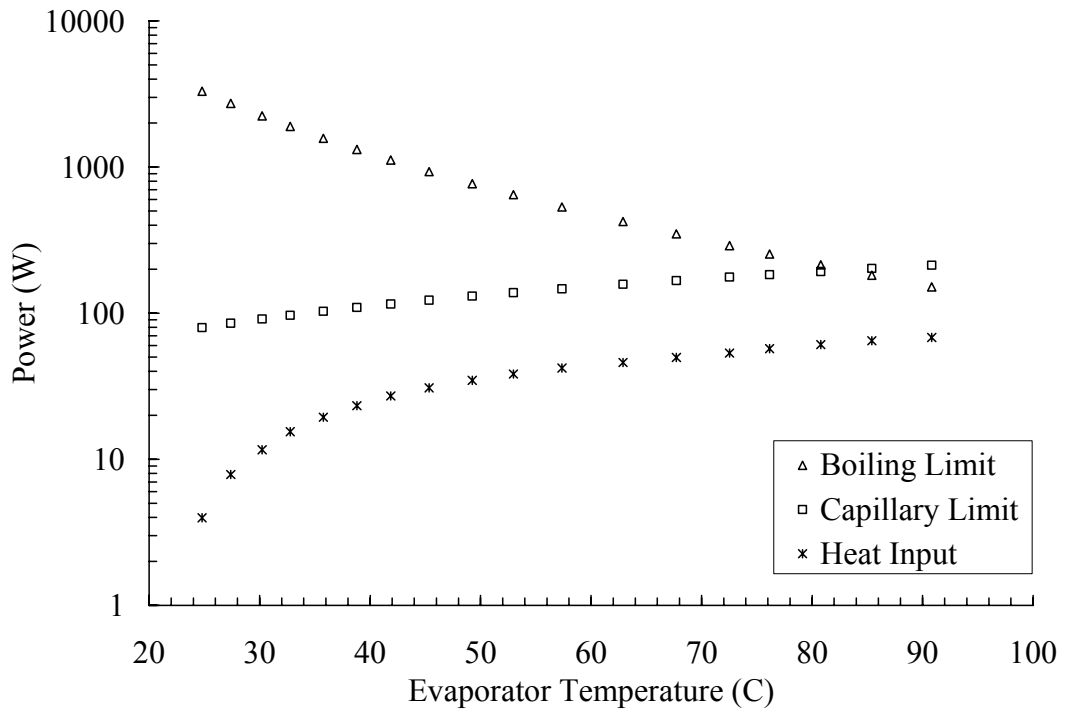


Figure 5.43: Capillary limit for HP02 in 15° bended vertical orientation

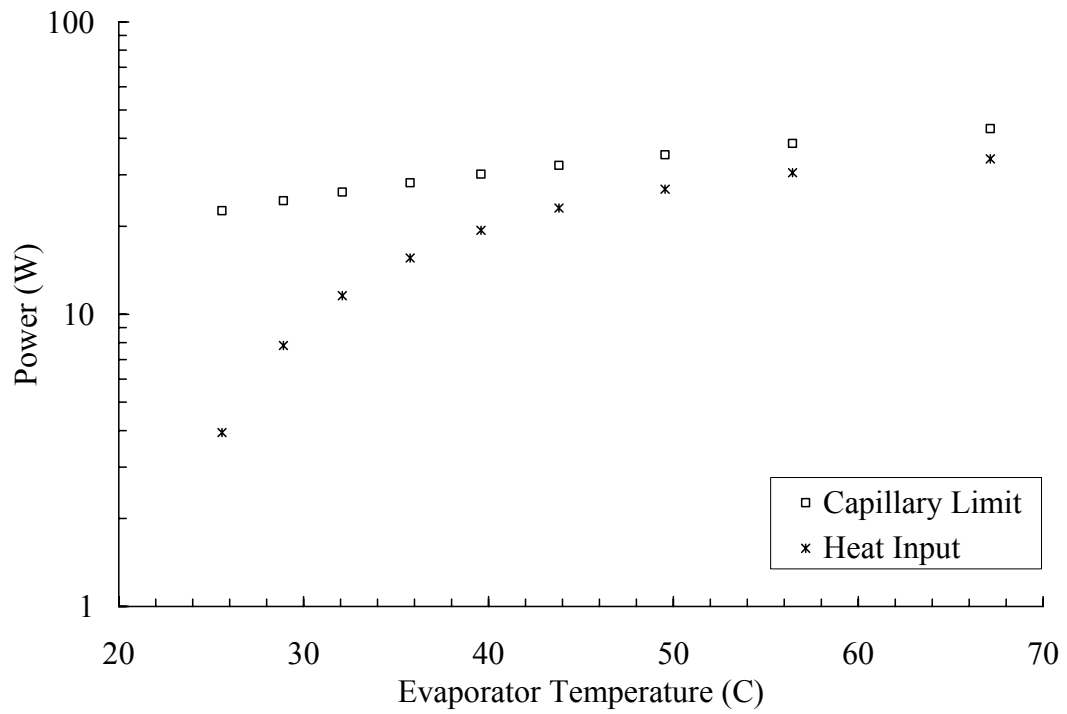


Figure 5.44: Capillary limit for HP02 in 30° bended horizontal orientation

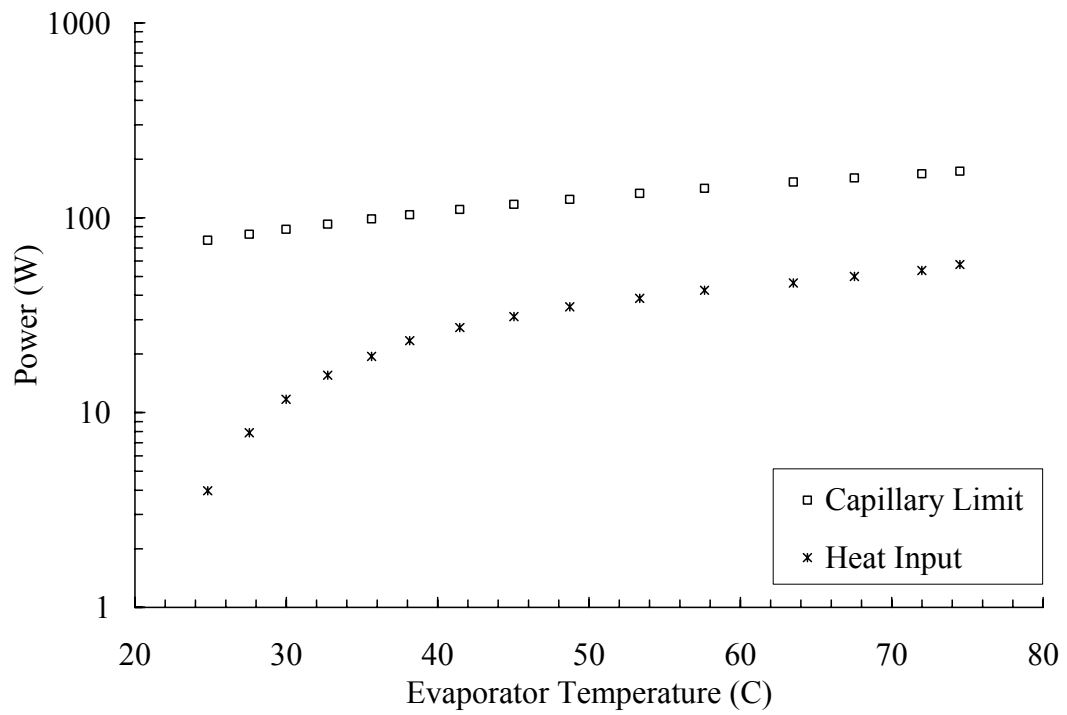


Figure 5.45: Capillary limit for HP02 in 30° bended vertical orientation

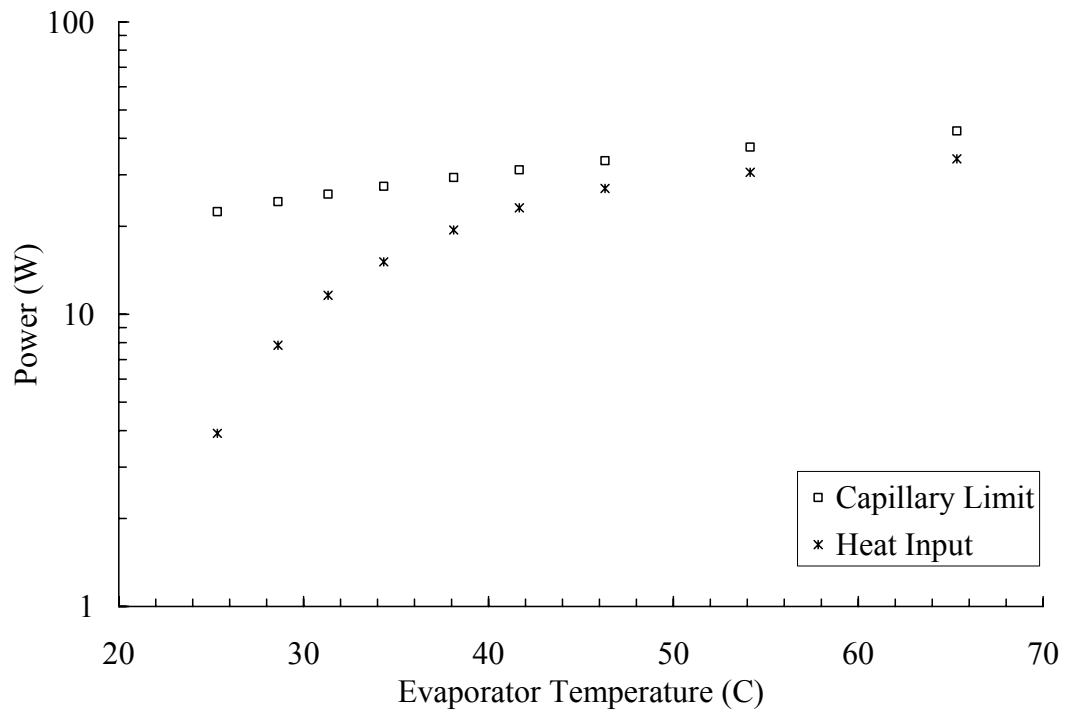


Figure 5.46: Capillary limit for HP02 in 45° bended horizontal orientation

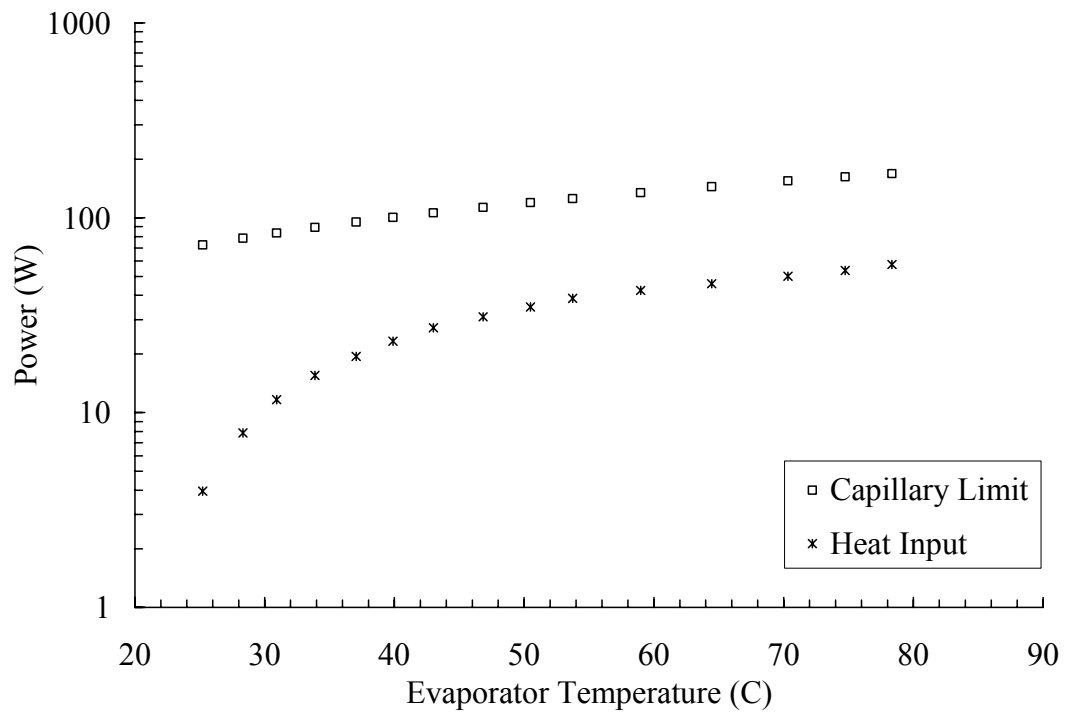


Figure 5.47: Capillary limit for HP02 in 45° bended vertical orientation



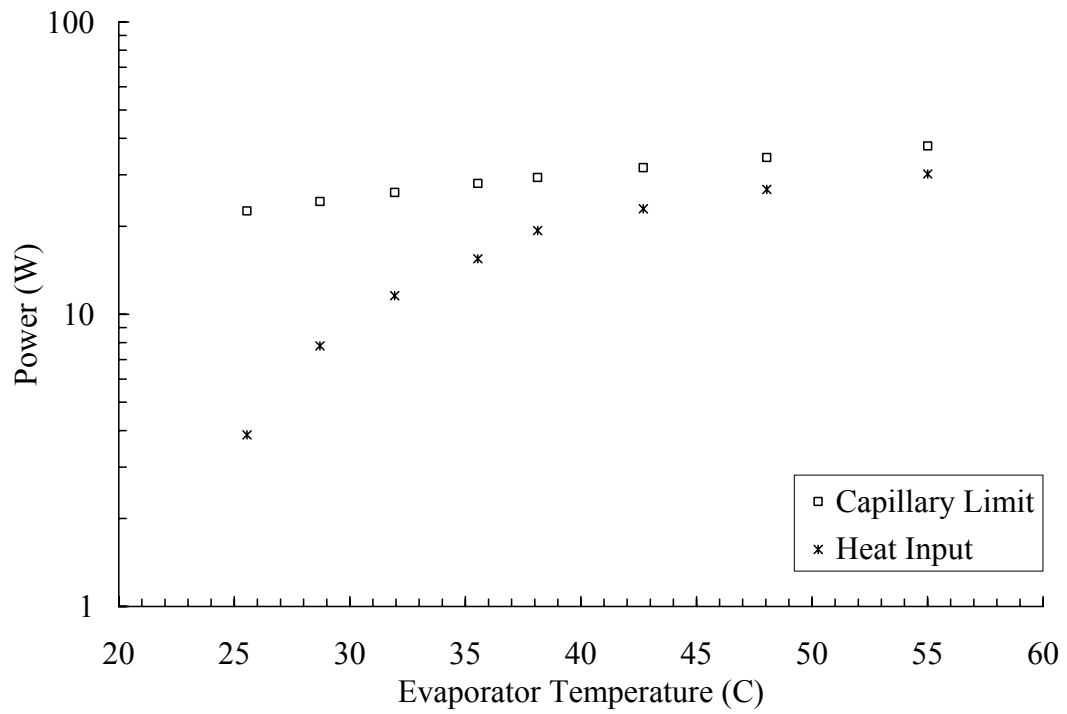


Figure 5.48: Capillary limit for HP02 in 60° bended horizontal orientation

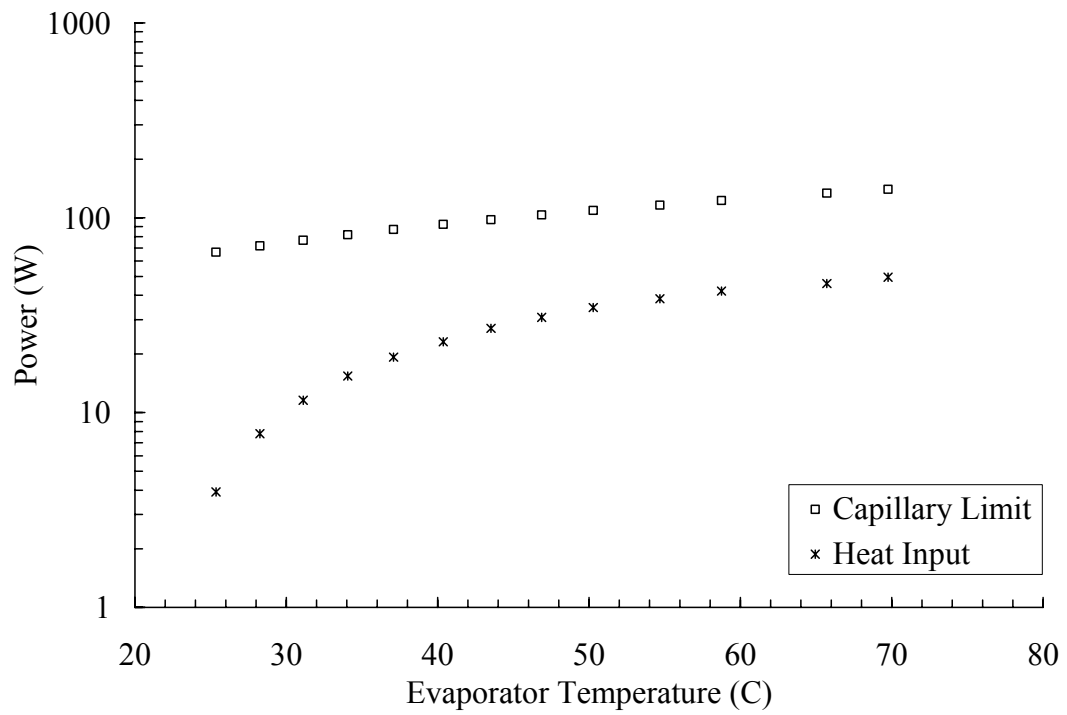


Figure 5.49: Capillary limit for HP02 in 60° bended vertical orientation

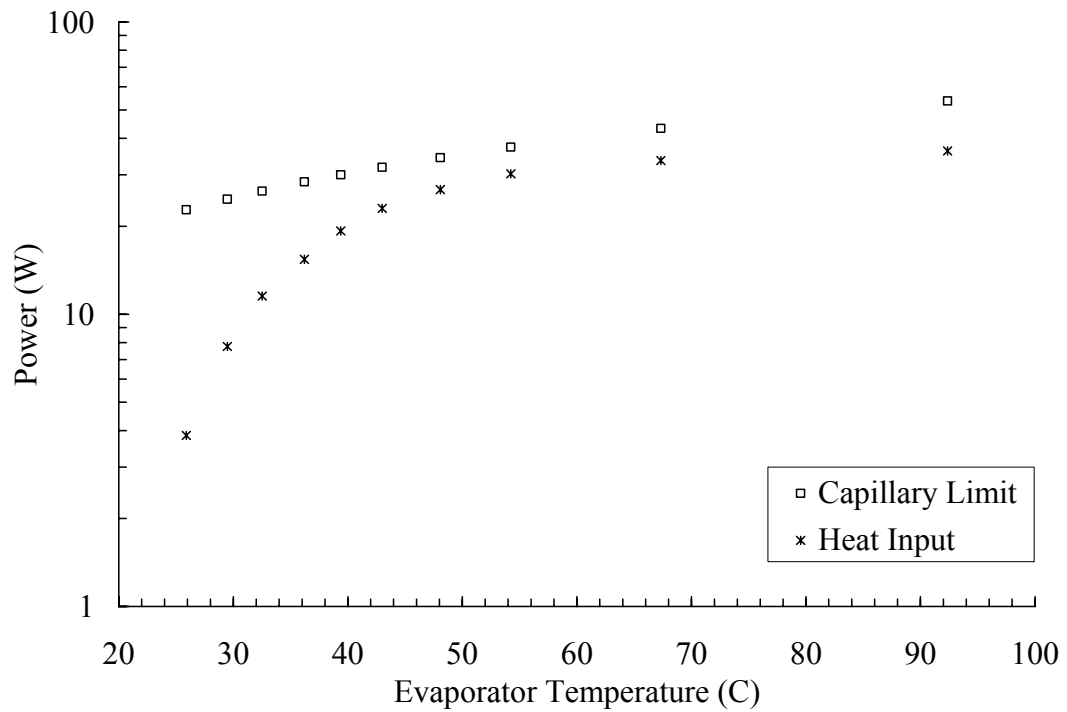


Figure 5.50: Capillary limit for HP02 in 90° bended horizontal orientation

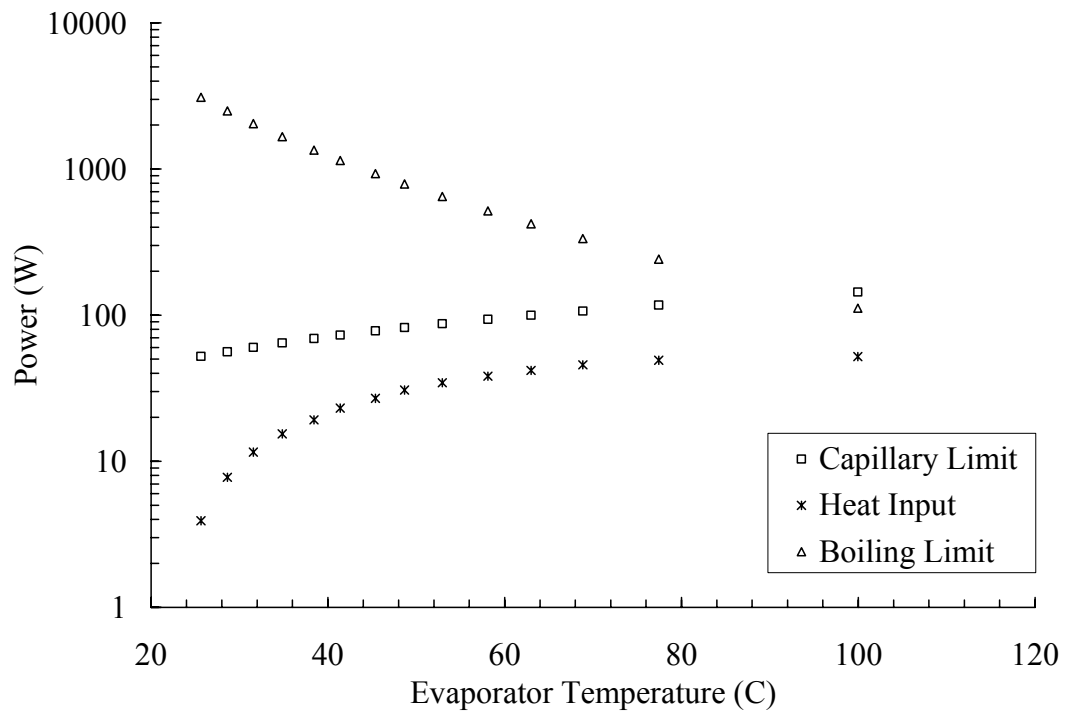


Figure 5.51: Capillary limit for HP02 in 90° bended vertical orientation

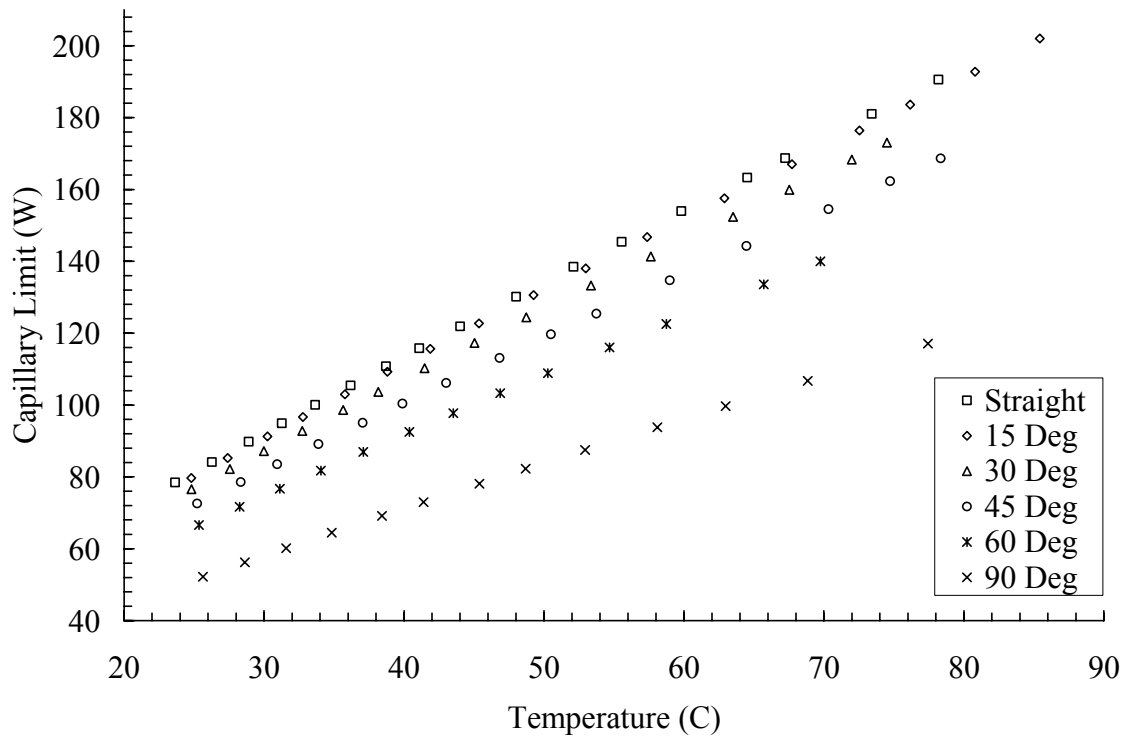


Figure 5.52: Effect of bending angle on capillary limit for HP02 in vertical orientation

Table 5.1: Effect of bending angle on capillary limit for HP02 in horizontal orientation

<b>Straight</b>		<b>15 Deg</b>		<b>30 Deg</b>		<b>45 Deg</b>		<b>60 Deg</b>		<b>90 Deg</b>	
<b>Temp (C)</b>	<b>Capillary Limit (W)</b>	<b>Temp (C)</b>	<b>Capillary Limit (W)</b>	<b>Temp (C)</b>	<b>Capillary Limit (W)</b>	<b>Temp (C)</b>	<b>Capillary Limit (W)</b>	<b>Temp (C)</b>	<b>Capillary Limit (W)</b>	<b>Temp (C)</b>	<b>Capillary Limit (W)</b>
24.36	21.90	24.80	22.15	25.58	22.59	25.33	22.45	25.55	22.57	25.90	22.76
27.19	23.49	27.90	23.88	28.91	24.44	28.62	24.27	28.71	24.32	29.48	24.74
31.23	25.72	31.13	25.66	32.09	26.18	31.32	25.75	31.94	26.08	32.53	26.39
34.02	27.23	34.25	27.35	35.76	28.15	34.34	27.38	35.54	28.01	36.21	28.35
35.81	28.19	38.15	29.41	39.60	30.16	38.11	29.37	38.13	29.36	39.38	30.00
39.50	30.13	42.62	31.71	43.81	32.30	41.67	31.20	42.70	31.71	43.01	31.84
44.67	32.76	49.31	35.02	49.56	35.13	46.30	33.52	48.04	34.36	48.07	34.35
50.77	35.74	63.85	41.73	56.45	38.38	54.16	37.30	55.01	37.68	54.24	37.29
61.88	40.87	88.60	52.24	67.14	43.17	65.33	42.36	–	–	–	–
79.56	48.51	–	–	–	–	–	–	–	–	–	–
95.87	55.11	–	–	–	–	–	–	–	–	–	–
105.54	58.56	–	–	–	–	–	–	–	–	–	–

From the above charts, it can be seen that the heat pipe was operating for all angles of the bending angle and the drop in the observed conductance values was because of the increased temperature drop along the heat pipe length. The termination of all the tests was either due to lack of steady state (Figure 5.38 and Figure 5.39) or stagnant conductance values (Figure 5.29 and Figure 5.31). As mentioned earlier for HP02, the bending loss was negligible and the capillary limit was mostly affected by the gravitational pressure drop. Hence the capillary limit variation for the horizontal orientation could not be plotted since all values overlap. A table is included showing the results (Table 5.1). It can be seen that similar to HP01, the capillary limit of HP02 in the vertical orientation decreases with increasing bending angle and this is mostly because of the decrease in the gravitational pressure drop in the axial direction.

## **5.5 Results**

In the last section, the data presented showed that the heat pipe performance in terms of copper equivalence decreased as the input power was increased until it no longer maintained steady state. This can be seen during testing of HP01 in Figure 5.8 through Figure 5.14 and HP02 in Figure 5.24 through Figure 5.35. The increase in power coupled with the increasing bending angle drove down the conductance values of the heat pipe. This was due to the rise in the temperature difference along the heat pipe length. The possible causes for this were described in Section 5.2. As previously reported by Merrigan et al. [20], the axial temperature drop showed an increasing trend with increasing bending angle (Figure 5.15, Figure 5.36 and Figure 5.37) and did not significantly affect the operation of the heat pipe. However, with HP01, in some cases the

maximum power transferred increased with an increase in the bending angle. This was later traced to erroneous data recording, which was rectified during the testing of HP02. During tests for HP02, it was noted that the maximum power for which a steady state reading could be recorded decreased and the time required for attaining steady state at higher power levels doubled to approximately 60-90 minutes from a normal time of 30 - 40 minutes.

The following limits are possible causes for heat pipe failures encountered during this work,

### **5.5.1 Possible Capillary Limit**

It can be seen that the capillary limits calculated using the test data were higher than the input power for most of the tests carried out in Figure 5.16 through Figure 5.22 and Figure 5.40 through Figure 5.51. When the heat pipe was in horizontal orientation the axial gravitational pressure drop was absent, capillary pumping pressure was the only driving factor. Therefore, all tests in horizontal orientation show a trend towards the capillary limit curve. Therefore, the possibility of encountering capillary limit in horizontal orientation was high.

### **5.5.2 Boiling Limit Encountered**

Since the boiling limit is a radial flux limitation, it was found that the heat pipe was limited by boiling phenomenon in situations where the capillary limit was high and the operating temperatures and input heat flux were high enough to initiate nucleate

boiling (Figure 5.20, Figure 5.22, Figure 5.43 and Figure 5.51). The lack of steady state indicated possibility of incipient boiling in the evaporator region.

### **5.5.3 Condenser Limit**

Apart from capillary and boiling limit, the third possibility was inadequate heat removal by the test setup. However, due to limitation of testing resources, this aspect could not be investigated and tubing of larger diameter was used in the water circulator to increase the flow rate of water over the condenser end of the heat pipe.

### **5.5.4 Bending Issues**

During calculations of energy losses in the bended section of the heat pipe, it was found that it was very low and practically incapable in affecting the capillary limit. This can be explained by considering the Reynolds numbers for the vapor flow. The vapor flow was laminar for all the tests and Reynolds number was in the range of 10-900. The low density and the high viscosity minimized the expected losses due to centrifugal forces at the bend and hence the frictional pressure drop was negligible. The bending losses increased at higher powers as the Reynolds number increased due to the increased vapor density.

## CHAPTER 6

### DISCUSSION

#### **6.1 Conclusion**

Two copper water heat pipes using sintered copper felt as the wick were fabricated. The aim of this investigation was to demonstrate the feasibility of bendable heat pipes. A thorough literature review showed that flexible heat pipes have attracted a lot of attention over the years. But all of the work published previously was geared towards making pipes which were either flexible or pre-bended during fabrication. It was found that no attempt was made to explore the possibility of stock heat pipes which can be bended or flexed in different shapes as required by the target application.

The ongoing work on heat pipes made using sintered copper felt as the wicking medium was extended to explore this possibility. The results for bendable heat pipes are encouraging as the heat pipe was found to work well in all orientations and up to a bend of 90°. The effect of pressure loss due to bending was found to be negligible and three to four orders of magnitude smaller than the capillary pumping pressure. This shows that the increase in the temperature drop due to bending is because of the obstruction in the flow of liquid returning to the evaporator from the condenser. The investigation of wick separation due to bending showed a noticeable separation of the wick from the



container walls. The vapor flow area was also reduced that directly reduced the heat carrying capacity. This lead to the build up of temperature at the evaporator end at constant heat input.

The heat pipe HP02 was found to work well against gravity even though theoretically the capillary pumping pressure was not capable of overcoming the axial hydrostatic pressure drop. This indicates that the wick had a higher capillary pumping capacity than the one calculated. The difference was traced down to the effective capillary radius which was established using an empirical relation. The performance in adverse orientation increased with increasing bending angle, which was expected as the axial hydrostatic pressure drop decreased with half of the heat pipe eventually being oriented horizontally after the 90° bend.

The benchmarking method used for comparing different heat pipes, which is designated as Copper Equivalence, was explained in detail. The usefulness and importance of copper equivalence was immediately recognized when the test setup had to be modified after testing of HP01. Copper equivalence allowed for comparing HP01 and HP02 even though both were tested on slightly different test setups.

## **6.2 Future Work**

The possibility of multiple bends needs to be explored for this concept to be feasible in practice. The current heat pipes were found to be capable of working after multiple bends although no systematic testing was carried out. The possibility of the heat pipe working beyond 90° could also be explored. Even though such studies have been published in the past, post-fabrication bending was never investigated for these cases.

Similarly, the aspect of different combinations of working fluids and wicking mediums could also be explored. This will allow testing of bendable heat pipes at different operating temperature ranges. The effect of relative radius of curvature on the heat pipe performance needs further investigation. This aspect is slightly complex as once bent, the same heat pipe might be damaged if the bending radius is changed later. There is a possibility that the diameter of the heat pipe will play some role in the number of bends that can be introduced in the heat pipe. This could be investigated by testing a batch of heat pipes of different sizes.

Wick separation studies could be performed for possible remedies including spring or mandrel supports during bending. The effective capillary radius for sintered copper felt should be measured experimentally.

Although copper equivalence eliminates the need for knowing the contact resistance in the test setup, the knowledge of actual contact resistance values will greatly elevate the validity of such testing in the future. During higher temperature testing the contact resistance would play a major role as other parasitic losses are considerably constant due to presence of good insulation.

## BIBLIOGRAPHY

- [1] Tohru Kishimoto, “Flexible-heat-pipe cooling for high-power devices”, *The International Journal of Microcircuits and Electronic Packaging*, vol. 17, no. 2, pp. 98-107, 1994.
- [2] Shaoning Lu and His-Shang Li, “Oscillatory mode with extremely high heat transfer rate in a flexible heat pipe”, *InterPACK '99: Pacific RIM/ASME International Intersociety Electronics Photonic Packaging Conference 'Advances in Electronic Packaging 1999'*, Maui, 1999.
- [3] P. D. Dunn and D. A. Reay, *Heat pipes*, 4th Ed, U.S.A., Pergamon, 1994.
- [4] M. N. Ivanovskii, V. P. Sorokin, and I. V. Yagodakin, *The physical principles of heat pipes*, 1982.
- [5] A. Faghri, *Heat pipe science and technology*. Washington, D.C., Taylor & Francis, 1995.
- [6] G. P. Peterson, *An Introduction to Heat Pipes – Modeling, Testing and Applications*, John Wiley & Sons, Inc., 1994.
- [7] A. Basiulis and T. A. Hummel, “The application of heat pipe techniques to electronic component cooling”, *ASME Winter Annual Meeting*, New York, 1972.
- [8] F. E. Bliss Jr., E. G. Clark Jr. and B. Stein, “Construction and test of a flexible heat pipe”, *ASME Conference Paper*, 1970.
- [9] F. Edelstein, “Deployable heat pipe radiator [Final Report]”, *NASA Report*, 1975.
- [10] E. W. Saaski and J. P. Wright, “A flexible cryogenic heat pipe”, *AIAA 10th Thermophysics Conference*, Denver, 1975.
- [11] J. P. Wright, P. J. Brennan and C. R. McCreight, “Development and test of two flexible cryogenic heat pipes (for spacecraft instrument cooling)”, *AIAA 11th Thermophysics Conference*, San Diego, 1976.
- [12] H. Koch, H. Kreeb and M. Perdu, “Modular axial grooved heat pipes (for spacecraft radiators)”, *European Space Agency Report*, 1976.

- [13] W. D. Muenzel, C. J. Savage, A. Accensi and B. G. M. Aalders, “Performance evaluation of the ESRO heat pipes included in the International Heat Pipe Experiment (IHPE) (using ammonia and acetone as working fluids)”, *European Space Agency Report*, 1976.
- [14] W. D. Muenzel, “Lifetests of the telecommunications satellite heat pipes [Final report]”, *European Space Agency report*, 1977.
- [15] M. Groll, W. D. Muenzel, W. Supper and C. J. Savage, “Development of an axial groove aluminum-ammonia liquid trap heat pipe thermal diode”, 3<sup>rd</sup> *International Heat Pipe Conference*, Palo Alto, 1978.
- [16] M. E. Peebles and L. D. Calhoun, “Fabrication and comparative performance of three variable conductance heat pipe concepts”, *ASME Paper*, 1977.
- [17] J. P. Mathieu, B. Moschetti and C. J. Savage, “Development of a high performance variable conductance heat pipe”, *AIAA 15th Thermophysics Conference*, Snowmass, 1980.
- [18] K. L. Meier, H. E. Martinez and J. E. Runyan, “Development of space reactor core heat pipes”, *Intersociety Energy Conversion Engineering Conference*, Atlanta, 1981.
- [19] D. M. Ernst, “Heat pipe heat rejection system and demonstration model for the nuclear electric propulsion (NEP) spacecraft [Final Report]”, *NASA Report*, 1981.
- [20] M. A. Merrigan, E. S. Keddy, J. T. Sena and M. G. Elder, “Heat pipe technology development for high temperature space radiator applications”, *Proceedings of the 19th Intersociety Energy Conversion Conference*, LaGrange Park, 1984.
- [21] R. M. Shaubach and N. J. Gernert, “High performance flexible heat pipes”, *AIAA 20th Thermophysics Conference*, Williamsburg, 1985.
- [22] D. M. Ernst and G. Y. Eastman, “High temperature heat pipe technology at Thermacore – an overview”, *AIAA 20th Thermophysics Conference*, Williamsburg, 1985.
- [23] H. A. N. Hwangbo and T. E. Joost, “A flexible variable conductance heat pipe design for temperature control of spacecraft equipment”, *AIAA Thermophysics, Plasmadynamics and Lasers Conference*, San Antonio, 1988.
- [24] G. P. Peterson, “Analytical development and computer modeling of a bellows-type heat pipe for the cooling of electronic components”, *Heat Transfer Engineering*, vol. 9, no.3, pp. 101-109, 1988.

- [25] R. S. Bhatti and S. Vanoost, "Qualification program on stainless steel A95 heatpipe for space application", *European Space Agency Symposium on Space Thermal Control and Life Support Systems*, pp. 575-582, 1988.
- [26] N. Gernert, D. Sarraf and M. Steinberg, "Flexible heat pipe cold plates for aircraft thermal control", *SAE Aerospace Technology Conference and Exposition, Long Beach*, 1991.
- [27] A. S. Gus'kov, Y. F. Gortyshov and Y. A. Poskonin, "Calculation of the thermophysical characteristics of an arterial flexible heat pipe", *Izvestiya Vysshikh Uchebnykh Zavedenij. Aviatsionnaya Tekhnika*, no. 4, pp. 38-43. 1993.
- [28] N. J. Gernert and J. Brown, "Development of a flexible loop heat pipe cold plate", *SAE Aerospace Atlantic Conference*, Dayton, 1995.
- [29] I. A. Zelenov, V. G. Zuev and U. A. Poskonin, "Flexible heat pipes, construction special features and test results", *ESA International Conference on Spacecraft Structures, Materials and Mechanical Testing*, pp. 1381-1384, Noordwijk, 1996.
- [30] S. K. Thomas and K. L. Yerkes, "Quasi-steady state thermal resistance of a flexible copper-water heat pipe subjected to transient acceleration loading", *Proceedings of the 31st Heat Transfer Conference*, pp. 349-356, Houston, 1996.
- [31] S. K. Thomas and K. L. Yerkes, "Quasi-steady state thermal resistance of a flexible copper-water heat pipe subjected to transient acceleration loading", *Journal of Thermophysics and Heat Transfer*, Vol. 11, no. 2, pp. 306-309, 1997.
- [32] R. B. Schweickart and M. M. Buchko, "Flexible heat pipes for CCD cooling on the Advanced Camera for Surveys", *Proceedings of the 5th Space Telescopes and Instruments*, pp. 292-300, Kona, 1998.
- [33] D. E. Glass, J. C. Stevens and V. V. Raman, "Flexible heat pipes for a lightweight spacecraft radiator", *Journal of Spacecraft and Rockets*, Vol. 36, no. 5, pp. 711-718, 1999.
- [34] T. Ozaki, A. Yao, Y. Ohkawa, H. Seko, A. Tsujihata and H. Noda, "Graphite faceskin deployable radiator panels for space satellites", *Proceedings of the 45th International SAMPE Symposium and Exhibition*, Long Beach, pp.1944-1953, 2000.
- [35] M. Marchetti, P. Testa, and F. R. Torrisi, "Measurement of thermal conductivity and thermal contact resistance in composite materials for space applications," *International Journal of Materials & Product Technology*, vol. 4, pp. 379-388, 1989.

- [36] C. C. Silverstein, Design and technology of heat pipes for cooling and heat exchange. Washington, D.C.: Hemisphere Pub. Corp., 1992.
- [37] B. N. Vadgama, "Experimental investigation of heat pipes with micro-fibrous metal felt wick and R134a working fluid", *Masters' Thesis*, Auburn University, 2004.
- [38] C. A. Busse, "Theory of the ultimate heat transfer limit of cylindrical heat pipes", *International Journal of Heat and Mass Transfer*, vol. 16, pp. 169-186, 1973.
- [39] R. W. Fox and A. T. McDonald, Introduction to Fluid Mechanics, John Wiley & Sons, Inc., 1985.
- [40] "Flow of Fluids through Valves, Fittings and Pipe.", Crane Company, New York, N.Y., Technical Paper No. 410, 1982.
- [41] U. A. Powle, "Energy losses in smooth pipe bends", *Mechanical Engineering Bulletin*, vol. 12, no. 4, pp. 104-109, 1981.
- [42] H. Ito, "Laminar flow in Curved Pipes", *Z. Angew. Math. Mech.*, vol. 49, pp. 653-656, 1969.
- [43] J. C. Misra, M. K. Patra and S. C. Misra, "Laminar boundary-layer flow of a Newtonian fluid through a curved pipe - some applications to arterial flow dynamics", *International Journal of Engineering Science*, vol. 32, no. 12, pp 1997-2010, 1997.
- [44] C. L. Tien and K. S. Chung, "Entrainment limits in heat pipes", *AIAA Journal*, vol. 17, no. 6, pp. 643-646, 1979.
- [45] F. P. Incropera and D. P. DeWitt, Introduction to Heat Transfer, John Wiley & Sons, Inc., 1985.